

RECEIVED	
BY <i>Q77u</i>	DATE <i>31/10/51</i>

55000 /



**MATHEMATICAL MODEL APPROACH FOR SEA SURFACE
TEMPERATURE BASED ON GMS-6 SATELLITE IMAGE**

CHAIROTE YAIPRASERT

**A DISSERTATION SUBMITTED IN PARTIAL FULFILLMENT
OF THE REQUIREMENTS FOR THE DEGREE OF
DOCTOR OF PHILOSOPHY IN COMPUTATIONAL SCIENCE
SCHOOL OF SCIENCE
WALAILAK UNIVERSITY**

2007

Dissertation Title Mathematical Model Approach for Sea Surface Temperature
Based on GMS-6 Satellite Image

Author Chairote Yaiprasert

Program Computational Science

Academic Advisor Committee

K. Jaroensutasinee.....Chairman

(Asst. Prof. Krisanadej Jaroensutasinee, Ph.D.)

M. Jaroensutasinee.....Committee

(Asst. Prof. Mullica Jaroensutasinee, Ph.D.)

Ph.D. Examination Committee

Teerakiat Kerdcharoen.....Chairman

(Asst. Prof. Teerakiat Kerdcharoen, Ph.D.)

Piyawut Srichaikul.....Committee

(Piyawut Srichaikul, Ph.D.)

K. Jaroensutasinee.....Committee

(Asst. Prof. Krisanadej Jaroensutasinee, Ph.D.)

M. Jaroensutasinee.....Committee

(Asst. Prof. Mullica Jaroensutasinee, Ph.D.)

Approved by Committee of Computational Science Graduate Program, School
of Science, Walailak University in Partial Fulfillment of the Requirements for the
Doctor of Philosophy of Science in Computational Science.

K. Jaroensutasinee.....

(Asst. Prof. Krisanadej Jaroensutasinee, Ph.D.)

Chairman Committee of Doctor of Philosophy
in Computational Science Graduate Program

ชื่อวิทยานิพนธ์	แบบจำลองทางคณิตศาสตร์สำหรับอุณหภูมิผิวน้ำทะเล บนพื้นฐานของ ภาพถ่ายดาวเทียม GMS-6
ผู้แต่ง	ชัยโรจน์ ไหญ่ประเสริฐ
สาขาวิชา	วิทยาศาสตร์เชิงคำนวณ
ปีการศึกษา	2550

บทคัดย่อ

การศึกษานี้มุ่งศึกษาพัฒนาวิธีการใหม่ในการทำนายและจำลองปริมาณรังสีดวงอาทิตย์ และอุณหภูมิจากค่าจุดภาพของภาพถ่ายดาวเทียมโดยใช้แบบจำลองทางคณิตศาสตร์, ข้อมูลภาพถ่ายดาวเทียม และการยืนยันภาคสนาม ค่าจุดภาพจะถูกใช้ทำนายอุณหภูมิผิวน้ำทะเลและตัวบ่งชี้ของอุณหภูมิอื่นๆ ของอุณหภูมิผิวน้ำทะเล ปริมาณรังสีดวงอาทิตย์เป็นปัจจัยที่สำคัญในการเพิ่มอุณหภูมิของโลก อย่างไรก็ตามข้อมูลที่เข้าถึงใช้ได้ไม่มีอยู่ในส่วนของพื้นที่ที่แยกตัวอยู่ห่างไกลออกไป เนื่องจากไม่มีสถานีอุตุนิยมวิทยาในพื้นที่นั้น แต่ยังมีช่องทางที่ดีจากการมีภาพถ่ายดาวเทียมของแผนที่แสดงปริมาณไอน้ำในอากาศที่เราสามารถเข้าถึงใช้ได้ทุกๆ ครึ่งชั่วโมงโดยอัตโนมัติ ผลของการศึกษานี้จะถูกเปรียบเทียบกับดัชนีอุณหภูมิของ NOAA จากผลของการศึกษาแสดงให้เห็นว่าค่าจุดภาพของภาพถ่ายดาวเทียมมีความสัมพันธ์ไปในทางเดียวกันกับปริมาณรังสีดวงอาทิตย์ ซึ่งรวมทั้งปริมาณรังสีดวงอาทิตย์นั้นยังมีความสัมพันธ์ไปในทางเดียวกันอุณหภูมิผิวน้ำทะเล ทั้งนี้วิธีการศึกษานี้สามารถนำไปประยุกต์ในทุกพื้นที่ของโลกได้

Dissertation Title	Mathematical Model Approach for Sea Surface Temperature Based on GMS-6 Satellite Image
Author	Chairote Yaiprasert
Major Program	Computational Science
Academic Year	2007

ABSTRACT

This study focused on developing a new approach for predicting and modelling solar radiation and temperature from the pixel value of satellite images using mathematical model, satellite data and field verification. The pixel values were used to predict sea surface temperature and other temperature indices. Solar radiation was considered as the most important parameter affecting an increase in global temperature. However, these data were not always available particularly in isolated sites due to the non-availability of the meteorological stations in these sites. Fortunately, the GMS-6 satellite images were always available because we could automatically download the vapour map satellite image at half an hour intervals. Our results were compared with temperature indices from NOAA. The results showed that the pixel value was positively associated with solar radiation, and also irradiance was positively associated with the sea surface temperature. This study suggests that the methodology could be applied to any geographical area in the world.

ACKNOWLEDGEMENTS

This project was supported in part by PTT Public Company Limited, TOTAL Foundation and TOTAL E&P Thailand, TRF/Biotec special program for Biodiversity Research Training grant BRT T_550001, Commission on Higher Education and CXKURUE, the Institute of Research and Development, Walailak University.

I would like to express my deep and sincere gratitude to my supervisor and co-supervisor, Assistant Professor Dr. Krisanadej Jaroensutasinee and Assistant Professor Dr. Mullica Jaroensutasinee for giving me a chance to study and grow academically at Walailak University. They kindly and closely gave me advices, supports and suggestions throughout my research. I was grateful to the committee members, Assistant Professor Dr. Teerakiat Kerdcharoen and Dr. Piyawut Srichaikul, for their affirmative suggestions and helpful comments.

Invaluable assistance in the comments on the previous versions of this dissertation was provided by Assistant Professor Dr. Krisanadej Jaroensutasinee and Assistant Professor Dr. Mullica Jaroensutasinee, Walailak University. I would like to intensely thank the National Oceanic and Atmospheric Administration (NOAA) for providing data.

Lastly, I indebted to my father, my mother, sisters and my friends for their understanding, loving and continuing support.

Chairote Yaiprasert

DISCLAIMER

I certify that the material contained in this dissertation is my own work and does not contain significant portions of unreferenced or unacknowledged material. I also warrant that the above statement applied to the implementation of the project and all associated documentation.

In the case of electronically submitted work, I also consent to this work being stored electronically and copied for assessment purposes, including the department's use of plagiarism detection systems in order to check the integrity of assessed work.

C. Vaighant

Signature

10 April 2008

Date

TABLE OF CONTENTS

	Page
Abstract (Thai)	i
Abstract (English)	ii
Acknowledgements	iii
Disclaimer	iv
Table of Contents	v
List of Illustrations	vii
Chapter I Introduction	1
Chapter II Comparing Two Estimating Techniques on Coral Growth Forms Using Random and Quadrat Sampling Techniques	36
Chapter III Coral Growth Forms and Biodiversity Indices at Khanom Mu Koh Talae Tai Marine National Park	55
Chapter IV The Pixel Value Data Approach for Rainfall Forecasting Based On Goes-9 Satellite Image Sequence Analysis	73
Chapter V Mathematical Model for Solar Radiation and Temperature Field Verification	97
Curriculum Vitae	127

LIST OF TABLES

	Page
Table 1 Summary of environmental factors alleged to cause/influence coral.	7
Table 2 Averaged seasonal rainfall (mm) in various parts of Thailand based on 1971-2000 period.	29
Table 3 Biodiversity index from % coral growth form classification.	49
Table 4 Coral biodiversity indices at Khanom - Mu Koh Talae Tai Marine National Park.	67
Table 5 The regression output for fitting the model $y_i = \beta_0 + \beta_1 x_i + e_i$, $*P < 0.001$.	88
Table 6 The regression output of pixel value and solar radiation for fitting the model $y_i = \beta_0 + \beta_1 x_i + e_i$, $*P < 0.001$.	118
Table 7 The regression output of solar radiation and temperature for fitting the model $y_i = \beta_0 + \beta_1 x_i + e_i$, $*P < 0.001$.	119

LIST OF ILLUSTRATIONS

	Page
Figure 1	World NOAA SSTs data.
	20
Figure 2	Coastal contour lines of Southeast Asia.
	25
Figure 3	Thailand coastal line (left) and Khanom-Mu Koh Talae Tai Marine National Park (right).
	26
Figure 4	The prevailing wind of the Gulf of Thailand; red, green, blue and purple arrows represent Northeast monsoon, Southwest monsoon, Tropical storm and Southern wind, respectively.
	27
Figure 5	Three study sites at Khanom - Mu Koh Talae Tai Marine National Park, Nakhon Si Thammarat, Thailand: Koh Tan, Koh Mud Soom and Ao Tong Yee.
	40
Figure 6	Seven coral growth forms.
	43
Figure 7	% coral form at (□) Koh Tan, (▣) Koh Mudsoom and (■) Ao Thong Yee. (a) random sampling technique and (b) quadrat sampling technique, * $P < 0.001$.
	48
Figure 8	SST NOAA, measured SST (upper line) and light intensity (lower line) at Koh Tan.
	50
Figure 9	Four study sites: Koh Tan, Koh Mud Soom, Ao Tong Yee and Koh Wang Nok.
	60
Figure 10	Seven coral growth forms.
	64

LIST OF ILLUSTRATIONS (CONTINUED)

		Page
Figure 11	% of seven coral growth forms at Koh Tan, Koh Mud Soom, Ao Thong Yee and Koh Wang Nok. White to black colour level represent to the percentage of Massive, Columnar, Encrusting, Branching, Foliaceous, Laminar and Free-living, respectively, $*P < 0.001$.	65
Figure 12	% of seven coral growth forms at Koh Tan, Koh Mud Soom, Ao Tong Yee and Koh Wang Nok respectively, $*P < 0.001$.	66
Figure 13	Snapshots of water vapour image from the GOES-9 satellite on Thailand.	79
Figure 14	A monochrome digital image.	83
Figure 15	The joint 95% confidence region of the regression parameters from model $y_i = \beta_0 + \beta_1 x_i + e_i$.	86
Figure 16	The association between the averaged pixel value of daily water vapour images and the amount of daily rainfall (mm) in Thailand from TMD.	89
Figure 17	Snapshots of water vapour image from the GMS-6 satellite on Thailand (October 2007).	101
Figure 18	Daily mean temperature data (red points) and moving average temperature (blue solid line) during January-December 2007.	101
Figure 19	Daily mean solar radiation data (red points) and moving average solar radiation (green solid line) during January-December 2007.	102

LIST OF ILLUSTRATIONS (CONTINUED)

	Page
Figure 20 Colour bar diagram; hue value (red), saturation (green), value (blue), and mathematical transformation (black).	104
Figure 21 The 95% confidence interval predicted responses of solar radiation (W/m^2).	111
Figure 22 The 95% confidence interval predicted responses of sea surface light intensity (W/m^2).	113
Figure 23 The 95% confidence interval predicted responses of SST ($^{\circ}\text{C}$).	114
Figure 24 Comparison between measured SST data (red solid line), calculated SST data (green solid line) by the proposed mathematical model and NOAA SST data (blue points), corresponding to year 2007.	115

LIST OF ABBREVIATIONS

ANOVA	Analysis of Variance
ATI	Area Time Integral
AVHRR	Advanced Very High Resolution Radiometer
CREWS	Coral Reefs Early Warning System
ENSO	El Niño-Southern Oscillation
GMS	Geostationary Meteorological Satellite
GMT	Greenwich Mean Time
GOES	Geostationary Operational Environmental Satellite
HSV	Hue, Saturation, Value
IR	Infrared Radar Spectrum
METEOSAT	Meteorological Satellite
MMM	Maximum Monthly Mean
MPM	Maximum Pentad Mean
MSG	METEOSAT Second Generation
MW	Microwave Spectrum
NASA	National Aeronautics and Space Administration
NESDIS	National Environmental Satellite, Data, and Information Service
NGDC	National Geophysical Data Center
NGO	Non-Governmental Organizations
NLSST	Non-Linear SST
NOAA	National Oceanic and Atmospheric Administration

POES	Polar Orbiting Environmental Satellites
PVI	Pixel Value Index
REI	Rain Exposure Index
RGB	Red, Green, Blue
SAR	Synthetic Aperture Radar
SEVIRI	Spinning Enhanced Visible and Infrared Imager
SST	Sea Surface Temperature
TMD	Thai Meteorological Department
UN	United Nations
VIS	Visible Spectrum
WV	Water Vapour

CHAPTER I

INTRODUCTION

SIGNIFICANCE OF RESEARCH

Coral bleaching poses a threat to coral reefs as temperatures rise due to the enhanced greenhouse effect. Mass coral bleaching again affected large parts of the world. Our knowledge of this event was greatly developed from GeoComputing index, and Rain Exposure Index (REI) experience (Ruairuen et al., 2005). Inversed REI values were used to predict Sea Surface Temperature (SST) and other temperature indices, which provided the basis for a more effective response to the bleaching event. The response incorporated regular monitoring of conditions on the Khanom-Mu Koh Talae Tai Marine National Park. The application of bleaching thresholds was determined from experimental work, field observations and knowledge of satellite data. Sea surface temperature products provided through NOAA/NESDIS were important to this effort. From early August 2007, daily updates of seawater temperatures (recorded by the data logger station network) were compared with average daily water temperatures and monitored against bleaching thresholds.

Coral reefs were the most diverse marine ecosystems. Geographically they were located in circumtropical shallow tropical waters along the shores of islands and continents (Buchheim, 1998). Scleractinian corals play a primary role in the construction and maintenance of reefs. They provided support and shelter for the many organisms that inhabit the coral reefs (Meesters et al., 1998). It was estimated

that 25% of all marine species inhabit coral reefs, where the number of individual species might be as high as one million (Davidson, 1998).

Marine ecosystems contribute about 63% of the estimated value of the biosphere \$16-\$54 trillion USD annually. Coral reefs in particular contribute to about 1.8% of this value (Costanza et al., 1997). Given that coral reefs constitute 0.2 % of the world's marine ecosystem (Bryant et al., 1998), these figures demonstrate that the contribution of coral reefs to the welfare of the world and the people living on it was disproportionately large (Souter and Linden, 2000).

One thing the countries which border the ocean had in common was the high dependency on coastal resources by the population living at the coast (Muthiga et al., 1998). Resources derived from coral reefs were essential to the livelihood of millions of people who live within tropical coastal communities (Souter and Linden, 2000). Economically they support artisanal fisheries; a source of livelihood to the most of the coastal population in tropical countries. Tourism was vital to economies of most countries where coral reefs were found. Coral reefs were invaluable for protecting the beach against strong ocean waves.

In the case of Southeast Asia, there had been a continual decline in reef condition; but there were some positive signs in some countries e.g. Indonesia and possibly Myanmar. The continued reef decline in the Philippines, Vietnam, Thailand and Singapore was a major concern (Wilkinson, 2004). The threats to reefs remain high and dominated by human pressures; over-fishing and damaging fishing was extensive, pollution from the land affects many reefs, sediments continue to damage reefs due to coastal development, dredging and deforestation, and reclamation of coral reef areas continues for industries, airports and marinas. However, there were more

active management initiatives throughout the region, and monitoring programs had improved and expanded, after a decade 42 Status of Coral Reefs of the World: 2004 of little progress. Some countries lack the expertise and resources for monitoring and there was a critical lack of effective coordination. Several major projects were starting to address the issues with assistance from UN and NGO agencies; but there was a major need for regional coordination and cooperation, and a sharing of resources for coral reef monitoring and management.

Bleaching in 1998, Moderate to severe damage was reported on Indonesia's coral reefs after the 1998 bleaching event and recovery had been variable. Reefs in the Philippines, Thailand, and Vietnam suffered widespread bleaching episodes leading to high variable mortality. Recovery was occurring, yet could take time due to continued anthropogenic threats causing further stress (Tun et al., 2004).

Bleaching from 1999-2004, There was evidence of coral recovery in Cambodia, Indonesia, Philippines, Thailand and Vietnam after extensive coral bleaching mortality, mostly in the northern parts of Southeast Asia. In Indonesia, recovery had been slow in Sumatra and Lombok, but rapid in the Seribu Islands adjacent to Jakarta where coral cover was 40% on some reefs. Coral recruitment was low in the Gulf of Thailand indicating that recovery from the 1998 bleaching could be delayed. The coral reefs in the World Heritage Tubbataha reefs south of Palawan were showing rapid recovery after years of blast fishing and the 1998 bleaching event. Coral reefs in Bali showed minimal bleaching and many corals were in excellent condition except for physical damage caused by dynamite explosions and localised anchor damage. In Tulamben and Seraya corals showed little sign of bleaching (Tun et al., 2004).

To address the above problems, this study aimed to provide meteorologists with an automatic spatial data method based on mathematically inverted technique to obtain indirect inferences of temperature and analysis in the GMS (Geostationary Meteorological Satellite) satellite image sequence with possible solar radiation in term mathematical model. It could be predicted so that effective drought control measures could be taken. The basic principle behind the method was to formulate from a recent collection data that the movement and propagation of water vapour dynamic systems over the west Pacific region. It was the crucial factor leading to the solar energy through coral reef, which provided the basis for a more effective response to the bleaching event. The response incorporated regular monitoring of conditions on the Khanom-Mu Koh Talae Tai Marine National Park in Thailand. The method used was data mining and knowledge discovery techniques. Firstly, the image sequences of water vapour map acquired from the GMS were used. The qualified of mathematical model technique was automatically identified by image processing and high computing techniques.

The mathematical model technique was achieving accurate identification and correct detecting of dryness from the remote sensing image sequences which was over daily updates of SST from data logger station network. The data were compared with average daily water temperatures from NOAA product and their monitored against bleaching thresholds.

It provided the indispensable premise for meteorologists to make further forecasts on coral bleaching events. Since the satellite image data were spatial temporal, we needed first identify and track water vapour and dryness from the entire image sequences correctly and efficiently, and then make the necessary

characterization of the pixel values by extracting meteorological features associated with them. To address this issue, it proposes a fast detecting and characterization method of water vapour and dryness according to their feature correspondences, derived from the meteorological satellite image sequences. The method was based on the fact that in a relatively small time-span. The technique was progressive and detectable, which guarantees a relatively similar area and texture in two consecutive satellite images.

It was then necessary to learn and understand the causes of bleaching in order to reduce the damages and losses. Therefore, developing a better way to predict the coral bleaching events could be needed.

CORAL REEF HAZARD

One of the major challenges facing science today was the response of ecosystems to global environmental change, and its retroaction on climate and human societies (Reynaud et al., 2003). The frequency, diversity and the rate at which humans were impacting coral reefs were increasing to the extent that reefs were threatened globally, throughout their geographical range (Hughes et al., 2003; Shepherd, 2003).

Assessments to late 2000 were that 27% of the world's reefs had been effectively lost, with the largest single cause being the massive climate-related coral bleaching event of 1998 (Almada-Villela et al., 2002). Coral reef ecosystems in the world had undergone a tremendous change due to environmental and anthropogenic factors. Though scientists did not yet know definitely what was causing the decline of some reefs (Dustan et al., 2001), factors known to contribute to this change include

over fishing and removal of grazers, use of destructive gear, bleaching (the loss of algal symbionts), storm damage, disease, increasing abundance of macro algae and pollution (Hoegh- Guldberg 1999, Rogers and Miller, 2006).

The link between increased greenhouse gases, climate change, and regional-scale bleaching of corals, considered dubious by many reef researchers only 10 to 20 years (Sheppard and Rioja-Nieto, 2005), was now incontrovertible. Moreover, future changes in ocean chemistry due to higher atmospheric carbon dioxide might cause weakening of coral skeletons and reduce the accretion of reefs, especially at higher latitudes (Hughes et al., 2003). It was predicted that coral reefs could suffer mounting stress associated with a global increase in atmospheric carbon dioxide over the coming decades (Mumby et al., 2001).

Coral bleaching was a very patchy phenomena (Wooldridge and Done, 2004). Often, bleached and unbleached corals were found in the same reef or next to each other (McClanahan, 2004). This provided evidence that temperature alone does not account for the bleaching patterns. The sources of this variation were poorly understood and had been variously attributed to extrinsic environmental patchiness e.g. temperature, light, turbulence, solar radiation, water flow, salinity, sediments as well as phenotypic and genetic differences among corals and their micro algal symbionts (Baker, 2001; Hughes et al., 2003). Average summer water temperatures differ enormously within the geographic boundaries of a typical coral species' range (Hughes et al., 2003). Wind speed, light, and clouds were all thought to influence bleaching intensity (Table 1). Satellite- derived SST had been widely used to identify the spatial extent of coral reef bleaching (Strong et al., 1997). However, to accurately monitor and predict coral bleaching, satellite observations of additional environmental

parameters such as wind, currents, cloud cover, and solar radiation were necessary as they could help to better relate environmental measurements.

Table 1 Summary of environmental factors alleged to cause/influence coral.

Variable	Field	Laboratory
Elevated sea water temperature	Glynn, (1993); Aronson et al., (2000); McClanahan and Maina, (2003); Sheppard, (2003); McClanahan et al., (2004); McClanahan et al., (2005)	Hoegh-Guldberg and Smith, (1989); Glynn and DŌCroz, (1990); Lesser et al., (1990); Fitt and Warner, (1995); Warner et al., (1996); Porter et al., (1999)
Decreased sea water temperature	Coles and Fadlallah, (1991); Kobluk and Lysenko, (1994)	Muscatine et al., (1991); Gates et al., (1992)
Solar radiation (including Ultraviolet radiation); and clouds	Fisk and Done, (1985); Gleason and Wellington, (1993); Brown et al., (1994); Gleason and Wellington, (1995); Mumby et al., (2001)	Hoegh-Guldberg and Smith, (1989); Lesser, (1989); Lesser and Shick, (1989); Lesser et al. (1990); Kinzie et al., (2001); Salih et al., (2000); Nakamura et al., (2005); Anderson et al., (2001)

Variable	Field	Laboratory
Combination of elevated temperature and solar radiation	Harriott, (1985); Brown and Suharsono, (1990); Williams and Bunkley-Williams, (1990); Glynn, (1993); Brown et al., (1995); Dunne and Brown, (2001); Brown et al., (2002)	Lesser et al., (1990); Glynn et al., (1992); Nakamura et al., (2005)
Water flow/current speed	McClanahan et al., (2005); Finelli et al., (2006)	Nakamura and van Woersk, (2001); Nakamura et al., (2003); Nakamura et al., (2005)
Reduced/increased salinity; river sediments	Fang et al., (1995); Obura, (1995); McClanahan and Obura, (1997)	Kushmaro et al., (1996); Porter et al., (1999); Kinzie et al., (2001)
Modelling approach; Water flow; Habitat; community; elevated temperature	Wooldridge and Done, (2004)	
temperature, wind speed, solar radiation and barometric pressure	Berkelmans, (2002)	

Source: modified and updated from Brown, 1996

BLEACHING MECHANISMS

It had been over two decades since the phenomenon of coral bleaching was first described (Brown, 1996). There was still however no simple explanation for the unusual increase in frequency and intensity of these events that had been occurring at a global scale (Huppert and Stone, 1998). Coral bleaching, defined as the loss of symbiotic dinoflagellates (zooxanthellae) from animals normally possessing them (Ware et al., 1996), was a response of tropical symbiotic corals and related cnidarians and molluscs to a variety of environmental stresses (Fitt et al., 2001).

Bleaching was the loss of algal symbionts (zooxanthellae) and/or their pigments from a coral (or other symbiotic animal) host, and occur in response to environmental stressors which vary regionally and seasonally, and which might act singly or synergistically (Fitt et al., 2001). The most apparent and globally documented of these was thermal stress. Corals and other zooxanthellate reef organisms occupy a restricted temperature range (approximately 18- 30°C). In the summertime, water temperatures surrounding reefs normally approach local maxima and/or the upper thermal tolerance limits of many species (Jokiel and Coles, 1990; Glynn, 1993; Hoegh-Guldberg, 1999). Sufficient and sustained positive temperature anomalies were deleterious to the coral-algal symbiosis, resulting in changes in photosynthesis reactions, production of damaging free oxygen radicals, and subsequent expulsion of the symbionts (reviewed by Hoegh-Guldberg, 1999). Prolonged bleaching results in coral mortality. For bleaching to occur in a particular area, thermal anomalies must exceed the local threshold, which lies between the highest locally-tolerated, non-bleaching temperature and the lowest temperature known to initiate bleaching in that area (Glynn, 1996; Brown, 1997). In general, Sea

Surface Temperatures (SSTs) $\geq 1^{\circ}\text{C}$ above local mean summer maximum temperatures, sustained over days or weeks, had been correlated with observed bleaching events (e.g. Jokiel and Coles, 1990; Podesta and Glynn, 1997; 2001).

Bleaching in the botanical sense usually refers to the destruction of photosynthetic pigments by photo-oxidative processes that could occur in both higher plants and algae (Venn et al., 2006). When corals were exposed to heat stress, the photosynthetic metabolism fails, a phenomenon generally known as photo inhibition. These conditions result in a decline in photochemical efficiency of symbiotic micro algae (zooxanthellae) which ultimately led to the expulsion of these symbionts.

Corals and their zooxanthellae were vulnerable to a variety of environmental stressors that could disrupt the symbiotic relationship (Reaser et al., 2000). If the stress was severe and prolonged, most of the corals on a reef might bleach, and many might die (Hughes et al., 2003). Competing hypotheses for the cause of coral bleaching include: nutrient enrichment, disease, increase in temperature, and excess light/ultraviolet exposure (Brown, 1996; Yentsch et al., 2002; Table 1). Of all these factors, SST had received the most attention (Ware et al., 1996), and had generally been considered as the primary stress which causes coral to bleach worldwide when their thermal tolerance was exceeded (Hoegh-Guldberg and Smith, 1989; Glynn and DeCroz, 1990; Hoegh-Guldberg 1999; Fitt et al., 2001; Liu, 2003; Jokiel, 2004; McClanahan et al., 2005).

CORAL AND CLIMATE CHANGE

Since 1979, there had been six major bleaching events, all of which were associated with period of exceptionally warm SSTs. The observed positive correlation

between rising global temperatures and the occurrence of the two strongest El Niño-Southern Oscillation (ENSO) events in this century leave little doubt that the unprecedented coral bleaching and mortality observed today was linked to climate change.

During the 1997-1998 ENSO, massive bleaching occurred along the entire length of the largest barrier reef in the Northern Hemisphere. Aronson et al. (2000) recently reported 100% mortality of once-abundant coral stands in the lagoon shoal reef habitat. To date, there had been no coral recovery at this site. A well-established sponge community had quickly overgrown the dead coral skeletons and was likely to prevent coral recruits from gaining a foothold in the foreseeable future. Reef cores retrieved from these sites revealed continuous coral growth as far back as 3000 years B.P. It appeared that massive coral mortality such as that observed in 2000 had not occurred in Belize over the past 3 millennia. Other evidence suggests that ENSOs occurred less frequently in the past. For example, a 400-year-long coral record collected at the "epicentre" of ENSO activity in the Galápagos Islands, indicates that in the mid-1600s, the frequency of ENSO progressively increased in a step-wise manner following the end of the Little Ice Age (Dunbar et al., 1994). In the mid-1600s, the recurrence interval was centred at one event every 6 years. By 1750, the frequency increased to 4.6 years and by the mid-1800s, the pace stepped up to one event every 3.4 years, close to the present rate. These data clearly indicate that the spacing of past ENSO intervals had not been driven by anthropogenic influences. However, we knew little about how fossil fuel burning since the beginning of the Industrial Era might have influenced the magnitude of the most recent ENSOs. The past two severe El Niño events set record-breaking global temperatures. In a recent

analysis by Karl et al. (2000), it had been noted that paleo-climate studies, extending back hundreds to thousands of years, indicate that the 20th century was warmer than any other period over the past 500 years or longer. Perhaps most alarming was that recent warming over the past couple of decades had already reached levels that were predicted to occur during the 21st century (Kattenberg et al., 1996).

Since 1982, coral reefs worldwide had been subjected to an increased frequency of the phenomenon known as coral bleaching. Bleaching involves the dramatic loss of pigmented, single-celled endosymbiotic algae that live within the gastrodermal cells of a coral host that depends on this relationship for survival. Prior to the 1980s, and as early as the 1920s when coral reef research intensified, localised bleaching events were reported and attributed to factors such as extremely low tides, hurricane damage, torrential rainstorms, freshwater runoff near reefs, or toxic algal blooms (Glynn, 1993). However, these early occurrences had recently been overshadowed by geographically larger and more frequent bleaching events whose impact had expanded to regional and global proportions. To underscore the problem, over 60 bleaching events were documented in the period 1979-1990, while there were only three events in 1876-1979 (Williams and Bunkley-Williams, 1990). A proximate explanation for the occurrence of these events points to meteorological extremes that intensify average summertime seawater temperatures, often in concert with increased penetration of ultraviolet radiation causing both thermal stress and photo-damage to coral tissues (Hoegh-Guldberg, 1999). A common condition in the timing of these events in the Northern Hemisphere had been the co-occurrence of ENSO events. However, during La Niña, when the northern sectors of the central and eastern Pacific were cooled, surface waters in the subtropical Southern Hemisphere could experience

above-average warming at such sites as Easter Island, the Cook Islands, Tahiti, and Fiji (Reynolds and Smith, 1994).

ENSO reflects a quasi-periodic reorganization in atmospheric and oceanic water masses leading to relaxation of the easterly trade winds with subsequent westerly wind bursts originating near the International Dateline. These changes, coupled with diminished upwelling, led to a weakening of the Pacific Cool Tongue and, under very severe ENSO conditions, its complete disappearance. During periods of La Niña, all of these ENSO conditions were reversed and sometimes elevated above average. However, a strong La Niña event in the Northern Hemisphere could result in extreme sea warming in area south of the equator. The most recent La Niña event, which began in August of 1998, had continued to persist into mid-2000 and had been ranked as one of the seven strongest La Nina events since 1949 (Wolter, 2000).

The last major occurrence of coral bleaching was in 1998, when corals bleached extensively as a result of elevated Sea surface temperatures, destroying about one- sixth of the world's coral colonies (Dennis, 2002). This event coincided with the largest ENSO on record (West and Salm, 2003). But the 2002, 2004 and 2005 bleaching was out of phase with El Niño, raising concerns that bleaching events were growing in frequency and intensity in response to climate change (Glynn, 1993; Dennis, 2002; McClanahan et al., 2005). This had stimulated research into modelling potential future scenarios of sea temperatures in reef regions e.g. Sheppard, 2003, Hoegh-Guldberg, 1999. Based on the temperature thresholds and a predicted recurrence of the El Niño events, Sheppard (2003) predicted that corals in the Western Indian Ocean's southern hemisphere could become ecologically extinct within the next 20 to 40 yrs. However, recent developments in Zooxanthellae genetics suggest

that resilience of coral reefs, through acclimation of the coral animal and the symbiotic algae might prevent extinction to occur (Sheppard, 2003; McClanahan et al., 2005). Andrea et al. (2006) observed that some species of bleached corals were able to adapt to bleaching state by increasing their feeding rates; suggesting that coral species with high Cnidarians feeding capability during bleaching and recovery, could be more resilient to bleaching events over the long term and might help to safeguard affected reefs from potential local and global extinction (Andrea et al., 2006).

Published projections of a baseline of increasing ocean temperature resulting from global warming had suggested that annual temperature maxima within 30 years might be at levels that could cause frequent coral bleaching and widespread mortality leading to decline of corals as dominant organisms on reefs (Coles and Brown, 2003; Hughes et al., 2003). However, these projections had not considered the high variability in bleaching response that occurs among corals both within and among species (Coles and Brown, 2003). The ‘adaptive bleaching hypotheses’ as described by Buddemeier and Fautin, 1993; Ware et al., 1996; Kinzie et al., 2001; stipulates that with coral bleaching, corals first lose their dinoflagellate symbionts and then regain a new mix of symbionts that were better suited to the imposed stress regime. It was formulated explicitly to account for the varied observations and experiments on bleaching (Ware et al., 1996). Several studies had carried on the debate through field and lab experiments. Baker, (2001) through molecular studies of corals noted that bleaching offers an ecological opportunity for reef corals to rid themselves rapidly of suboptimal algae and to acquire new partners. This inferred that bleaching might sometimes help reef corals to survive environmental change (Baker, 2001; Hoegh-Guldberg et al., 2002). In support of the adaptive bleaching hypotheses was the long-

term data sets on mass coral bleaching and mortality, which reveals that far fewer corals in the far-eastern Pacific Ocean died after the 1997–98 El Niño event (0–26%) than after the 1982–83 El Niño event (52–97%) even though the magnitude and duration of sea-surface temperature anomalies in the region in 1997–98 exceeded those of 1982–83 (Baker, 2001; Glynn et al., 2001). McClanahan et al. (2004) analysed the frequency of four possible responses to anomalous warm water (not bleach and live; not bleach and die; bleach and live; bleach and die). He observed similar frequencies for the taxa that bleached and died, and those that bleached and lived. To support the adaptive bleaching hypotheses based on his study, the frequency of survival after bleaching should be high than those that beached and died (McClanahan, 2004).

Current severe, thermally-driven disturbances to coral reefs worldwide did not bode well for the future health of this ecosystem, particularly if genetic responses were unable to keep pace with an increasing frequency and/or magnitude of ENSO/La Niña activity.

CORAL COMMUNITY RECOVERY

It was imperative that historical environmental conditions did shape the community structure of the population and their response to disturbances. The challenge for coral reef researchers and managers was to identify specific locations with environmental conditions that enhance the coral community resilience, i.e. resistance to heat stress, survival during bleaching, and reef recovery after bleaching-related mortality (Obura, 2005; Marshall and Schuttenberg, 2006). Coral resistance to heat stress; their tolerance to disturbances, and potential to recover from large scale

disturbances were determined by the ecosystem conditions; biological diversity; connectivity between areas; and the local environmental conditions (Marshall and Schuttenberg, 2005; 2006).

From the perspective of modelling resilience, biological diversity and ecological conditions could be represented by estimates of species richness, coral abundance and the management status of a reef system. Connectivity or location of an area with respect to the 'transport network' of the larvae could be estimated using the current vectors and the network of marine protected areas (Cowen et al., 2000; Cowen et al., 2006; Dawson et al., 2006; Roberts, 2006). West and Salm (2003) in their review compiled environmental factors which were likely correlates of resistance and resilience to coral bleaching. These factors included cloud cover, temperature variability, turbidity, absorption, wind, high wave energy, upwelling and adjacent to deep water. They listed broad size and species distributions and history of corals surviving bleaching events as indirect indicators of bleaching tolerance.

MODELLING OF CORAL REEF SYSTEMS

A modest number of studies had attempted to model coral reef processes including coral bleaching using different approaches: e.g. Sheppard, 2003; Langmead and Sheppard, 2004; Wooldridge and Done, 2004; Sheppard and Rioja-Nieto, 2005.

The modelling of coral reef ecological processes, like in many ecosystem modelling was complicated by the imprecise nature of ecological interrelationships, and the subjectivity inherent in the judgments by field observers (Bosserman and Ragade, 1982; Silvert, 1997). Traditional models of reef processes often require unavailable data and precision (Meesters et al., 1998). Frequently important

observations were lacking, and potentially valuable information might be non quantitative in nature (Silvert, 1997). This might limit the success and usefulness of these models.

Fuzzy set theory, first introduced by Zadeh (1965) offers a methodology for dealing with these problems, and provides an alternative approach to modelling highly complex systems. It was an extension of classical set theory where elements of a set had grades of membership ranging from zero for non-membership to one for full membership. A fuzzy set was a collection of paired numbers that consist of members and degrees of support or the level of confidence for those numbers (Juang et al., 1992). In classical set theory, every element could be classified as to whether or not it belongs to a particular set.

In considering the modelling of coral reef resilience, defining strong resilience of a reef system in terms of crisp sets for attributes presumes the ecosystem manager could make a sharp, unambiguous distinction between an ecosystem that was strongly resilient and one that was not by comparing measured attributes to resilience thresholds for those attributes. A crisp set was a set in which all members match the class concept and the class boundaries were sharp, and allow only binary membership functions (Burrough and McDonnell, 2005). However, fuzzy set theory deals with situations where membership in a set was unclear and allows for this division to be removed. Instead, the uncertainty of the boundary between these regions, and the measurements on which they were based, could be modelled (Burrough and McDonnell, 2005; Malins and Metternicht, 2006). The boundaries or control points of a membership function for some fuzzy set A were defined as the region of the universe containing elements that had non zero membership function but not complete

membership (Ross, 2004; Burrough and McDonnell, 2005). The control points along the x-axis bound the elements of the universe with some degree of fuzziness, or only partial membership in fuzzy set A in the form $0 < \mu_A(x) < 1$ (Ross, 2004). Fuzzy modelling provides a framework which allows a greater ability to make decisions about ecosystems and to develop ecosystem concepts (Bosserman and Ragade, 1982).

In literature, application studies of fuzzy logic concept to modelling coral reef processes include the work of Meesters et al., 1996. They constructed a coral reef model that predicts changes in coral cover and diversity under anthropogenic stress. Hendee et al., 1998 constructed an expert system application, termed the coral reefs early warning system (CREWS) to identify oceanographic conditions conducive to coral bleaching. This application was programmed to send bleaching alerts in fuzzy terms when the real time input oceanography data was favourable for bleaching (Hendee et al., 1998). CREWS used SST, wind speed, and photosynthetically available radiation as input parameters.

SST DATA TO PREDICT CORAL REEF BLEACHING

A weather satellite was a type of satellite that was primarily used to monitor the weather and climate of the Earth. These meteorological satellites, however, saw more than clouds and cloud systems. City lights, fires, effects of pollution, auroras, sand and dust storms, snow cover, ice mapping, boundaries of ocean currents, energy flows, and etc., were other types of environmental information collected using weather satellites. In the last year, meteorological data such as rainfall estimation based on remote sensors in the visible (VIS), infrared (IR) radar, and microwave (MW) ranges of the spectrum, had been carried out on board several launched

platforms. In particular, the launch of the newest generation of geostationary satellites, the Geostationary Operational Environmental Satellite GOES-I-M series (Menzel and Purdom, 1994) and the newest METEOSAT Second Generation (MSG) (Schmetz et al., 2002) with its Spinning Enhanced Visible and Infrared Imager (SEVIRI), adds new channels to the traditional VIS-IR-WV (Water vapour) triplet. Some of the new channels had been tested for decades as part of the AVHRR series on board the NOAA polar orbits or had other heritages (Levizzani and Amorati, 2002). One of the satellite data that nowadays was becoming an object of interest by the scientific community was the GMS satellite imagery.

GMS weather imagery and quantitative sounding data was a continuous and reliable stream of environmental information used to support weather forecasting, severe storm tracking, and meteorological research theoretically. GMS collects and distributes weather data to other Asia Pacific countries and contributes to weather forecast services in countries from Australia northward to China, including Japan, Burma, Indonesia, Korea, Laos, Malaysia, Mongolia, New Zealand, the Philippines, Taiwan, Thailand, Tibet, and Vietnam (Space Systems/Loral, 2007).

Satellites did not measure temperature as such. They measured radiances in various wavelength bands, which must then be mathematically inverted to obtain indirect inferences of temperature (Uddstrom, 1998; National Academy of Sciences, 2000). The resulting temperature profiles depend on details of the methods that were used to obtain temperatures from radiances. As a result, different groups that had analysed the satellite data to calculate temperature trends had obtained a range of values.

Since 1972, SSTs from satellite data were produced by NOAA (Figure 1). Monitoring of SST from Earth-orbiting infrared radiometers had a wide impact on oceanographic science. Currently, one of the principal sources of infrared data for SST measurement was from the Advanced Very High Resolution Radiometer (AVHRR) carried on NOAA's Polar Orbiting Environmental Satellites (POES), beginning in 1978. AVHRR was a broad-band, four or five channel (depending on the model) scanner, sensing in the visible, near-infrared, and thermal infrared portions of the electromagnetic spectrum. The POES satellite system offers the advantage of daily global coverage, by making near-polar orbits roughly 14.1 times daily. In-situ SSTs, from buoys (drifting and moored) were used operationally to maintain accuracy removing any biases, and compiling statistics with time (McClain et al., 1985; Strong, 1991; Strong et al., 2000).

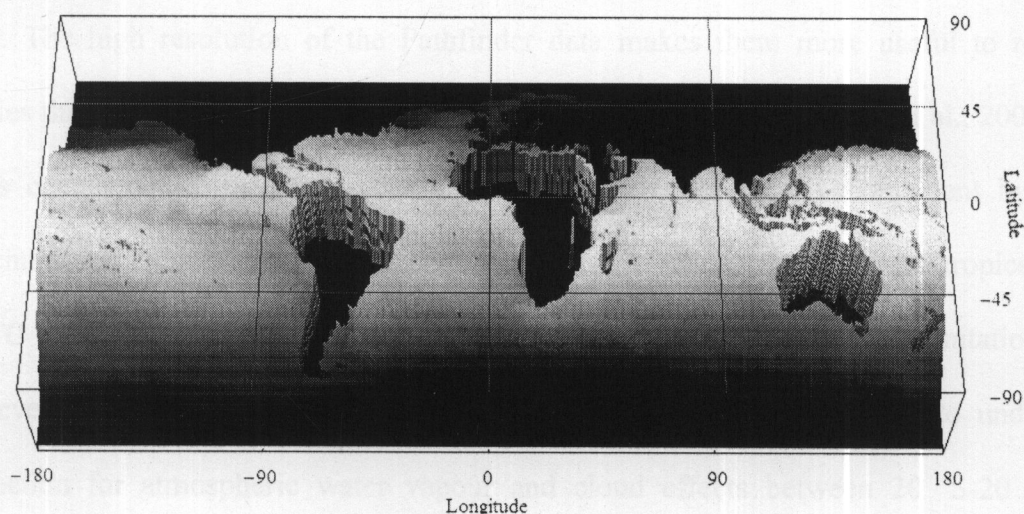


Figure 1 World NOAA SSTs data.

Goreau and Hayes (1994) first mapped HotSpot anomalies in retrospect using monthly SSTs. In 1997, NOAA initiated twice-weekly, global HotSpot anomaly mapping at 50km resolution. HotSpot thresholds were based on a satellite-only maximum monthly mean (MMM) climatology (MCSST, 1984-1993) computed from nighttime's SSTs (Strong et al., 1997). Mapped HotSpots (particularly those exceeding the MMMs by 1°C) predicted areas of thermally-induced bleaching worldwide during the 1997-1998 El Niño.

Recently, Toscano et al. (in press) revised the MMM climatology and improved HotSpot mapping resolution and accuracy using 9 km NOAA/NASA Oceans Pathfinder SST data (Kearns et al., 2000; Kilpatrick et al., 2001), a recalibrated AVHRR dataset derived from the Pathfinder version of the non-linear SST (NLSST) algorithm, spanning 17 years (1985-2001). Pathfinder data provided long time series of cloud-cleared temperatures that were internally consistent over time. The high resolution of the Pathfinder data makes them more useful to reef studies than operational 1° or 0.5° data (e.g. Davies et al., 1997; Mumby et al., 2001). SSTs calculated by the Pathfinder algorithm were calibrated by coincident buoy matchups and exhibit small biases, both globally ($+0.1\text{ °C} \pm 0.5$) and in the tropics (-0.1 °C to -0.2 °C). The Pathfinder algorithm was not without potential limitations, however. In the tropics, the algorithm slightly under-predicts SSTs due to under-correction for atmospheric water vapour and cloud effects between 20 °S-20 °N (Kilpatrick et al., 2001). Additionally, the global Pathfinder algorithm might not account for region-specific deviations, and might discard certain useable data via cloud clearing routines and specific temperature thresholds in quality testing. Also, the 9km resolution might still be too coarse to pinpoint conditions in small reef sites,

and a coarse (pre-processing) land mask had effectively eliminated SSTs from numerous pixels in coastal zones and near reefs between 1985 and 1998 (Kilpatrick, Halliwell, and Kearns, pers. comm.). In these cases neighbouring pixels obtained by retrieving SSTs from a 9-pixel grid centred on the desired location were used. While only small differences were seen between SSTs from a single target pixel and the 3x3 pixel grid, the averaging of data from 9 (or fewer) pixels further reduces the record of actual variability in the reef environment.

Because of these potential limitations and the fact that the Pathfinder algorithm was designed to minimise global biases and might have had larger regional errors, Pathfinder SSTs were tested against available in situ records at specific reef locations to verify their applicability in the highly variable coastal zones. If Pathfinder SSTs were highly correlated to the field data from these monitored localities, and exhibit minimal SST-in situ differences, they could be an invaluable resource for studying the temperature histories of reefs in remote or otherwise un-monitored regions, and provided longer-term temperature histories for areas with short-term in situ monitoring. Correlated time series of in situ and Pathfinder SSTs from 1985-2001 were examined along with high-resolution HotSpot thresholds for field sites from 9-km Pathfinder data (average of daytime and nighttime maximum pentad mean (MPM) climatological SSTs over the 9-yr baseline period 1985-1993; Casey and Toscano in prep.). Bleaching thresholds were set at 1 °C above the local MPM value, which represents the local mean summer maximum temperature. MPM values and bleaching thresholds might be used to calculate the magnitude of thermal anomalies and their rate of change in association with occurrence and severity of bleaching.

APPLICATIONS OF IMAGE PROCESSING TECHNIQUE

The likelihood ratio edge detector was used for the segmentation of SAR images. The edge position estimate was biased toward the darker region. This technique could be used to improve the accuracy of edge estimation and the statistical active contour. The combinations of two methods achieve accurate regularised edge location (Germain and Réfrégier, 2001).

Kitamoto and Ono (2001) enhance the quality of typhoon imagery over Southeast Asia in an attempt to minimise typhoon damage. Satellite data from two types of satellites (geostationary satellite and polar orbiting satellite) were combined and created a comprehensive collection of high quality typhoon imagery. Data mining methods had been applied to the analysis and prediction of typhoons by using typhoon image collection from GMS-5 (Kitamoto, 2001). The analysis was applied various methods such as principal component analysis and self-organising mapping to characterise or visualise the statistical properties of typhoon cloud patterns. An instance-based learning method was applied for analogy-based prediction using past similar patterns, and also established similarity-based image retrieval system for the typhoon image collection. He also points out that we should not overlook the fundamental difficulty in typhoon prediction due to the chaotic nature of the atmosphere.

Lin et al. (1997) describe methods of approximating images with polygons when many scales were present. With one technique, smoothing of image boundaries was achieved by an iterative method. Shapes were reduced to curvature extreme, which serve as vertices of reconstruction polygons. The ratio of the arc length along the boundary to the total length of the segments measured the goodness of fit. A

Gaussian filter was applied and a curvature function was defined by the first and second derivatives of points along the feature boundary. The width of the filter was proportional to the square root of the distance between vertices. Iterations continue until the number of extremes stabilises. A second proposed method represents features according to specified compression ratios. Iterations continue until a desired compression ratio (i.e. the number of peaks) was attained. If the number of vertices exceeds the specified number, more smoothing was done to obtain a more compact representation.

Han et al. (1997) used an application of a Kalman filter to derive water vapour profiles from Raman lidar, a microwave radiometer, an acoustic sounding system, and surface observations. Microwave radiometers provide integrated water contents but lack structural information. Hence, the approach was to combine the measurements based on the relative strengths of the sensors. As a first step, a Kalman filter was applied to a time history of the lidar data. Then a statistical analysis was done to combine the lidar and microwave data by climatological information. In the second step, the profile of estimated water vapour from the filter was mapped with the integrated water vapour and cloud liquid. The profile structure was largely determined from the lidar data and the climatological information. Limited verification accomplished by withholding a portion of the lidar data showed considerable skill.

STUDY SITES

Water vapour satellite image was covered at latitude -5°S to 45°N and longitude 90°E to 150°E . We used 2-min (1 min of latitude = 1 nautical mile, or

approximately 1.852 km) resolution terrain and topography data (NGDC, 2007) to generate coastal contour lines for Southeast Asia (Figure 2).

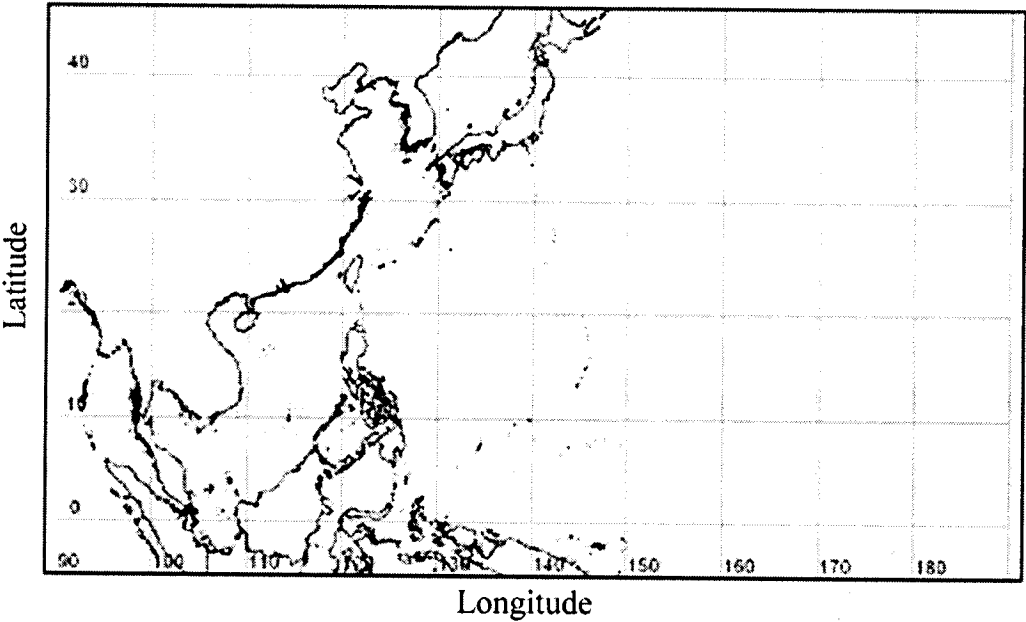


Figure 2 Coastal contour lines of Southeast Asia.

Thailand was located in the northern part of Indochina and situated in the Southeast Asia mainland. It covered an area of 513,115 km² between latitude 6°-21 °N and longitude 98°-105 °E. Thailand had coastal lines of approximately 1,840 km on the Gulf of Thailand and 861 km along the Andaman Sea. Khanom-Mu Koh Talae Tai Marine National Park was coral study site area. It was located in Nakhon Si Thammarat province, Thailand (Figure 3).

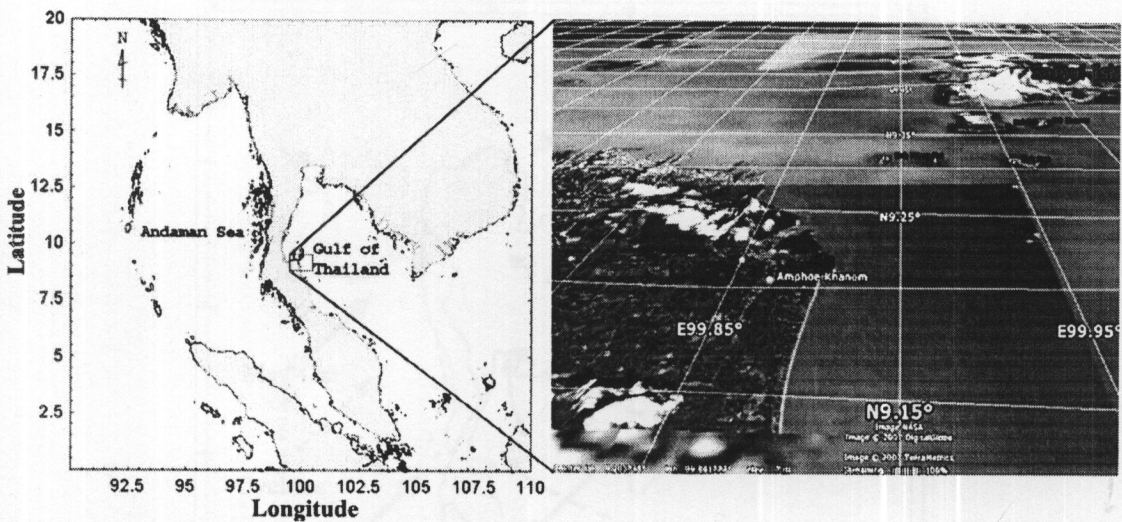


Figure 3 Thailand coastal line (left) and Khanom-Mu Koh Talae Tai Marine National Park (right).

In the topography, Thailand was geographically divided into four regions: the North, the Central or the Chao Phraya River Basin, the Northeast or the Korat Plateau and the South or the Southern Peninsula. The northern region was mountainous area prone to flood, earthquake, and landslide. The northeast region was arid area on the Korat Plateau, frequently faces sudden flood during rainy season, severe draught and cold during hot and cold seasons. The central region was the fertile area but this area often inundates during rainy season. The Southern region was hilly to mountainous and several offshore islands. The severe disasters in these regions were occasional floods, tropical storms, landslides and forest fire.

Thailand composed of two tropical monsoons: Northeast and Southwest monsoons. Northeast monsoon prevails in November to February. Southwest monsoon prevails in May to September. There were two transition periods between the opposing monsoon winds as depicted in the Figure 4.

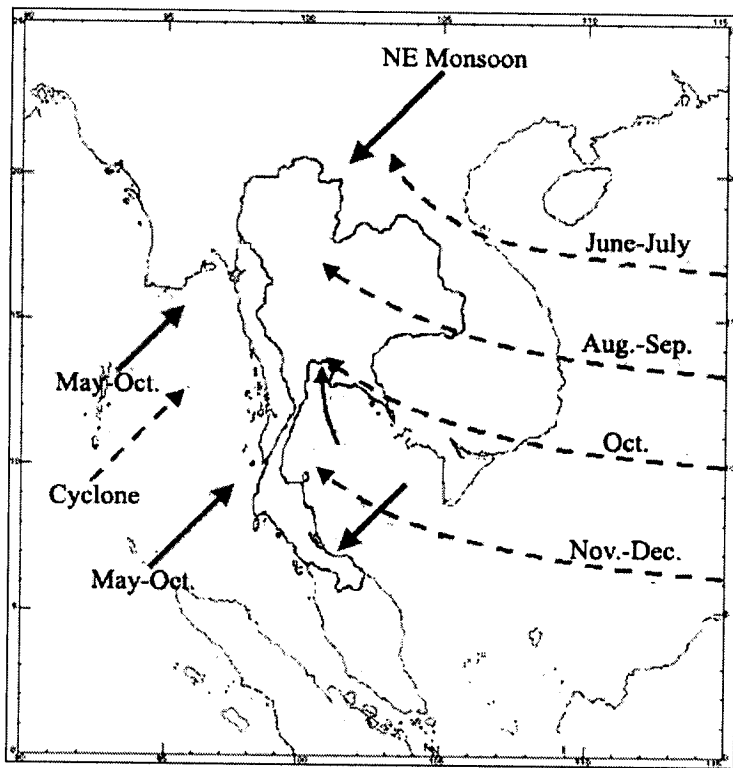


Figure 4 The prevailing wind of the Gulf of Thailand; red, green, blue and purple arrows represent Northeast monsoon, Southwest monsoon, Tropical storm and Southern wind, respectively.

Source: http://www.tmd.go.th/knowledge/image_know/season_03.jpg

Every summer, Southern Asia and especially India, was drenched by rains that come from moist air masses that move in from the Indian Ocean to the south. These rains and the air masses that bring them were known as monsoons. However, the term monsoon refers not only to the summer rains but to the entire cycle that consists of both summer moist onshore winds and rain from the south as well as the offshore dry winter winds that blow from the continent to the Indian Ocean.

In the summer, a high-pressure area lies over the Indian Ocean while a low exists over the Asian continent. The air masses move from the high pressure over the ocean to the low over the continent, bringing moisture-laden air to South Asia.

During winter, the process was reversed and a low sits over the Indian Ocean while a high lies over the Tibetan plateau so air flows down the Himalaya and south to the ocean. The migration of trade winds contributes to the monsoons.

The seasonal distribution of rainfall was closely related to the monsoons. Rainfall intensity could be high, producing a rapid rate of runoff and serious flooding. According to a general annual rainfall pattern, most areas of the country receive 1,200 - 1,600 mm a year. Some areas on the windward side, particularly Trat province in the Eastern Part and Ranong province in the Southern Thailand West Coast had more than 4,000 mm a year. Annual rainfall less than 1,200 mm occurs in the leeward side areas, which were clearly seen in the central valleys and the uppermost portion of the Southern Part. Approximately 70 percent of the rainfall was occurring during the main rainy season from May to September/October. The uneven distribution of rainfall was one of the main causes of flooding.

Table 2 Averaged seasonal rainfall (mm) in various parts of Thailand based on 1971-2000 period.

Seasonal rainfall (mm) in various parts of Thailand				
Region	Winter	Summer	Rainy	Annual rainy days
North	105.5	182.5	952.1	123
Northeast	71.9	214.2	1,085.8	117
Central	124.4	187.1	903.3	113
East	187.9	250.9	1,417.6	131
South				
-East Coast	759.3	249.6	707.3	148
-West Coast	445.9	383.7	1,895.7	176

Source: http://www.tmd.go.th/climate/climate_04.html

REFERENCES

- Aronson R. B., Precht W. F., McIntyre I. and Murdoch T. J. T. (2000). Coral bleaching out in Belize. *Nature*, 405, 36.
- Brown B. E. (1997). Coral Bleaching: Causes and Consequences. *Coral Reefs*, 16, 129-138.
- Casey K. S. and Toscano M. A. (in press). Satellite Observation of Thermal Stress in Coral Reefs. *Coral Reefs*, submitted for publication.
- Davies J. M., Dunne R. P. and Brown B. E. (1997). Coral Bleaching and Elevated Sea Water Temperature in Milne Bay Province, Papua New Guinea, 1996. *Marine and Freshwater Research*, 48, 513-516.
- Dunbar D. B., Wellington G. M., Colgan M. W. and Glynn P. W. (1994). Eastern Pacific sea surface temperature since 1600 A.D.: the $\delta^{18}\text{O}$ record of climate variability in Galapagos corals. *Paleoceanography*, 9, 291-315.
- Fitt W. K., Brown B. E., Warner M. E. and Dunne R. P. (2001). Coral Bleaching: Interpretation of Thermal Tolerance Limits and Thermal Thresholds in Tropical Corals. *Coral Reefs*, 20, 51-56.
- Germain O. and Re'fre'gier P. (2001). Edge location in SAR images: Performance of the likelihood ratio filter and accuracy improvement with an active contour approach. *IEEE Transactions on Image Processing*, 10, 72-78.
- Glynn P. W. (1993). Coral Reef Bleaching: Ecological Perspectives. *Coral Reefs*, 12, 1-17.
- Glynn P. W. (1996). Coral Reef Bleaching: Facts, Hypotheses and Implications. *Global Change Biology*, 2, 495-509.

- Goreau T. J. and Hayes R. L. (1994). Coral Bleaching and Ocean Hot Spots. *Ambio*, 23, 176-180.
- Han Y., Westwater E. R. and Ferrare R. A. (1997). Applications of Kalman filtering to derive water vapour profiles from Raman lidar and microwave radiometers. *Journal of Atmosphere and Oceanic Technology*, 14, 480-487.
- Hoegh-Guldberg O. (1999). Climate Change, Coral Bleaching and the Future of the World's Coral Reefs. *Marine Freshwater Resources*, 50, 839-866.
- Jokiel P. L. and Coles S. L. (1990). Response of Hawaiian and Other Indo-Pacific Reef Corals to Elevated Temperature. *Coral Reefs*, 8, 155-162.
- Karl T. R., Knight R. W. and Baker B. (2000). The record-breaking global temperatures of 1997 and 1998: Evidence for an increase in the rate of global warming? *Geophysical Research Letters*, 27, 719-722.
- Kattenberg A., Giorgi F. G., Meehl H. G. A., Mitchell J. F. B., Stouffer R. J., Tokioka T., Weaver A. J. and Mitchell T. M. L. (1996). Climate models, projections of future climate, in Climate Models, 1995. *The Science of Climate Change, contribution of WGI to the Second Assessment Report of the Intergovernmental Panel on Climate Change*, Houghton J. T. et al., (Editors), Cambridge University Press, Cambridge, UK, pp. 285-357.
- Kearns E. J., Hanafin J. A., Evans R. H., Minnett P. J. and Brown O. B. (2000). An Independent Assessment of Pathfinder AVHRR Sea Surface Temperature Accuracy Using the Marine Atmosphere Emitted Radiance Interferometer. *Bulletin of the American Meteorological Society*, 81, 1525-1536.
- Kilpatrick K. A., Podesta G. and Evans R. (2001). Overview of the NOAA/NASA Advanced Very High Resolution Radiometer Pathfinder Algorithm for Sea

Surface Temperature and Associated Matchup Database. *Journal of Geophysical Research*, 106, 9179-9197.

Kitamoto A. (2001). Data Mining for Typhoon Image Collection. Second International Workshop on Multimedia Data Mining (MDM/KDD'2001). *Proceedings of the 2nd International Workshop on Multimedia Data Mining*, San Francisco, USA, 26th, August.

Kitamoto A. and Ono K. (2001). The collection of typhoon image data and the establishment of typhoon information databases under international research collaboration between Japan and Thailand. *National Institute of Informatics Journal*, 2, 15-25.

Levizzani V., Amorati R. and Meneguzzo F. (2002). A review of satellite-based rainfall estimation methods. *European Commission Project MUSIC Report (EVK1-CT-2000-00058)*, 66.

Lin H. C., Wang L. L. and Yang S. N. (1997). Fast heuristics for polygonal approximation of a 2D shape boundary. *Signal Processing*, 60, 235-241.

McClain E. P., Pichel W. G. and Walton C. C. (1985). Comparative performance of AVHRR-based multichannel sea surface temperatures. *Journal Geophysical Research*, 90(C6), 11587-11601.

Menzel W. P. and Purdom J. F. W. (1994). Introducing GOES-I, The First of a New Generation of Geostationary Operation Environmental Satellites. *Bulletin of the American Meteorological Society*, 75, 757-782.

Mumby P. J, Chisholm J. R. M., Edwards A. J., Clark C. D., Roark E. B., Andrefouet S. and Jaubert J. (2001). Unprecedented Bleaching Induced Mortality in

Porites spp. at Rangiroa Atoll, French Polynesia. *Marine Biology*, 139, 183-187.

National Academy of Sciences (2000). Issues in the Integration of Research and Operational Satellite Systems for Climate Research: Part I. *Science and Design*, Space Studies Board, National Research Council 2101 Constitution Avenue, NW Washington, DC 20418, 152.

NGDC (2007). Marine Geology and Geophysics Surface of the Earth (ETOPO2v2) 2 minute colour relief images. Retrieved 12 March 2007 from <http://www.ngdc.noaa.gov/mgg/image/2minrelief.html>.

Podesta G. P. and Glynn P. W. (1997). Sea Surface Temperature Variability in Panamá and Galápagos: Extreme Temperatures Causing Coral Bleaching. *Journal of Geophysical Research*, 102, 15749-15759.

Podesta G. P. and Glynn P. W. (2001). The 1997-98 El Niño Event in Panamá and Galápagos: an Update of Thermal Stress Indices Relative to Coral Bleaching. *Bulletin of Marine Science*, 69, 43-59.

Reynolds R. and Smith T. (1994). Improved global sea surface temperature analysis using optimum interpolation. *Journal of Climate*, 7, 929-948.

Schmetz J., Pili P., Tjemkes S., Just D., Kerkmann J., Rota S. and Ratier A. (2002). An Introduction to Meteosat Second Generation (MSG). *Bulletin of the American Meteorological Society*, 83, 977-992.

Strong A. E., Barrientos C. S., Duda C. and Sapper J. (1997). Improved Satellite Techniques for Monitoring Coral Reef Bleaching. *Proceedings, 8th International Coral Reef Symposium*, 2, 1495-1498.

- Strong A. E. (1991). Sea surface temperature signals from space. *Encyclopedia of Earth System Science*, Nierenberg W. A. (Editor), Academic Press, San Diego, CA, 4, 69-80.
- Strong A. E. and McClain E. P. (1984). Improved ocean surface temperature from space-comparisons with drifting buoys. *Bulletin of the American Meteorological Society*, 65(2), 138-142.
- Strong A. E., Kearns E. and Gjovig K. K. (2000). Sea Surface Temperature Signals from Satellites - An Update. *Geophysical Research Letters*, 27(11), 1667-1670.
- Toscano M. A., Liu G., Guch I. C., Casey K. S., Strong A. E. and Meyer J. E. (in press). Improved Prediction of Coral Bleaching Using High-Resolution Hotspot Anomaly Mapping. *Proceedings of the 9th International Coral Reef Symposium*, Bali, Indonesia, submitted for publication.
- Tun K., Loke M. C., Cabanban A., Vo S. T., Philreefs Y. T., Suharsono S. K. and Lane D. (2004). Status of coral reefs, coral reef monitoring and management in Southeast Asia, 2004, Status of Coral Reefs of the World: 2004. *Australian Institute of Marine Science*, Townsville, Queensland PMB No 3, Townsville MC Qld 4810.
- Uddstrom M. J. (1998). Retrieval of Atmospheric Profiles from Satellite Radiance Data by Typical Shape Function Maximum a Posteriori Simultaneous Retrieval Estimators. *Journal of Applied Meteorology*, 27(5), 515-549.
- Water Vapour Map. (2007). Index of /archdat/pacific/western/tropics/vapour. Retrieved 12 March 2007 from <http://www.nrlmry.navy.mil/archdat/pacific/western/tropics/vapour>.

- Wilkinson C. (2004). Status of Coral Reefs of the World: 2004. *Australian Institute of Marine Science*, Townsville, Queensland PMB No 3, Townsville MC Qld 4810.
- Williams E. H. Jr. and Bunkley-Williams L. (1990). The world-wide coral reef bleaching cycle and related sources of mortality. *Atoll Research Bulletin*, 33, 1-71.
- Wooldridge S. and Done T. J. (2004). Learning to predict large-scale coral bleaching from past events: A Bayesian approach using remotely sensed data, in-situ data, and environmental proxies. *Coral Reefs*, 23, 96–108.

CHAPTER II

COMPARING TWO ESTIMATING TECHNIQUES ON CORAL GROWTH FORMS USING RANDOM AND QUADRAT SAMPLING TECHNIQUES

PUBLICATION (ORAL PRESENTATION)

Chairote Yaiprasert, Suntorn Surabun, Siriwan Wongkoon, Mullica Jaroensutasinee, and Krisanadej Jaroensutasinee, 2007. Comparing two estimating techniques on coral growth forms using random and quadrat sampling techniques. *The 33rd Congress on Science and Technology of Thailand*, Nakhon Si Thammarat, Thailand. 18-20th October, pp. 125-126.

ABSTRACT

This study aimed at estimating coral growth forms at Khanom - Mu Koh Talae Tai Marine National Park. Two techniques were used to estimate coral growth forms: random and quadrat sampling techniques. Researcher took coral photographs with a digital camera and underwater casing. Coral images were classified into one of seven coral forms and used these percentages to calculate coral biodiversity indices (i.e. Shannon-Wiener index and Simpson index). The biodiversity indices did not differ between two techniques.

Keywords: Coral, Biodiversity index, Shannon-Wiener index, Simpson index, Sea Surface Temperature

INTRODUCTION

Coral reefs were ecosystems of high biodiversity which having the greatest number of species of any marine ecosystem. Unfortunately, the condition of many of the world's coral reefs had reached a crisis point. In addition to the general trend toward reef degradation had addressed the question of acute problems, and had estimated that as much as 10 % of the global reef area had been degraded beyond recovery, with another 30% predicted to collapse within the next 10-20 years (Knowlton, 2001; Wilkinson, 2002; 2004). The reefs at greatest risk were those in Southeast, East and South Asia, East Africa, and the Caribbean. Coral bleaching worldwide including Thailand was largely related to the warming of sea water (Bryant et al., 1989; Burke et al., 2002; Wilkinson, 2002; 2004).

The world was facing a global biodiversity crisis (Novacek and Cleland, 2001; Bellwood et al., 2004). The rapid loss of marine and terrestrial biodiversity had prompted efforts to catalogue this biodiversity, such as the census of marine life and the all species foundation, the goal of the latter being to catalogue all the biodiversity on the Earth within the next 25 years (Wilson, 2003). The challenges facing such efforts were great in that a small fraction of the existing biodiversity was presently described (May, 1988; Wilson, 2003). Compounding this problem was the well-documented decline in number of taxonomists (Buyck, 1999; Hopkins and Freckleton, 2002) and funding for taxonomy resulting in both insufficient funding and personnel to pursue this vast taxonomic undertaking (Wilson, 2003).

The coral reefs of Indo–West Pacific were the world's most diverse (Roberts et al., 2002) and most threatened (Burke et al., 2002). However, data from many taxonomic groups suggest that the biodiversity of this region was underestimated (e.g.

Barber et al., 2002; Paulay and Meyer, 2002; Meyer, 2003). Thorough documentation of marine biodiversity in this region was difficult because the size of this region and complexity of the habitat.

By any measure, coral reefs were among the most diverse and valuable ecosystems on earth. Coral reefs occur in over 100 countries, most of them developing countries without the capacity or financial resources to adequately manage these vital resources. Reefs support at least a million described species of animals and plants, and another 8 million coral reef species were estimated to be as yet undiscovered. According to one estimate, coral reefs provided goods and services worth in each year - a staggering figure for an ecosystem which covers less than one percent of the earth's surface. Reef systems provided economic and environmental services to millions of people as shoreline protection from waves and storms, as places for recreation and tourism, and as sources of food, pharmaceuticals, livelihoods, and revenues.

In developing countries, coral reefs contribute about one-quarter of the total fish catch, providing food to an estimated one billion people in Asia alone. Globally, half a billion people were estimated to live within 100 km of a coral reef and benefit from its production and protection. In light of expected climate change and associated sea level rises, coral reefs could offer a natural, self-building and self-repairing breakwater against wave and storm damage. These extremely valuable ecosystems constitute the economic base and future hope for sustained development in many countries, particularly small island nations.

This study was a part of long term coral reef monitoring project. This study aimed at comparing two techniques that commonly used in coral reef studies. To

estimate seven coral reefs growth forms using random and quadrat sampling techniques at three locations. These percentages of coral growth forms were used to estimate coral biodiversity.

MATERIALS AND METHODS

This study was undertaken at three locations: Koh Tan (S1), Koh Mud Soom (S2) and Ao Tong Yee (S3) located at Khanom - Mu Koh Talae Tai Marine National Park, Nakhon Si Thammarat, Thailand (Figure 5).

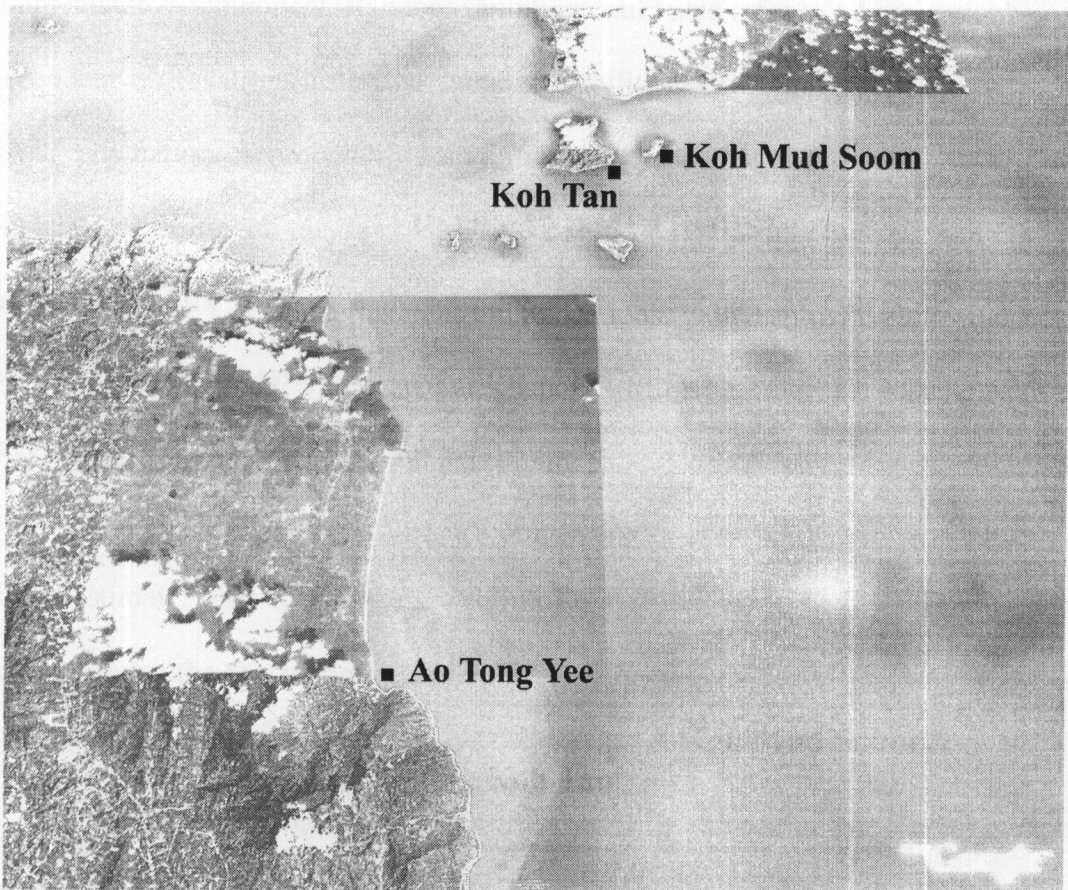


Figure 5 Three study sites at Khanom - Mu Koh Talae Tai Marine National Park, Nakhon Si Thammarat, Thailand: Koh Tan, Koh Mud Soom and Ao Tong Yee.

Two techniques were used to estimate coral growth forms: random and quadrat sampling techniques. Sampling was that part of statistical practice concerned with the selection of individual observations intended to yield some knowledge about a population of concern, especially for the purposes of statistical inference. Each observation measures one or more properties of an observable entity enumerated to distinguish objects or individuals. Results from probability theory and statistical theory were employed to guide practice. A sample was a subject chosen from a population for investigation. A random sample was one chosen by a method involving an unpredictable component. Random sampling could also refer to taking a number of independent observations from the same probability distribution, without involving any real population. A probability sample was one in which each item had a known probability of being in the sample. The sample could usually not be completely representative of the population from which it was drawn that random variation in the results was known as sampling error. In the case of random samples, mathematical theory was available to assess the sampling error. Thus, estimates obtained from random samples could be accompanied by measures of the uncertainty associated with the estimate. This could take the form of a standard error, or if the sample was large enough for the central limit theorem to take effect, confidence intervals might be calculated.

In random sampling, also known as probability sampling, every combination of items from the frame, or stratum, had a known probability of occurring, but these probabilities were not necessarily equal. With any form of sampling there was a risk that the sample might not adequately represent the population but with random sampling there was a large body of statistical theory which quantifies the risk and thus

enables an appropriate sample size to be chosen. Furthermore, once the sample had been taken the sampling error associated with the measured results could be computed. With non-random sampling there was no measure of the associated sampling error. While such methods might be cheaper this was largely meaningless since there was no measure of quality. There were several forms of random sampling. For example, in simple random sampling, each element had an equal probability of being selected. Another form of random sampling was Bernoulli sampling in which each element had an equal probability of being selected, like in simple random sampling. However, Bernoulli sampling leads to a variable sample size, while during simple random sampling the sample size remains constant. Bernoulli sampling was a special case of Poisson sampling in which each element might had a different probability of being selected. Other examples of probability sampling include stratified sampling and multistage sampling.

Sampling with quadrats (plots of a standard size) could be used for most ecosystems (Cox, 1990). A quadrat delimits an area in which coral cover could be estimated, coral counted, or species listed. Quadrats could be established randomly, regularly, or subjectively within a study site. The appropriate size for a quadrat depends on the items to be measured. If cover was the only factor being measured, size was relatively unimportant. If coral numbers per unit area were to be measure, then quadrat size was critical. A plot size should be large enough to include significant numbers of individuals, but small enough so that plants could be separated, counted and measured without duplication or omission of individuals (Barbour et al., 1987; Cox, 1990). The reliability of the estimate depends on (1) the population in each quadrat must be known exactly, (2) the area of each quadrat must be known and

(3) the quadrats must be representative of the sampling area. Quadrats were commonly used to measure plant populations.

Coral photographs were taken with digital cameras, Canon Power Shot A620 and Olympus uD600/S600 with underwater casings. For quadrat sampling technique, a 50 x 50 cm² quadrat was placed on top of corals and a photograph was taken that contained the whole quadrat area. There were resampled by taking 50 more quadrat and random photographs with new coral locations in order to avoid pseudo-replications. Coral photographs were classified into seven coral growth forms: massive, encrusting, branching, foliaceous, laminar, free-living, and columnar (Veron, 2000) (Figure 6).

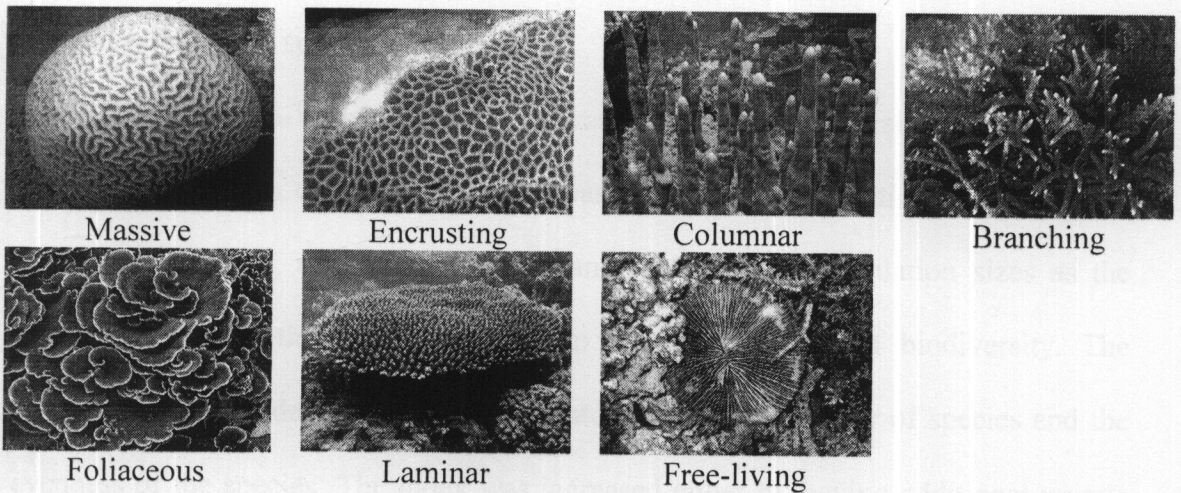


Figure 6 Seven coral growth forms.

There were randomly selected 40 out of all coral photographs/study site for a quadrat and random sampling technique to estimate % coral growth form/photography. These percentages of coral growth forms were used to calculate Shannon-Wiener index and Simpson index (Simpson, 1949; Zar, 1984; Krebs, 1989).

Shannon-Wiener index, this diversity measure was based on information theory simply, the measure of order (or disorder) within a particular system. For our used, this order could be characterised by the number of species and/or the number of individuals in each species, within our sample plot. By applying these numbers to the Shannon-Wiener equations we could determine what was referred to as the degree of uncertainty. With this number we could then specify our degree of diversity. In questioning how difficult it would be to predict correctly the species of the next individual collected, we defined uncertainty, in turn defining diversity. For example, if our number of uncertainty was low, i.e. we felt confident in naming the next individual's species, which our types of species were few. If our number of uncertainty was high, the number of species was greater and our chances of knowing the next individual's species were low.

The Shannon-Wiener Index, (H') was one of several diversity indices used to measure diversity in categorical data. It was simply the Information entropy of the distribution, treating species as symbols and their relative population sizes as the probability. This article treated its use in the measurement of biodiversity. The advantage of this index was that it takes into account the number of species and the evenness of the species. The index was increased either by having additional unique species, or by having greater species evenness.

$$H' = - \sum_{i=1}^S p_i \ln p_i \quad (1)$$

Where n_i was the number of individuals in each species; the abundance of each species. S was the number of species, also called species richness. N was the total number of all individuals $\sum_{i=1}^S n_i$ and p_i was the relative abundance of each

species, calculated as the proportion of individuals of a given species to the total number of individuals in the community $\frac{n_i}{N}$.

Simpson's diversity index was a measure of diversity. In ecology, it was often used to quantify the biodiversity of a habitat. It took into account the number of species present, as well as the relative abundance of each species. The Simpson index represents the probability that two randomly selected individuals in the habitat belong to the same species. Simpson's diversity index was a simple mathematical measure that characterises species diversity in a community. The proportion of species relative to the total number of species was calculated and squared. The squared proportions for all the species were summed, and the reciprocal was taken:

$$D = \frac{\sum_{i=1}^S n_i(n_i - 1)}{N(N - 1)} \quad (2)$$

Where S was the number of species, N was the total percentage cover or total number of organisms and n was the percentage cover of a species or number of organisms of a species.

When using the Simpson Index for lower numbers, misleading results could be obtained, with obviously less diverse areas having a higher index than they should. One way around this when studying on land was to include bare earth as an extra species, which yields more realistic results (Simpson, 1949; Zar, 1984; Krebs, 1989).

A 1 m² empty area was located within coral reef with sandy bottom where was selected to deploy four HOBO Pendant temperature and light data loggers model UA-002-64 to measure water temperature and light intensity at Koh Tan (latitude 9.36871 °N, longitude 99.95840 °E) during 2-18 June 2007. Four 1.5 kg weights were placed

at 1 m² empty area and tied these four data loggers to each weight in four diagonal corners. This allowed each data logger to receive an accurate and maximum light intensity. A waterproof shuttle used to upload the water temperature and light intensity data from data loggers.

RESULTS

There was higher % massive form at *S3* than *S2* ($F_{2,234} = 6.033$, $P < 0.01$, Figure 7). There were higher % massive form found in random sampling than quadrat sampling technique ($F_{1,234} = 6.584$, $P < 0.05$). Their interaction terms were not different ($F_{2,234} = 1.470$, ns).

For the percentage of columnar form, study site, sampling technique and their interaction terms did not differ (study site: $F_{2,234} = 1.831$, ns; sampling techniques: $F_{1,234} = 0.574$, ns; and interaction term: $F_{2,234} = 0.150$, ns). There was higher % encrusting form at *S3* than *S1* ($F_{2,234} = 8.330$, $P < 0.001$) but sampling technique and their interaction terms did not differ (sampling technique: $F_{1,234} = 1.964$, ns; interaction term: $F_{2,234} = 0.048$, ns). There was higher % branching form at *S2* than *S1* ($F_{2,234} = 28.633$, $P < 0.001$) but sampling technique and their interaction terms did not differ (sampling technique: $F_{1,234} = 0.377$, ns; interaction term: $F_{2,234} = 1.089$, ns). There was higher % foliaceous form at *S1* than *S2* and *S3* and higher in quadrat than in random sampling technique (study site: $F_{2,234} = 20.452$, $P < 0.001$; sampling technique: $F_{1,234} = 4.094$, $P < 0.05$) but their interaction terms did not differ ($F_{2,234} = 0.449$, ns).

For % laminar form, study site, sampling technique and their interaction terms did not differ (study site: $F_{2,234} = 3.915$, $P < 0.05$, ns; sampling technique: $F_{1,234} = 0.400$, ns; interaction term: $F_{2,234} = 0.292$, ns). For % free-living form, study site, sampling technique and their interaction terms did not differ (study site: $F_{2,234} = 1.838$, ns; sampling technique: $F_{1,234} = 1.838$, ns; interaction term: $F_{2,234} = 1.838$, ns). This suggests that there were different coral forms present in different study areas. At *S1*, foliaceous form was found more than other study sites and there was no columnar form present at *S1*. At *S3*, massive, encrusting, and laminar forms were found than other study sites, and there was no branching form present at *S3*. Free-living form was found very low number in all three study sites. Biodiversity indices did not differ between two techniques: random and quadrat sampling techniques (Table 3).

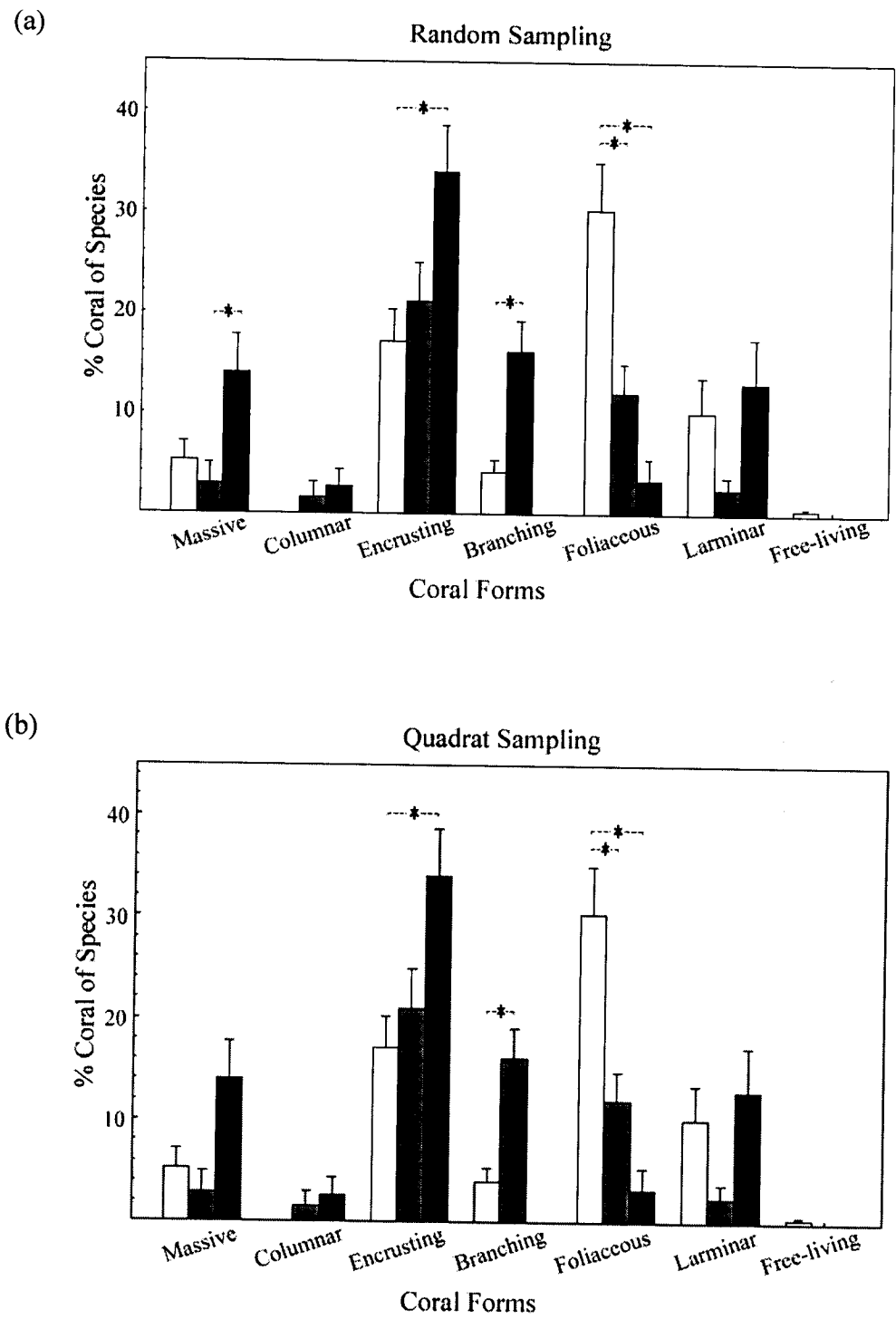


Figure 7 % coral form at (□) Koh Tan, (■) Koh Mudsoom and (■) Ao Thong Yee. (a) random sampling technique and (b) quadrat sampling technique, $*P < 0.001$.

Table 3 Biodiversity index from % coral growth form classification.

Study site	Shannon-Wiener Index		Simpson Index	
	Random	Quadrat	Random	Quadrat
Koh Tan	1.73	1.59	0.86	0.80
Koh Mud Soom	1.63	1.59	0.91	0.89
Ao Tong Yee	1.61	1.57	0.85	0.81

SST at Koh Tan during 2-18 June 2007 ranged from 28.67-33.17 °C. The field investigation SST data and NOAA SST were plotted. This SST was validated by comparison between the NOAA SST data, the measured SST data and NOAA SST that were good agreement between the series (Figure 8). Temperature seems to be very high due to several reasons: the circulation in the ocean, wind surface, and high solar radiation. The effects of future climate change on species could be profound, as indicated by the earlier example of SST and light intensity in Koh Tan. Species might be unable to tolerate changed conditions within their current range, or that cannot migrate fast enough to keep up with moving climate zones, face eventual extinction.

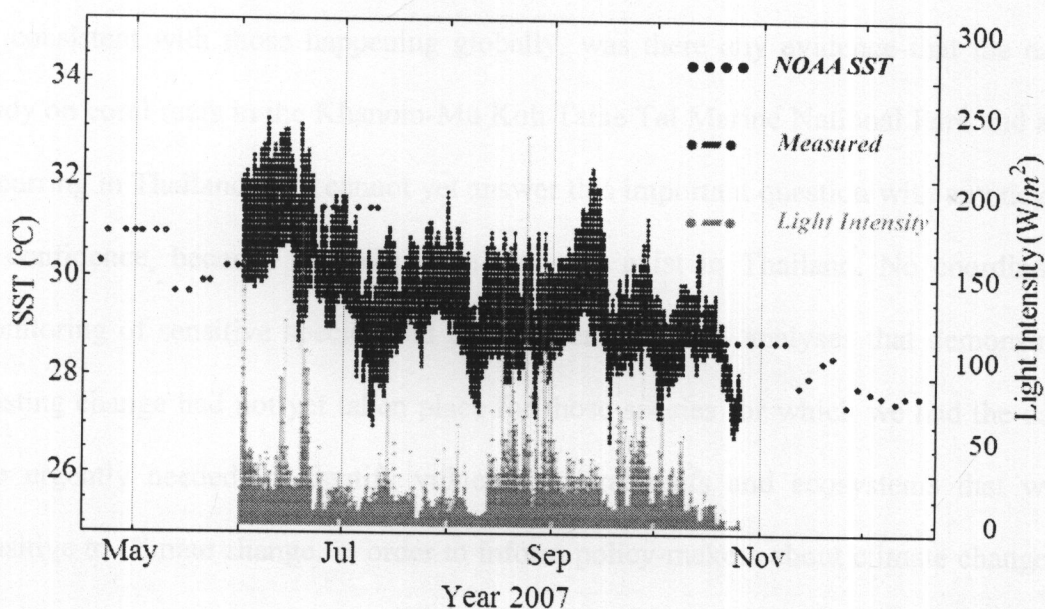


Figure 8 SST NOAA, measured SST (upper line) and light intensity (lower line) at Koh Tan.

DISCUSSION

We found the biodiversity index from % coral growth form classification did not differ between two techniques: random and quadrat sampling techniques. We also suggest the random sampling technique, which could make it easier to sampling on snorkel diving research.

One direct measure of coral stress was the phenomenon of coral bleaching and mortality associated with widespread elevated SSTs during the last decade (Hoegh-Guldberg, 1999). This was frequently associated with warm temperatures and had been widely predicted to increase in the future. Exposure for one month at temperatures 1 or 2 °C higher than the mean averages at the warmest time of year was sufficient to cause the corals to bleach.

Considering that temperature and other climatic trends in Koh Tan appear to be consistent with those happening globally, was there any evidence that the early study on coral reefs in the Khanom-Mu Koh Talae Tai Marine National Park and also occurring in Thailand? We cannot yet answer this important question with any degree of confidence, because few long-term data-sets exist in Thailand. No coordinated monitoring of sensitive species had been undertaken, and analyses that demonstrate existing change had not yet taken place for those species for which we had the data. We urgently needed to identify vulnerable coral reefs and ecosystems that were sensitive to climate change, in order to inform policy-makers about climate change in relation to conservation management.

ACKNOWLEDGEMENTS

This work was supported in part by PTT Public Company Limited, TOTAL Foundation and TOTAL E&P Thailand, TRF/Biotec special program for Biodiversity Research Training grant BRT T_550001, Commission on Higher Education, the Thailand Research Fund grant PHD/0201/2548 and CXKURUE, the Institute of Research and Development, Walailak University.

REFERENCES

- Barber P. H., Palumbi S. R., Erdmann M. V. and Moosa M. K. (2002). Sharp genetic breaks among populations of a benthic marine crustacean indicate limited oceanic larval transport: patterns, causes, and consequences. *Molecular Ecology*, 11, 659–674.
- Barbour M. G., Burk J. H. and Pitts W. D. (1998). Terrestrial Plant Ecology. *Chapter 9: Method of sampling the plant community*, Menlo Park, CA: Benjamin/Cummings Publishing Co.
- Bellwood D. R., Hughes T. P., Folke C. and Nystrom M. (2004). Confronting the coral reef crisis. *Nature*, 429, 827–833.
- Bryant D., Burke L., McManus J. and Spalding M. (1998). Reefs at Risk: A map-based indicator of threats to the world's coral reefs. *World Resources Institute*, 56.
- Burke L., Selig E. and Spalding M. (2002). Reefs at Risk in Southeast Asia. *World Resources Institute*, Washington, D.C., 1-72.
- Buyck B. (1999). Taxonomists were an endangered species in Europe. *Nature*, 401, 321.
- Cox G. (1990). *Laboratory manual of general ecology (6th edition)*, Dubuque, Iowa, William C. Brown (Editors).
- Hoegh-Guldberg O. (1999). Coral bleaching, climate Change and the future of the world's coral reefs. *Marine and Freshwater Research*, 50, 839-866.

- Hopkins G. W and Freckleton R. P. (2002). Declines in the numbers of amateur and professional taxonomists: implications for conservation. *Animal Conservation*, 5, 245-249.
- Knowlton N. (2001). The future of coral reefs. *Proceedings of the National Academy of Sciences of the United States of America*, 98(10), 5419–5425.
- Krebs C. J. (1989). Ecological Methodology. *Species Diversity Measures*, Harper and Row, Publishers. New York, 361-367.
- May R. M. (1998). How many species were there on Earth? *Science*, 241, 1441–1449.
- Meyer C. P. (2003). Molecular systematics of cowries (Gastropoda: Cypraeidae) and diversification patterns in the tropics. *Biological Journal of the Linnean Society*, 79, 401–459.
- Novacek M. J. and Cleland E. E. (2001). The current biodiversity extinction event: scenarios for mitigation and recovery. *Proceedings of the National Academy of Sciences of the United States of America*, 98, 5466–5470.
- Paulay G. and Meyer C. (2002). Diversification in the tropical pacific: comparisons between marine and terrestrial systems and the importance of founder speciation. *Integrative and Comparative Biology*, 42, 922–934.
- Roberts C. M., McClean C. J., Veron J., Hawkins J. P., Allen G. R., McAllister D. E., Mittermeier C. G., Schueler F. W., Spalding M., Wells F., Vynne C. and Werner T. B. (2002). Marine biodiversity hotspots and conservation priorities for tropical reefs. *Science*, 295, 1280–1284.
- Simpson E. H. (1949). Measurement of diversity. *Nature*, 163, 688.
- Veron J. (2000). Coral of the world. *Australian Institute of Marine Science*, PMB 3, Townsville MC, Qld 4810, Australia.

- Wilkinson C. R. (Editor) (2002). Status of Coral Reefs of the World: 2002. *Australian Institute of Marine Science*, PMB 3, Townsville MC, Qld 4810, Australia.
- Wilkinson C. R. (Editor) (2004). Status of Coral Reefs of the World: 2004. *Australian Institute of Marine Science*, PMB 3, Townsville MC, Qld 4810, Australia.
- Wilson E. O. (2003). The encyclopedia of life. *Trends in Ecology and Evolution*, 18, 77–80.
- Zar J. H. (1984). Biostatistical Analysis. *Measures of dispersion and variability*, Prentice-Hall, Inc. Englewood Cliffs, New Jersey, 32-36.

CHAPTER III

CORAL GROWTH FORMS AND BIODIVERSITY INDICES AT KHANOM MU KOH TALAE TAI MARINE NATIONAL PARK

PUBLICATION

Suntorn Surabun, Chairote Yaiprasert, Siriwan Wongkoon, Mullica Jaroensutasinee, and Krisanadej Jaroensutasinee, 2007. Coral growth forms and biodiversity indices at Khanom Mu Koh Talae Tai Marine National Park. *The 33rd Congress on Science and Technology of Thailand*, Nakhon Si Thammarat, Thailand. 18-20th October, 129.

ABSTRACT

This study aimed at estimating % coral growth forms at Khanom-Mu Koh Talae Tai Marine National Park. We compared coral growth forms at four study sites using random photographic technique. We took coral photographs with a digital camera and underwater casing. Coral images were classified into one of seven coral forms and used these percentages to calculate coral biodiversity indices (i.e. Shannon-Wiener index and Simpson index). The biodiversity indices were higher at Koh Tan and Koh Mud Soom than at Ao Tong Yee and Koh Wang Nok.

Keywords: Coral, Biodiversity index, Shannon-Wiener index, Simpson index.

INTRODUCTION

The shape of reef corals was affected by light level and by wave stress leading to the well-known zonation of coral form associations with exposure and depth. Growth form was constrained by geometric factors. Similarly, coral calcification rate, of importance both for coral form and for net reef growth, was light dependant, and might be affected by other factors such as wave stress and sediment flux (Vaughan, 1907; Morton, 1974; Graus and Macintyre, 1976; Geister, 1977; Jaubert, 1997).

The existence of a coral reef framework creates a three dimensional, topographically complex habitat and the high levels of species (and hence genetic) diversity on coral reefs would not be possible without this physical structure. Corals were the main builders of the reef framework through the accumulation of limestone by a process known as calcification, but a diversity of other organisms, encrusting coralline algae, foraminifera, molluscs, and echinoderms were also needed in the building of the reef. Coral calcification was intimately related to the internal symbiosis with the zooxanthellae and overall reefs precipitate half of the calcium delivered to the sea each year (Done et al., 1996).

Coral reefs were the most diverse and beautiful of all marine habitats. Large wave resistant structures had accumulated from the slow growth of corals. The development of these structures was aided by algae that were symbiotic with reef-building corals, known as zooxanthellae. Coralline algae, sponges, and other organisms, combined with a number of cementation processes also contribute to reef growth. The dominant organisms were known as framework builders, because they provided the matrix for the growing reef. Corals and coralline algae precipitate calcium carbonate, whereas the framework- building sponges might also precipitate

silica. Most of these organisms were colonial, and the slow process of precipitation moves the living surface layer of the reef upward and seaward. Reef-building corals might occur in a variety of growth forms, and there often was strong variation in coral shape even within a species (Done et al., 1996; Birkeland, 1997).

The reef was topographically complex. Much like a rain forest, it had many strata and areas of strong shade, cast by the over towering coral colonies. Because of the complexity, thousands of species of fish and invertebrates live in association with reefs, which were by far our richest marine habitats. In Caribbean reefs, for example, several hundred species of colonial invertebrates could be found living on the undersides of platy corals. It was not unusual for a reef to have several hundred species of snails, sixty species of corals, and several hundred species of fish. Of all ocean habitats, reefs seem to have the greatest development of complex symbiotic associations.

However, while zooxanthellae photosynthesis certainly enhances coral calcification rates and was responsible for forming most of the solid coral reef framework, the way in which this operates was yet to be fully determined. Photosynthesis raises the pH which provides more carbonate ions for deposition and zooxanthellae were also believed to remove inorganic chemical inhibitors. Energy for active calcification might be provided to the coral by the zooxanthellae but only in shallow water corals where the fixation of carbon exceeds their own respiratory needs. What was certain was that all the goods and services of the reef were directly or indirectly dependent on the reef building corals and their zooxanthellae (Birkeland, 1997).

This symbiosis required sufficient light and good water circulation, and generally exists in a rather narrow range of water temperature, with low nutrient and sedimentation loads. As a result corals were sensitive to environmental factors which perturb any of these factors. For example, corals at individual localities appear to have become adapted to quite narrow temperature regimes and exposure to warmer water was often sufficient to cause bleaching, which the appearance was caused by the expulsion of zooxanthellae by coral. It was not evidence of the death of the coral, but could lead to death if the triggering condition for the expulsion was not improved (Done et al., 1996; Birkeland, 1997).

Coral reefs had different shapes and patterns because of the growth pattern of the millions of tiny individual animals that make up a colony. Reefs could look like beautiful underwater gardens. Some corals resemble the tendrils of plants, while some might look like leaves. The brain coral was nearly spherical and had grooves that make it look like a human brain. Corals with flat, fan-shaped structures that spread out from a narrower base were called sea fans. The organ-pipe corals, which were found in the tropical oceans of the Indo-Pacific, were typically long rigid tubes. The coral's skeletons, external or internal, had a stone like, horny, or leathery texture. The body of a coral animal consists of a polyp, a hollow, cylindrical structure attached at its lower end to some surface. The largest of the solitary polyps grows to a diameter of about 10 in (25 cm). The polyps of the corals that form reefs range from 0.04 to 1.2 in (0.1 to 3 cm) in diameter.

This study aimed at comparing % coral forms at four study sites, Khanom Mu Koh Talae Tai Marine National Park. We estimated the percentage of seven coral reef

growth forms using random sampling technique. These percentages of coral growth forms were used to estimate coral biodiversity indices.

MATERIALS AND METHODS

We selected four coral study sites at Khanom Mu Koh Talae Tai Marine National Park: Koh Tan (*S1*), Koh Mud Soom (*S2*), Ao Tong Yee (*S3*) and Koh Wang Nok (*S4*) (Figure 9).

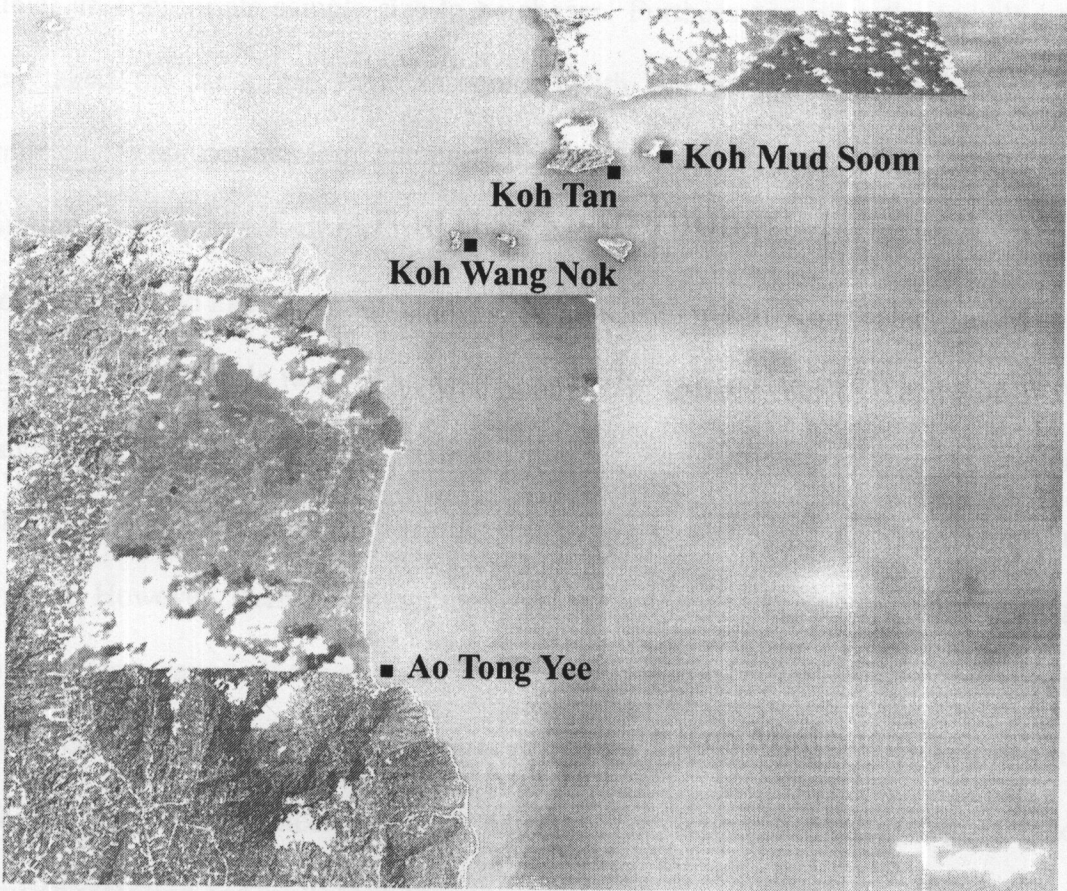


Figure 9 Four study sites: Koh Tan, Koh Mud Soom, Ao Tong Yee and Koh Wang Nok.

We took coral photographs with digital cameras, Canon Power Shot A620 and Olympus uD600/S600 with underwater casings. At each study site, we took 100 coral pictures and randomly selected 40 out of 100 pictures/study sites.

In random sampling, also known as probability sampling, every combination of items from the frame, or stratum, had a known probability of occurring, but these probabilities were not necessarily equal. With any form of sampling there was a risk that the sample might not adequately represent the population but with random sampling there was a large body of statistical theory which quantifies the risk and thus enables an appropriate sample size to be chosen. Furthermore, once the sample had been taken the sampling error associated with the measured results could be computed. With non-random sampling there was no measure of the associated sampling error. While such methods might be cheaper this was largely meaningless since there was no measure of quality. There were several forms of random sampling. For example, in simple random sampling, each element had an equal probability of being selected. Another form of random sampling was Bernoulli sampling in which each element had an equal probability of being selected, like in simple random sampling. However, Bernoulli sampling leads to a variable sample size, while during simple random sampling the sample size remains constant. Bernoulli sampling was a special case of Poisson sampling in which each element might had a different probability of being selected. Other examples of probability sampling include stratified sampling and multistage sampling.

Forty coral photographs per study area were classified into one of seven coral growth forms: massive, encrusting, branching, foliaceous, laminar, free-living, and columnar (Veron, 2000) (Figure 10). The coral growth process generates a wide range

of colony morphologies; examples were spherical, plate-like and branching growth forms. These morphologies were species specific, but also showed high intra-specific variability. This intra-specific variability was probably caused by environmental parameters, such as light availability and the amount of water flow. The effect of light availability was studied in two pioneering coral modelling studies (Graus and Macintyre, 1976; Graus and Macintyre, 1982), and the effect of fluid flow on coral growth was studied in previous work by Kaandorp (1996), Kaandorp and Sloot (2001), and Kaandorp (2001).

We used the percentage of coral growth forms to calculate Shannon-Wiener index and Simpson index. The Shannon-Wiener Index, (H') was one of several diversity indices used to measure diversity in categorical data. The index was increased either by having additional unique species, or by having greater species evenness.

$$H' = - \sum_{i=1}^S p_i \ln p_i \quad (1)$$

Where n_i was the number of individuals in each species; the abundance of each species. S was the number of species, also called species richness. N was the total number of all individuals $\sum_{i=1}^S n_i$, and p_i was the relative abundance of each species, calculated as the proportion of individuals of a given species to the total number of individuals in the community $\frac{n_i}{N}$ (Zar, 1984; Krebs, 1989).

Simpson's diversity index was a measure of diversity. It took into account the number of species present, as well as the relative abundance of each species. The Simpson index represents the probability that two randomly selected individuals in

the habitat belong to the same species. The proportion of species relative to the total number of species was calculated and squared. The squared proportions for all the species were summed, and the reciprocal was taken:

$$D = \frac{\sum_{i=1}^S n_i(n_i - 1)}{N(N - 1)} \quad (2)$$

Where S was the number of species, N was the total percentage cover or total number of organisms and n was the percentage cover of a species or number of organisms of a species (Simpson, 1949).

Data were tested for normality and using the two-way ANOVA test to test the differences between study sites, coral growth forms and their interaction between study sites and coral growth forms. If there were some differences, post-hoc with Bonferroni adjustment were tested.

The Bonferroni simply calculates a new pairwise alpha to keep the family wise alpha value at .05 (or another specified value). The formula for doing this was as follows:

$$\alpha_B = \frac{\alpha_{FWE}}{c} \quad (3)$$

Where α_B the new alpha was based on the Bonferroni test that should be used to evaluate each comparison or significance test, α_{FWE} was the family wise error rate as computed in the first formula, and c was the number of comparisons (statistical tests).

The Bonferroni was probably the most commonly used posthoc test, because it was highly flexible, very simple to compute, and could be used with any type of statistical test (e.g., correlations)—not just posthoc tests with ANOVA. The

traditional Bonferroni, however, tends to lack power. The loss of power occurs for several reasons; (1) the family wise error calculation depends on the assumption that, for all tests, the null hypothesis was true. This was unlikely to be the case, especially after a significant omnibus test, (2) all tests were assumed to be orthogonal (i.e., independent or non overlapping) when calculating the family wise error test, and this was usually not the case when all pairwise comparisons were made, (3) the test does not take into account whether the findings were consistent with theory and past research. If consistent with previous findings and theory, an individual result should be less likely to be a Type I error and (4) Type II error rates were too high for individual tests. In other words, the Bonferroni overcorrects for Type I error (Keppel and Wickens, 2004)

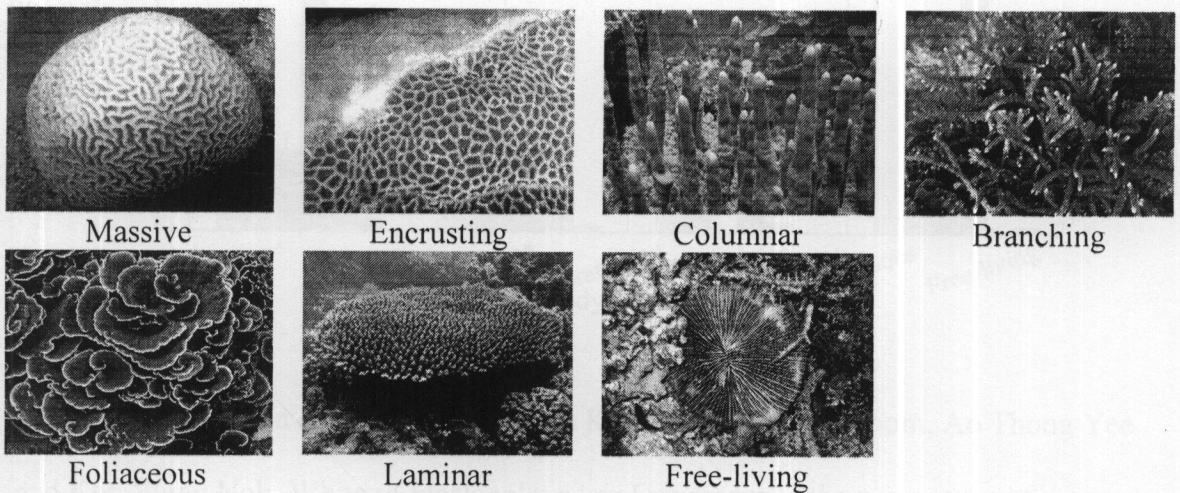


Figure 10 Seven coral growth forms.

RESULTS

Percent coral growth forms did not differ among study sites ($F_{3,1078} = 2.418$, ns). There were some difference percentages of coral growth forms ($F_{6,1078} = 47.087$,

$P < 0.001$) and their interaction between study sites and % coral growth forms ($F_{18,1078} = 10.804$, $P < 0.001$). There were significantly different in the percentage of seven coral forms in each study site (Koh Tan: $F_{6,273} = 10.525$, $P < 0.001$; Koh Mud Soom: $F_{6,273} = 20.025$, $P < 0.001$; Ao Thong Yee: $F_{6,259} = 27.888$, $P < 0.001$; Koh Wang Nok: $F_{6,273} = 21.255$, $P < 0.001$, see

Figure 11)

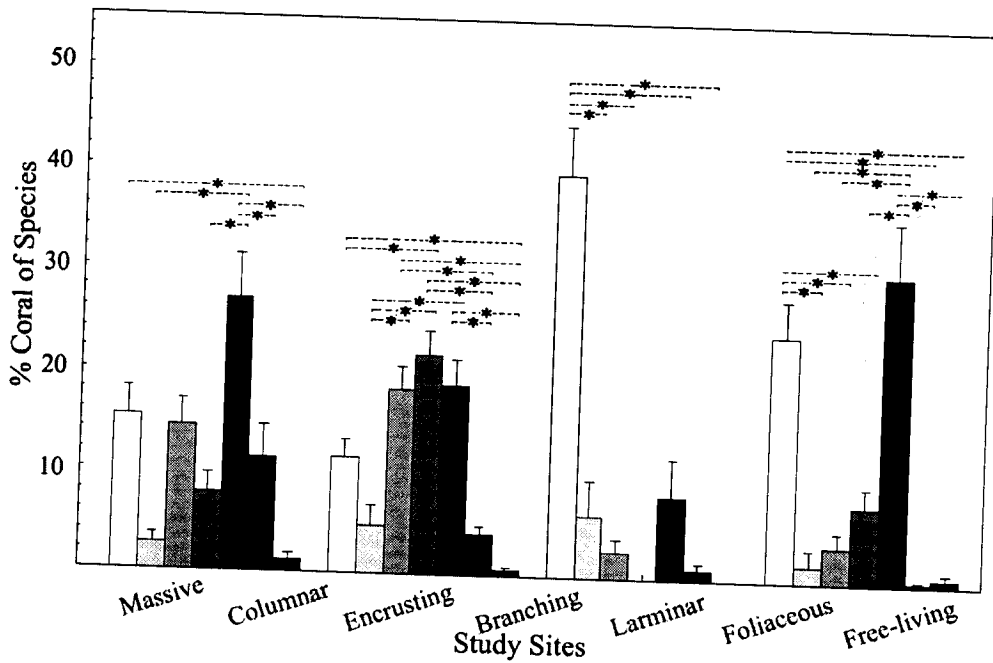


Figure 11 % of seven coral growth forms at Koh Tan, Koh Mud Soom, Ao Thong Yee and Koh Wang Nok. White to black colour level represent to the percentage of Massive, Columnar, Encrusting, Branching, Foliaceous, Laminar and Free-living, respectively, * $P < 0.001$.

There was the highest percentage of massive form at Ao Tong Yee than other three study sites ($F_{3,154} = 13.694$, $P < 0.001$, Figure 12). For % columnar form and

free living form, there were no different among four study sites (columnar form: $F_{3,154} = 0.820$, ns; free living for: $F_{1,154} = 1.458$, ns, Figure 12). There was the highest percentage of encrusting and branching forms at Koh Mud Soom than other three study sites (encrusting form: $F_{1,154} = 15.184$, $P < 0.001$; branching forms: $F_{1,154} = 25.126$, $P < 0.001$, Figure 12). There was higher % foliaceous form at Koh Wang Nok than Ao Thong Yee and Koh Mud Soom ($F_{1,154} = 5.484$, $P < 0.01$, Figure 12). There was the highest percentage of laminar form at Koh Tan than other three study sites ($F_{1,154} = 8.277$, $P < 0.001$, Figure 12). This suggested that there were different coral forms present in different study areas.

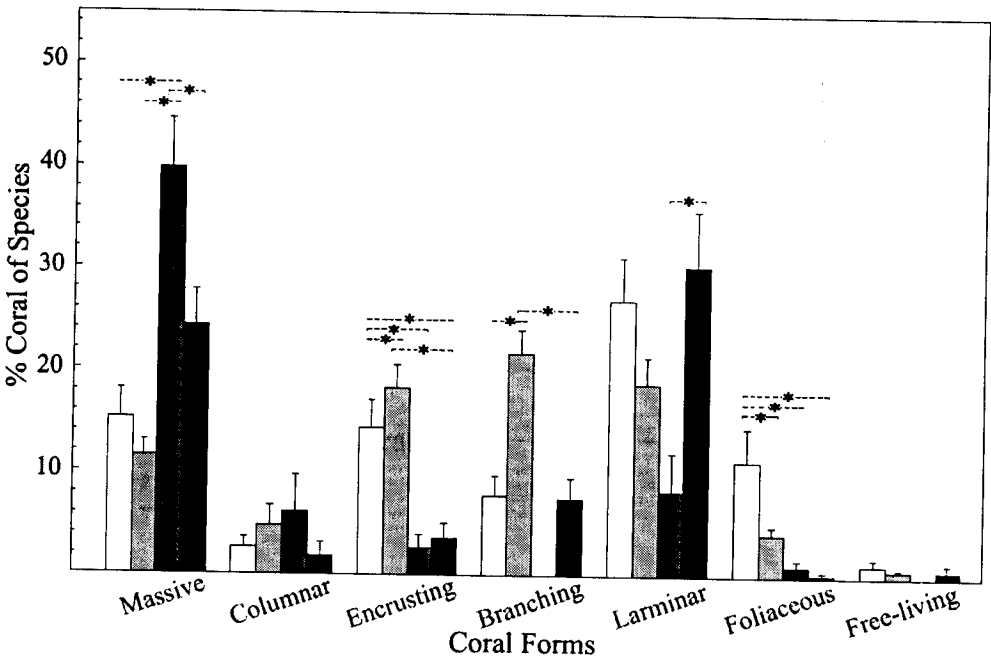


Figure 12 % of seven coral growth forms at Koh Tan, Koh Mud Soom, Ao Tong Yee and Koh Wang Nok respectively, * $P < 0.001$.

Table 4 Coral biodiversity indices at Khanom - Mu Koh Talae Tai Marine National Park.

Study site	Shannon-Wiener Index	Simpson Index
Koh Tan	2.18	0.86
Koh Mud Soom	2.18	0.87
Ao Tong Yee	1.28	0.83
Koh Wang Nok	1.68	0.84

DISCUSSION

At Ao Tong Yee, we found the highest percentage of massive form but no branching and free living forms. This indicates that Ao Tong Yee area was under strong waves and wind. Coral with branching form such as stag horn coral species could not be able to grow under this condition. Their branches could be breaking off easily under strong waves and wind.

Koh Tan and Koh Mud Soom had higher biodiversity indices than Ao Tong Yee and Koh Wang Nok (Table 4). Ao Tong Yee had the lowest biodiversity indices than other three study areas (Table 4). This could be due to the fact that the other three study areas were islands but Ao Tong Yee was a part of Khanom mainland with rocky shore and strong wave fronts.

One of the main questions in the study of the morphogenesis of branching corals was the branching mechanism. The branching pattern of many stony corals was probably tightly genetically regulated, since branches in many corals were added according to typical, species specific architectural rules (Dauget, 1991). In *Stylophora pistillata*, for example, such architectural rules generate a nearly spherical colony shape, that regenerates when damaged (Loya, 1976; Rinkevich, 2001; 2002). This

regulation of the growth form was often thought to be mediated by chemical signals excreted into the water, the isomones (Rinkevich and Loya, 1985). Branching patterns also often arise in abiotic growth processes, such as viscous fingering, electric discharge and crystallisation. The development of such patterns was explained with models of diffusion-limited aggregation (Witten and Sander, 1981) and Laplacian growth (e.g. Mineev-Weinstein and Dawson, 1994; Magdaleno and Casademunt, 1998). In such models, the growth of the pattern depends locally on the value of an external field that might either describe the concentration of aggregating particles, as in the case of diffusion-limited aggregation, or a pressure or electric field, as in the case of viscous fingering or electric discharge. The branching patterns that arise from such abiotic growth processes were often similar in appearance to the patterns that arise in biotic growth processes, such as coral growth. This similarity suggested the possibility that in these biotic growth processes a comparable Laplacian growth mechanism might be at work.

We suggested whether natural coral growth might be considered a Laplacian growth process by considering the real time-scales of growth and transport. These were compared by estimating the time needed to diffuse over the yearly skeletal extension rate (i.e. the growth caused by extension of vertical skeletal elements, ignoring secondary thickening). Assuming a transport mechanism that could be approximated by diffusion, the time needed to transport a resource over a distance. The skeletal extension rate varies between coral species and on environmental parameters such as the SST (Lough and Barnes, 2000).

ACKNOWLEDGEMENTS

This work was supported in part by PTT Public Company Limited, TOTAL Foundation and TOTAL E&P Thailand, TRF/Biotec special program for Biodiversity Research Training grant BRT T_550001, Commission on Higher Education, the Thailand Research Fund through the Royal Golden Jubilee Ph.D. Program (Grant No. PHD/0201/2548) and CXKURUE, the Institute of Research and Development, Walailak University.

REFERENCES

- Birkeland C. (Editor) (1997). Interactions between corals and their symbiotic algae. *Life and Death of Coral Reefs*, Chapman and Hall, New York, 96-112.
- Dauget J. M. (1991). Application of tree architectural models to reef coral growth forms. *Marine Biology*, 111, 157–165.
- Done T. J., Ogden J. C., Wiebe W. J. and Rosen B. R. (1996). Biodiversity and ecosystem function of coral reefs. *Functional Roles of Biodiversity: A Global Perspective*, Mooney H. A., Cushman J. H., Medina E., Sala O. E. and Schulze, E. D. (Editors), 393-423.
- Geister J. (1977). The influence of wave exposure on the ecological zonation of Caribbean reefs. *Proceeding 3rd International Coral Reef Symposium*, 1, 23–39.
- Graus R. R. and Macintyre I. G. (1976). Light control of growth form in colonial reef corals: Computer Simulation. *Science*, 193, 895–897.
- Graus R. R. and Macintyre I. G. (1982). Variation in growth forms of the reef coral *Montastrea annularis* (Ellis and Solander): a quantitative evaluation of growth response to light distribution using computer simulations. *Smithsonian Contributions to the Marine Sciences*, 12, 441–464.
- Jaubert J. (1997). Light, metabolism and growth forms of the hermatypic scleractinian coral *Synaraea convexa* Verrill in the lagoon of Moorea (French Polynesia). *Proceeding 3rd International Coral Reef Symposium*, Miami, USA, Rosenstiel School of Marine and Atmospheric Science, University of Miami, 483–488.

- Kaandorp J. A. (2001). *The Algorithmic Beauty of Seaweeds, Sponges and Corals, The Virtual Laboratory*, Springer, Kaandorp J.A. and Kübler J. (Editors), Berlin, Heidelberg, New York, 114–144.
- Kaandorp J. A. and Sloot P. M. A. (2001). Morphological models of radiate accretive growth and the influence of hydrodynamics. *Journal of Theoretical Biology*, 209, 257–274.
- Kaandorp J. A., Lowe C. P., Frenkel D. and Sloot P. M. A. (1996). Effect of nutrient diffusion and flow on coral morphology. *Geophysical Research Letters*, 77, 2328–2331.
- Keppel G. and Wickens T. D. (2004). Design and analysis. *A researchers handbook (4th Edition)*, Upper Saddle River, NJ: Pearson
- Krebs C. J. (1989). Ecological Methodology. *Species Diversity Measures*, Harper and Row, Publishers. New York, 361-367.
- Lough J. M. and Barnes D. J. (2000). Environmental controls on growth of the massive coral *Porites*. *Journal of Experimental Marine Biology and Ecology*, 245, 225–243.
- Loya Y. (1976). Skeletal regeneration in a red sea scleractinean coral population. *Nature*, 261, 490–491.
- Magdaleno F. X. and Casademunt J. (1998). Surface tension and dynamics of fingering patterns. *Physical Review E*, 57, R3707–R3710.
- Mineev-Weinstein M. B. and Dawson, S. P. (1994). Class of non-singular exact-solutions for Laplacian pattern formation. *Physical Review E*, 50, R24–R27.

- Morton J. (1974). The coral reefs of the British Salomon Islands; A comparative study of their composition and ecology. *Proceeding 2nd International Coral Reef Symposium*, 2, 31-54.
- Rinkevich B. and Loya Y. (1985). Coral isomone: a proposed chemical signal controlling intraclonal growth patterns in a branching coral. *Bulletin Marine Science*, 36, 319–324.
- Rinkevich B. (2001). Genetic regulation in the branching stony coral *Stylophora pistillata*. *The Algorithmic Beauty of Seaweeds, Sponges, and Corals*, Kaandorp, J. A., Kubler, J. E. (Editors), Springer, Berlin, 62–66.
- Rinkevich B. (2002). The branching coral *Stylophora pistillata*: contribution of genetics in shaping colony landscape. *Israel Journal of Zoology*, 48, 71–82.
- Simpson, E. H. (1949). Measurement of diversity. *Nature*, 163, 688.
- Vaughan, T. W. (1907). Recent Madreporaria of the Hawaiian Islands and Laysan. *Bulletin of the United States National Museum*, 59(9), 427.
- Veron J. (2000). Coral of the world. *Australian Institute of Marine Science*, PMB 3, Townsville MC, Qld 4810, Australia.
- Witten Jr. T. and Sander L. (1981). Diffusion-limited aggregation, a kinetic critical phenomenon. *Geophysical Research Letters*, 47, 1400–1403.
- Zar J. H. (1984). Biostatistical Analysis. *Measures of dispersion and variability*, Prentice-Hall, Inc. Englewood Cliffs, New Jersey, 32-36.

CHAPTER IV

THE PIXEL VALUE DATA APPROACH FOR RAINFALL FORECASTING BASED ON GOES-9 SATELLITE IMAGE SEQUENCE ANALYSIS

PUBLICATION

Chairote Yaiprasert, Krisanadej Jaroensutasinee and Mullica Jaroensutasinee, 2007.

The Pixel Value Data Approach for Rainfall Forecasting Based on GOES-9
Satellite Image Sequence Analysis. *International Journal of Mathematical,
Physical and Engineering Sciences*, 1(4), 222-227.

ABSTRACT

To develop a process of extracting pixel values over the using of satellite remote sensing image data in Thailand, it was a very important and effective method of forecasting rainfall. This paper presented an approach for forecasting a possible rainfall area based on pixel values from remote sensing satellite images. First, a method used an automatic extraction process of the pixel value data from the satellite image sequence. Then, a data process was designed to enable the inference of correlations between pixel value and possible rainfall occurrences. The result, when we had a high averaged pixel value of daily water vapour data, we could also had a high amount of daily rainfall. This suggests that the amount of averaged pixel values could be used as an indicator of raining events. There were some positive associations between pixel values of daily water vapour images and the amount of daily rainfall at each rain gauge station throughout Thailand. The proposed approach was proven to be a helpful manual for rainfall forecasting from meteorologists by which using automated analysing and interpreting process of meteorological remote sensing data.

Keywords: pixel values, satellite image, water vapour, rainfall, image processing.

INTRODUCTION

Meteorological satellite data had been operational in weather services for more than 30 years. During this period, forecasting of severe weather based on satellite remote sensing data had been a challenging task (Lucas et al., 2007; Errico and Fasano, 2008; Vescovo and Gianelle, in press). Early warnings of severe weather, made possible by timely and accurate forecasting could help prevent casualties and damage caused by natural disasters. This was particularly significant and urgent in Thailand, where had so often suffered from flooding due to inadequate flood controls, preventions and mitigations in the country.

For example, at least 176 people died and more than 450,000 were homeless or in hardship following the severe flooding that engulfed northern Thailand after Typhoon Usagi swept through the area in August, 2001. The worst affected area had been the Lom Sak district in the mountainous north-central province of Phetchabun. Massive mudslides tore down the mountainside in the early hours of August 11, uprooting vegetation and burying seven villages with more than two metres of water and mud. Since almost all flash floods were caused by intensive heavy rainfall, the responsible authorities had a key and clear mandate to provide both accurate and advanced forecasting of possible heavy rainfall (British Broadcasting Corporation, 2001; Brakenridge and Anderson, 2002; Divjak and Conachy, 2004).

Meanwhile, detail study of water vapour quantity in the atmosphere remains a challenge and an important issue for the meteorological community. These flash flooding phenomena were often caused by severe weather such as heavy rainfalls, thunderstorms and hurricanes (Houze et al., 1990; Fisher and Mustard, 2007; Meyer et al., 2007; Boussetta et al., 2008).

In order to improve the current measures of severe flood controls in Thailand, it was necessary to accurately predict and/or gather the amount of rainfall in order to be able to determine the possibility of excess amount of water in stream causing flash flooding. However, it was not practical to install a vast number of automatic rainfall sensors throughout the hot spots in the montane that could transmit this rainfall information to achieve the measures. It was then desirable to look for a continuous source of weather information and the meteorological satellites could provide such information. Therefore, it would be of urgent task to determine the amount of rainfall and correlate these quantities to water vapour satellite data by using image processing technique over Thailand region (Bonazountasa et al., 2007; Feidasa et al., 2007; Marconi, 2007; Pardé et al., 2007; Wong et al., 2007).

A meteorological analysis of all Pixel Value Index (PVI) could be performed by taking into account their corresponding environmental, physical variables to the ground, such as temperature, wind divergence and water vapour flux divergence. As a result, the correlations and causalities between the PVI technique and heavy rainfall occurrences could be deduced from the historical remote sensing scenarios and it could be represented as knowledge assisting to predict potential occurrences of heavy precipitation. Unfortunately, meteorologists continue to manually track, characterise and analyse air dynamic systems using so-called expert-eye-scanning technique. The meteorologists carry out extensive manual work to discover the moving trajectories and devolvment trends of air dynamic systems from the satellite remote sensing images. They used professional experience and knowledge (Arnaud et al., 1992). However, the volumes of satellite image data could be huge, making this method inadequate for tracking air dynamic systems covering wide ranges and long time

periods. The method was time consuming, ineffective and often yields unstable and variable results from the different experts involved, it was affecting the reliability of heavy rainfall forecasting.

To address the above problems, this paper aimed to provide meteorologists with an automatic spatial data method based on PVI technique and analysis in the satellite image sequence with possible heavy rainfall. It could be predicted so that effective flood control measures could be taken. The basic principle behind the method was to formulate from a recent collection data that the movement and propagation of water vapour dynamic systems over the west Pacific region. It was the crucial factor leading to the heavy rainfall in Thailand. The method used was data mining and knowledge discovery techniques. Firstly, the image sequences of water vapour map acquired from the GMS were used. The qualified of PVI was automatically identified by image processing and high computing techniques.

DATA SOURCES

Satellite images had been used extensively to study temporal changes. Information and knowledge of water vapour dynamic systems were crucial to heavy rainfall forecast the collection of large amounts of satellite data with high spatial and temporal resolutions was indispensable (Guo et al., 2007; Xiaoa and Wengb, 2007)

For this purpose, satellite remote sensing images of the water vapour data, taken by the GOES-9 satellite, and data of the number of rainfall were provided by the Thailand Meteorology Department (TMD) for use in this study. The data covers the time period from January to December 2004, a representative period when the Thailand suffered from intensive heavy rainfall.

The meteorological satellite, GOES-9 image was one of a new series of advanced geostationary sensors with improved infrared spatial resolution and radiometric sensitivity (Ellrod et al., 1998). GOES-9 had been placed in a geosynchronous orbit at 155° E since 23 May 1995 and started its operational observation over the west Pacific region on 30 September 1995. The geosynchronous plane was about 35,800 km above the Earth, high enough to allow the satellites a full-disc view of the Earth. Because they stay above a fixed spot on the surface, they provided a constant vigil for the atmospheric for severe weather conditions such as tornadoes, flash floods, hail storms, and hurricanes. When these conditions develop the GOES-9 satellites were able to monitor storm development and track their movements (NASA-GSFC and NOAA, 2007)

Water vapour absorbs and reradiates electromagnetic radiation in various wavelength bands. Such infrared radiation emitted by the Earth/atmosphere and intercepted by satellites. Water vapour molecules in the atmosphere absorb outgoing terrestrial radiation in the infrared region of the electromagnetic spectrum. The AVHRR sensor on the NOAA polar orbiting satellites had two thermal channels, near 11 and 12 μm , which were designed to correct for water vapour effects when predicting sea-surface temperatures. Several investigators had employed these thermal channels in estimating total column water vapour from the AVHRR sensor (~1.1 km at nadir) in a technique referred to as the split-window technique (Dalu, 1986; Kleespies and McMillin, 1990; Roger and Vermote, 1998). Figure 13 was illustrates the GOES-9 satellite images.

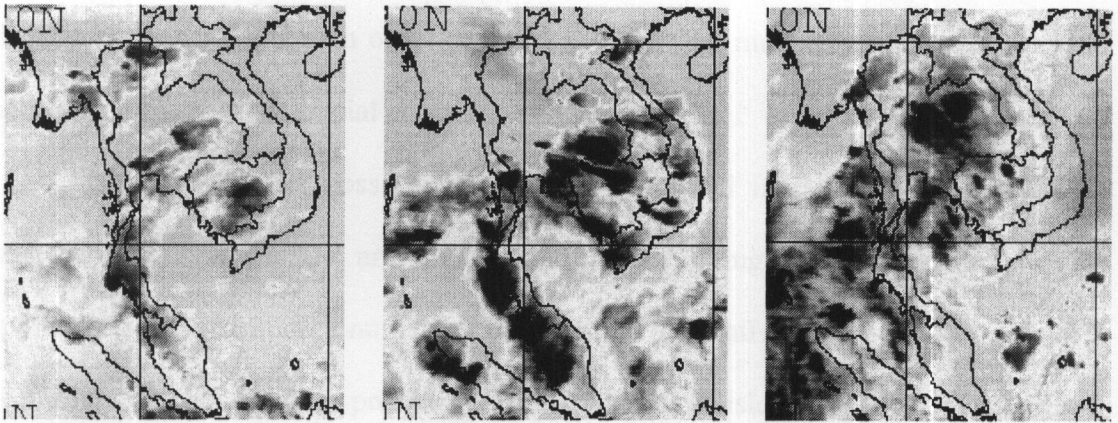


Figure 13 Snapshots of water vapour image from the GOES-9 satellite on Thailand.

METHODOLOGY

Related Work

The meteorological community had already established a number of numerical cloud analysis and forecasting systems. Much cloud analysis work had been carried out by using the empirical models and different types of satellite imaging or satellite observed data. For example, researcher proposed a cloud analysis method for rainfall forecasting in the Galician region of Spain (Roger and Vermote, 1998). They were applied a high-resolution non-hydrostatic numerical model to the satellite observations. They performed high-resolution cloud analysis based on statistical threshold of satellite imaging and numerical modelling (Plonski et al., 2000; Souto et al., 2003).

However, rather than using image processing techniques to handle satellite images, they were treated and handled as ordinary data. Although this method works very well on many problems and had wide application, it was difficult to integrate spatial information and the intrinsic spatial correlations between the image pixels and

the observed data values, in order to build an empirical model for the specific cloud analysis problems with spatial correlation considerations.

Although it was possible to build an empirical model in some cases, the unmanageable complexity and inadequate understanding might impede its wide application. Apart from the numerical methods, an alternative means could be chosen, according to the specific problem definition that considers spatial relationships. Researcher presented a cloud analysis method that automatically tracked clouds in meteorological satellite infrared images, based on area-overlapping analysis (Arnaud et al., 1992). They took the basic image processing and segmentation techniques to detect and track the clouds, without any assumptions of empirically physical models. From a meteorological perspective, Arnaud's approach had taken into account some basic meteorological phenomena, such as separation or merging of clouds. The method was fast and easy to compute, but the accuracy of correct cloud tracking was comparatively low, which affects its reliability when used for cloud analysis.

Image Processing Technique

Water vapour images were defined as a two-dimensional function, $f(x, y)$, where x and y were spatial (plane) coordinates, and the amplitude of f at any pair of coordinates x, y was called the intensity or grey level of the image at that point. When x, y and the amplitude values of f were all finite, discrete quantities, we called the image a digital image. The field of digital image processing refers to processing digital images by means of a digital computer (Gonzalez and Woods, 2002). A digital image results from a sampling of water vapour and produces a finite 2D array of

values uniformly distributed over the field of view, while the brightness was restricts the sample values to a finite integer range. These necessary operations converted real-world analogue sensory data to a form suitable for computer processing and storage.

Water vapour data from GOES-9 were obtained from IR sensors, which came in 0 to 255 values. Water vapour data were then transformed to RGB colours by Naval Department, USA, in JPEG format. We downloaded the vapour maps from the navy website to our local archive automatically at half an hour intervals. After that we were read and wrote of these common image formats of water vapour data from GOES-9 satellite and store in one of the computer supported image formats (Wolfram, 2004). The RGB colour scheme of water vapour was just one of many colour representation methods used in practice. The three so-called primary colours were combined (added) in various proportions to produce a composite, full-colour image.

For image processing applications, it was often useful to decouple the colour information from luminance. The HSV (hue, saturation, value) model had this property. Hue represents the dominant colour as seen by an observer, saturation refers to the amount of dilution of the colour with white light, and value defines the average brightness. The luminance component might, therefore, be processed independently of the image's colour information.

When processing colour images, we desired to change the colour format of the image. Colour format conversions were implemented as point operations. The RGB colour was converted to returns a three-channel image given specifies real colours in terms of hue, saturation and brightness, each between 0 and 1. Then, we were used image processing technique transform hue of three-channel HSV colour specification

to single channel monochrome image that given raw image data. This monochrome raw image data had a range between 0 and 1. We were used point transformations technique convert the raw image data to 0 to 255 values.

A monochrome digital image $f(x, y)$ was a 2D array of luminance (brightness) values (1).

$$f(x, y) = \begin{pmatrix} f(0,0) & f(0,1) & \cdots & f(0,N-1) \\ f(1,0) & f(1,1) & & f(1,N-1) \\ \vdots & & \ddots & \vdots \\ f(M-1,0) & f(M-1,1) & \cdots & f(M-1,N-1) \end{pmatrix} \quad (1)$$

With $f(x, y) \in Z$ where Z was the domain of the integers, and $0 \leq f(x, y) \leq L - 1$, where typically $L = 256$. Each element of the array was called a pixel (i.e. picture element). Values in this range could be efficiently represented by 8 binary digits (note that $2^8 = 256$) and therefore, each pixel occupied one byte in memory. Total storage requirements for an image were therefore of the order of $M \times N$ bytes, where M and N were the number of rows and columns in the image arrays.

The water vapour map was a two-dimensional geographic coordinate system. We transformed the plane coordinates (east and north or x, y) to geographic coordinates (longitude and latitude). Then it was deducted of the scale map, because the real earth's shape was irregular (Zhilin, 2007). Some information was lost in the first step of satellite products, in which an approximating, regular model was chosen. The scale was considered to be part of transforming plane coordinates to geographic coordinates. We used interpolating computational technique transform plan coordinates of water vapour image to geographic coordinates. The images were randomly opened to preview the monochrome images, which was illustrate in Figure 14.

We extracted the pixel value from monochrome grayscale images. The method was an automatic extracted pixel value data from the satellite image sequence. The data covers the time period from January to December 2004 that it was about 17,568 images in total process. The pixel value was extracted on water vapour image specify geographic coordinates from the rain gauge locations of number rainfall from TMD. It was automatic contribution geographic coordinates of rain gauge locations over water vapour images. Besides we were got pixel value form monochrome grayscale images, we were extracted date and time from file name of water vapour image. The spatial and temporal data of pixel value was integrated the intrinsic spatial correlations between the image information and the observed rainfall data values.

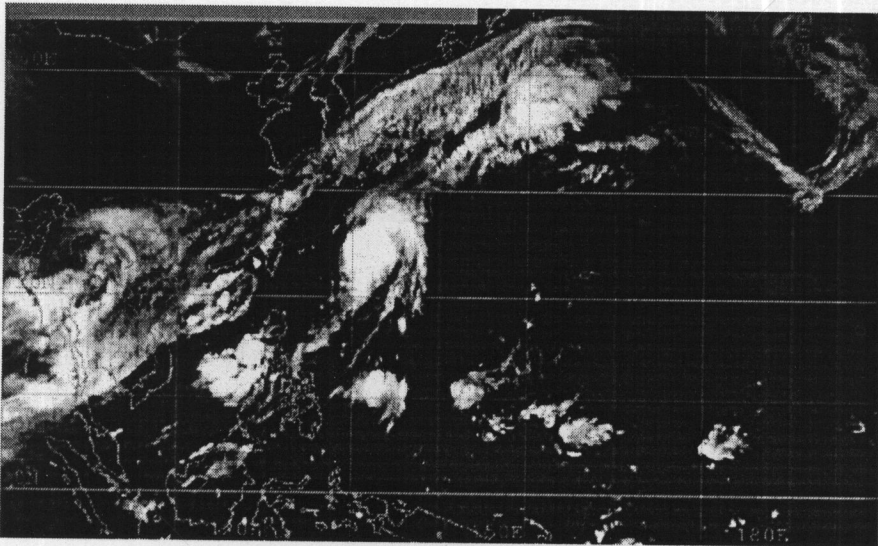


Figure 14 A monochrome digital image.

Rainfall occurred in the short time scales (generally less than 3 hr) over small spatial scales. Therefore, 48 monochrome images (24 hrs) were used for number daily rainfall from TMD. PVI was constructed by integrating all 48 images using mean and total pixel value technique. An image was designed to search the qualified pixels in

the satellite images, whose TMD values satisfy. This was followed by a general data analysis process, which aimed to segment the remaining qualified pixels image into several different clusters.

If there was a high amount of water vapour in all 48 images, PVI would be high value. The high PVI was means a high probability of rainfalls in 24 hours. Each image was transformed to pixel with a value ranging from 0-255. It contained only principal grey-level regions. The method could integrate spatial information and the intrinsic spatial correlations between the image pixels and the observed data values, in order to build an empirical model for the specific cloud analysis problems with spatial correlation considerations.

The PVI was achieving accurate identification and correct detecting of water vapour from the remote sensing image sequences which was over the rain gauge locations from TMD. It provided the indispensable premise for meteorologists to make further forecasts on weather events. Since the satellite image data were spatial temporal, we needed first identify and track water vapour from the entire image sequences correctly and efficiently, and then make the necessary characterization of the PVI by extracting meteorological features associated with them. To address this issue, we proposed a fast detecting and characterization method of water vapour according to their feature correspondences, derived from the meteorological satellite image sequences. The method was based on the fact that in a relatively small time-span. The pixel value was progressive and detectable, which guarantees a relatively similar area and texture in two consecutive satellite images.

EXPERIMENTAL RESULTS

The mathematical model was obtained from a least-square fit to a list of data as a linear combination of the specified basis functions. The fit function was giving a list of commonly required diagnostics such as the coefficient of determination R squared, the analysis of variance ANOVA table, and the mean squared error estimated variance. The output of regression functions could be controlled so that only needed information was produced. The basic functions f_i specify the predictors as functions of the independent variables. The resulting model for the response variable was $y_i = \beta_1 f_{1i} + \beta_2 f_{2i} + \dots + \beta_p f_{pi} + e_i$, where y_i was the i^{th} response, f_{ij} was the j^{th} basis function evaluated at the i^{th} observation, and e_i was the i^{th} statistical error.

Estimates of the coefficients β_1, \dots, β_p were calculated to minimise $\sum e_i^2$, the error or residual sum of squares. For example, simple linear regression was accomplished by defining the basic functions as $f_1 = 1$ and $f_2 = x$, in which case β_1 and β_2 were found to minimise $\sum [y_i - (\beta_1 + \beta_2 x_i)]^2$.

ANOVA table, a table for analysis of variance, provides a comparison of the given model to a smaller one including only a constant term. The table includes the degrees of freedom, the sum of squares and the mean squares due to the model (in the row labeled model) and due to the residuals (in the row labeled error). The residual mean square was also available in estimated variance, and was calculated by dividing the residual sum of squares by its degrees of freedom. The F -test compares the two models using the ratio of their mean squares. If the value of F was large, the null hypothesis supporting the smaller model was rejected.

To evaluate the importance of each basis function, we could get information about the parameter estimates from the parameter table. This table included the estimates, their standard errors, and t -statistics for testing whether each parameter was zero. The p -values were calculated by comparing the obtained statistic to the t distribution with $n-p$ degrees of freedom, where n was the sample size and p was the number of predictors. Confidence intervals for the parameter estimates, also based on the t distribution. We could be specified parameter confidence region the ellipsoidal joint confidence region of all fit parameters associated with basic functions $\{f_{i1}, f_{i2}, \dots\}$, a subset of the complete set of basic functions. Figure 15 illustrates the joint 95% confidence region of the regression parameters.

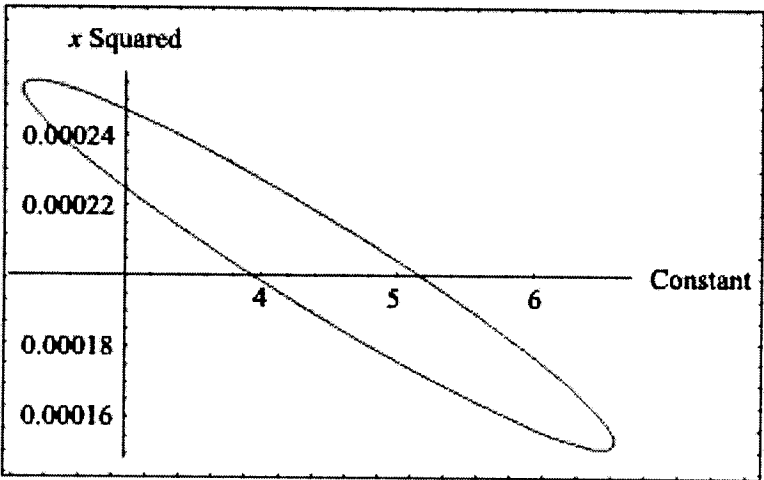


Figure 15 The joint 95% confidence region of the regression parameters from model $y_i = \beta_0 + \beta_1 x_i + e_i$.

The square of the multiple correlation coefficients was called the coefficient of determination R^2 , and was given by the ratio of the model sum of squares to the total

sum of squares. It was a summary statistic that describes the relationship between the predictors and the response variable. Adjusted R squared was defined as $\bar{R}^2 = 1 - \left(\frac{n-1}{n-p}\right)(1 - R^2)$, and gives an adjusted value that we could use to compare subsequent subsets of models. The coefficient of variation was given by the ratio of the residual root mean square to the mean of the response variable. If the response was strictly positive, this was sometimes used to measure the relative magnitude of error variation.

We had carried out experiments to evaluate PVI method with the amount of number rainfall proposed in the paper. We compared our PVI approach with the area-overlapping locations of number rainfall from TMD. We used the linear regression to examine the association between the averaged pixel value of daily water vapour images and the amount of daily rainfall (mm). The averaged pixel value of daily water vapour images was positively associated with the amount of daily rainfall.

The null hypothesis supporting the model was rejected ($F_{1,5162} = 92.1516$, $P < 0.001$, Table 5). This means that when we had a high averaged pixel value of daily water vapour data, we could also had a high amount of daily rainfall. This suggests that the amount of averaged pixel values could be used as an indicator of raining events. There were some positive associations between pixel values of daily water vapour images and the amount of daily rainfall at each rain gauge station throughout Thailand.

Table 5 The regression output for fitting the model $y_i = \beta_0 + \beta_1 x_i + e_i$, $*P < 0.001$.

ANOVA	df	SS	MS	F
Model	1	30240.400	30240.400	92.000*
Error	5162	0.169×10^{-5}	328.100	
Total	5163	0.172×10^{-5}		
Parameter	Estimate	SE	t-Value	
Constant	4.400	0.886	4.991	
x^2	0.200×10^{-3}	0.200×10^{-4}	9.599	
R ²	Adjust R ²	Estimated Variance		
0.017	0.017	328.159		

This means that when we had a high averaged pixel value of daily water vapour data, we could also had a high amount of daily rainfall (Figure 16). This suggests that the amount of averaged pixel values could be used as an indicator of raining events. There were some positive associations between pixel values of daily water vapour images and the amount of daily rainfall at each rain gauge station throughout Thailand.

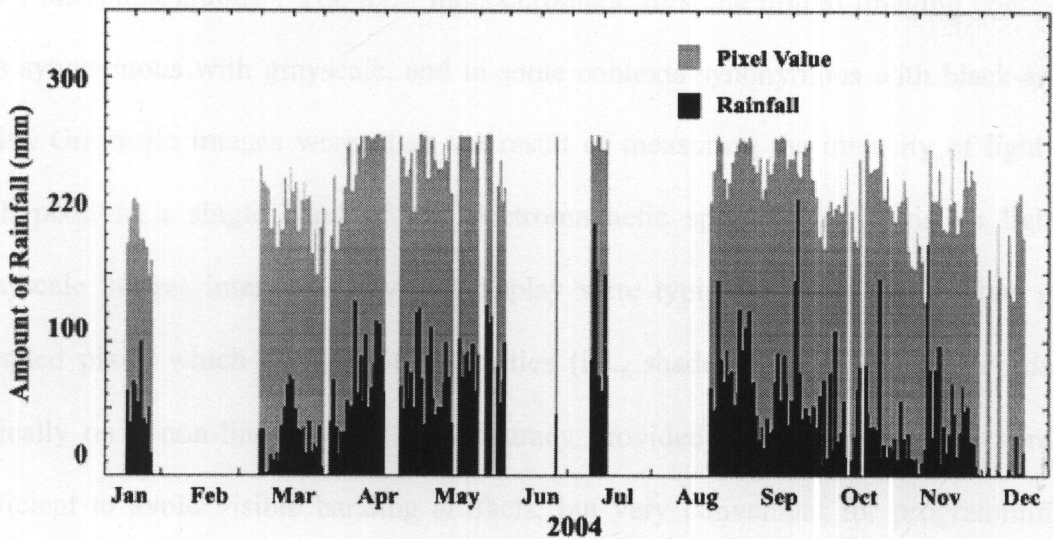


Figure 16 The association between the averaged pixel value of daily water vapour images and the amount of daily rainfall (mm) in Thailand from TMD.

The mathematical model was an abstract model that used mathematical language to describe the behaviour of a system. PVI mathematical consider a pixel value of water vapour image which describes an amount of daily rainfall. It was modelled by a function $y = 0.000203415x^2 + 4.424$ gave it an amount of daily rainfall in Thailand.

CONCLUSION

Grayscale images were distinct from black-and-white images, in which the contexts of computer imaging were images with only two colours, black and white; grayscale images had many shades of gray in between. In most contexts other than digital imaging, however, the term "black and white" was used in place of "grayscale"; for example, photography in shades of gray was typically called "black-

and-white photography". The term monochromatic in some digital imaging contexts was synonymous with grayscale, and in some contexts synonymous with black-and-white. Grayscale images were often the result of measuring the intensity of light at each pixel in a single band of the electromagnetic spectrum (e.g. visible light). Grayscale images intended for visual display were typically stored with 8 bits per sampled pixel, which allows 256 intensities (i.e., shades of gray) to be recorded, typically on a non-linear scale. The accuracy provided by this format was barely sufficient to avoid visible banding artifacts, but very convenient for programming. Technical used (e.g. in remote sensing applications) often require more levels, to make full use of the sensor accuracy (typically 10 or 12 bits per sample) and to guard against round off errors in computations. Sixteen bits per sample (65,536 levels) appears to be a popular choice for such uses.

PVI was another method that could be used for approximating the amount of daily rainfall from water vapour data from GOES-9 satellite. Image processing applications was often useful to decouple the colour information from luminance. The HSV model had this property. Hue represents the dominant colour as seen by an observer, saturation refers to the amount of dilution of the colour with white light, and value defines the average brightness. The luminance component might, therefore, be processed independently of the image's colour information.

We desired to change the colour format of the image. Colour format conversions were implemented as point operations. The RGB colour was converted to returns a three-channel image given specifies real colours in terms of hue, saturation and brightness, each between 0 and 1. Then, we used image processing technique transform hue of three-channel HSV colour specification to single channel

monochrome image that given raw image data. This monochrome raw image data had a range between 0 and 1. The final image was used point transformations technique convert the raw image data to 0 to 255 values.

The PVI was extracted pixel value from monochrome image. The monochrome images were given grayscale digital image. It was an image in which the value of each pixel was a single sample. Displayed images of this sort were typically composed of shades of gray, varying from black at the weakest intensity to white at the strongest, though in principle the samples could be displayed as shades of any colour, or even coded with various colours for different intensities. Characteristic of high amount water vapour on monochrome images could detect with black shade of images. Also, the contour and grid line of map was black shade similar high amount of water vapour on monochrome images. There were few spatial data available on TMD locations that overlapping on contour line of geographic map and grid of geographic coordinates. Some information of water vapour pixel value was failed to spot over contour and grid line of map. We were used a nearest pixel value replace some pixel lost information.

Besides, there were associated between the averaged pixel value of daily water vapour images and the amount of daily rainfall. Therefore, the pixel value of water vapour was a new way to predict the raining events. Then in the future, we could use these data to predict raining season in each areas. Moreover, this technique could be used to study climate change in term of anomalies in the amount of water vapour data because our results could provide a more accurate estimation of climate change and more data points because we could estimate the water vapour data every half an hour.

However, there were some limitations of this current technique. This technique depended on a real time availability of GOES-9 satellites data. Then, if the Internet was down or not reliable, downloading the GOES-9 satellite data could not be possible and satellite data, that were already downloaded, might be corrupted. This application required high bandwidth of the Internet connection. Another limitation was the resolution of the on-board satellite sensors. For current GOES-9 satellites, the resolution was somewhat at mesoscale, so it was not possible to pinpoint a small size. Finally, at the time of doing this research, we had very limited access to data from Thai meteorological department to validate our technique. These data were rain gauge collected data from 75 stations.

In the future, this technique should be modified to use for prediction a drought risk area as an inverse function. NASA was launching a CloudSat satellite that would be closely related to this work. Data from this mission should also be used to fine tune of this technique.

ACKNOWLEDGEMENTS

This work was supported in part by PTT Public Company Limited, TOTAL Foundation and TOTAL E&P Thailand, TRF/Biotec special program for Biodiversity Research Training grant BRT T_550001, Commission on Higher Education, and CXKURUE, the Institute of Research and Development, Walailak University. The authors thank Thailand Meteorological Department for their supporting the amount of daily rainfall at each rain gauge station in Thailand. The authors were also grateful to the editors and reviewers for their valuable comments and suggestions on this manuscript.

REFERENCES

- Arnaud Y., Desbios M. and Maizi J. (1992). Automatic tracking and characterization of African convective systems on meteosat pictures. *Journal of Applied Meteorology*, 31(5), 443-453.
- Bonazountasa M., Kallidromitoub D., Kassomenosc P. and Passasd N. (2007). A decision support system for managing forest fire casualties. *Journal of Environment Management*, 84, 412-418.
- Boussetta S., Koike T., Yang K., Graf T. and Pathmathevan M. (2008). Development of a coupled land-atmosphere satellite data assimilation system for improved local atmospheric simulations. *Remote Sensing of Environment*, 112(3), 720-734.
- Brakenridge G. R. and Anderson E. (2002). 2001 Global Register of Extreme Flood Events, *Dartmouth Flood Observatory*, Retrieved 25 January 2002 from <http://www.dartmouth.edu/~floods/Archives/2001sum.htm>.
- British Broadcasting Corporation. (2001). Thailand floods kill 70. *BBC News*, Retrieved 12 August 2001 from <http://www.wsws.org/articles/2001/sep2001/thai-s04.shtml>.
- Dalu G. (1986). Satellite remote sensing of atmospheric water vapour. *International Journal of Remote Sensing*, 7, 1089-1097.
- Divjak C. and Conachy J. (2001). Flood tragedy in Thailand linked to deforestation, *World Socialist Web Site*. Retrieved 4 September 2001 from <http://www.wsws.org/articles/2001/sep2001/thai-s04.shtml>.

- Ellrod G. P., Achutuni R. V., Daniels J.M., Prins E. M. and Nelson J. P. (1998). An assessment of GOES-8 imager data quality. *Bulletin of the American Meteorological Society*, 79, 2509-2526.
- Errico M. D. and Fasano G. (2008). Design of interferometric and bistatic mission phases of COSMO/SkyMed constellation. *Acta Astronautica*, 62(2-3), 97-111
- Feidas H., Kontosa T., Soualakellisa N. and Lagouvardosb K. (2007). A GIS tool for the evaluation of the precipitation forecasts of a numerical weather prediction model using satellite data. *Computers and Geosciences*, 33, 989-1007.
- Fisher J. I. and Mustard J. F. (2007). Cross-scalar satellite phenology from ground, Landsat, and MODIS data. *Remote Sensing of Environment*, 109, 261-273.
- Gonzalez, R. C. and Woods, R. E. (2002). Image Segmentation. *Digital Image Processing (2nd Edition)*, Euclid W.M. (Editor), Pearson Education (Singapore) Pte. Ltd., Indian Branch, 567-636.
- Guo J., Fu G., Li Z., Shao L., Duan Y. and Wang J. (2007). Analyses and numerical modelling of a polar low over the Japan Sea on 19 December 2003, *Atmospheric Research*, 85, 395-412.
- Houze R., Smull B. and Dodge P. (1990). Mesoscale organization of springtime rainstorms in Oklahoma. *Monthly Weather Review*, 118(3), 613-654.
- Kleespies, T. J. and McMillin, L. M. (1990). Retrieval of precipitable water from observations in the split window over varying surface temperatures. *Journal of Applied Meteorology*, 29, 851-862.
- Lucas R., Rowlands A., Brown A., Keyworth S. and Bunting P. (2007). Rule-based classification of multi-temporal satellite imagery for habitat and agricultural

- land cover mapping. *ISPRS Journal of Photogrammetry and Remote Sensing*, 62, 165-185.
- Marconi M. L. (2007). A kinetic model of Ganymede's atmosphere. *Icarus*, 190, 155-174.
- Meyer K., Yang P. and Gao B. C. (2007). Tropical ice cloud optical depth, ice water path, and frequency fields inferred from the MODIS level-3 data. *Atmospheric Research*, 85, 171-182.
- NASA-GSFC and NOAA. (2007). GOES-J Status, Retrieved 12 March 2007 from <http://rsd.gsfc.nasa.gov/goes/text/goesjstatus.html>.
- Pardé M., Goïta K. and Royer A. (2007). Inversion of a passive microwave snow emission model for water equivalent estimation using airborne and satellite data. *Remote Sensing of Environment*, 111(2-3), 346-356.
- Plonski M. P., Gustafson G., Shaw B., Thomas B. and Wonsick M. (2000). High resolution cloud analysis and forecast system. *Proceeding of the 10th Conferences on Satellite Meteorology and Ocean of American Meteorology Society*, Long Beach, CA, USA, 114-117.
- Roger, J. C. and Vermote, E. F. (1998). A method to retrieve the reflectivity signature at 3.75 μ m from AVHRR Data. *Remote Sensing of the Environment*, 64, 103-114.
- Souto M. J., Balseiro C. F., Pe'rez-Mun~uzuri V., Xue M. and Brewster K. (2003). Impact of cloud analysis on numerical weather prediction in the Galician region of Spain. *Journal of Applied Meteorology*, 42, 129-140.
- Vescovo L. and Gianelle D. (in press). Using the MIR bands in vegetation indices for the estimation of grasslands biophysical parameters from satellite remote

sensing in the Alps region of Trentino (Italy), *Advances In Space Research*, submitted for publication.

Wolfram S. (2004). The Mathematica Book, *Book News*, (5th edition), Oregon.

Wong N. H., Jusuf S. K., Win A. A. L., Thu H. K., Negara T. S. and Xuchao W. (2007). Environmental study of the impact of greenery in an institutional campus in the tropics. *Building and Environment*, 42, 2949-2970.

Xiaoa H. and Wengb Q. (2007). The impact of land use and land cover changes on land surface temperature in a karst area of China. *Journal of Environment Management*, 85, 245-257.

Zhilin, S. I. (2007). Simple method for outlier detection in fitting experimental data under interval error. *Chemometrics and Intelligent Laboratory Systems*, 88, 60-68.

CHAPTER V

MATHEMATICAL MODEL FOR SOLAR RADIATION AND TEMPERATURE FIELD VERIFICATION

PUBLICATION

Chairote Yaiprasert, Krisanadej Jaroensutasinee and Mullica Jaroensutasinee, 2007.

Mathematical Model for Solar Radiation and Temperature Field Verification

(in preparation).

ABSTRACT

Solar radiation data was considered as the most important parameter in renewable energy application. However, these data were not always available particularly in isolated sites due to the non-availability of the meteorological stations in these sites. Fortunately, the GMS-6 satellite images were always available because we could automatically download the vapour map satellite image at half an hour intervals. This paper was introduced a new approach for predicting and modelling of solar radiation data and temperature from pixel value of satellite images by using mathematical model. The pixel value was positively associated with solar radiation, and also irradiance was positively associated with the temperature. The methodology could be applied to any geographical area in the world.

Keywords: GMS-6 satellite images, image processing, pixel value, solar radiation, temperature.

INTRODUCTION

Daily total solar radiation data was considered such as the most important parameter in the meteorology, solar conversion, and renewable energy application (Hokoi et al., 1990; Egido and Lorenzo, 1992; Shrestha and Goel, 1998; Mellit et al., 2003; 2005b). Unfortunately, this parameter was not always available particularly in remote areas, where there were no meteorological stations installed in these locations. For this reason several researchers had been interested in developing several approaches for generating this parameter (Aguilar and Collares-Pereira, 1992; Lopez and Sidrash-de-Cardona, 1998; Guessoum et al., 1998), some more recent works were interesting to predict this parameter using the artificial intelligence techniques (Mohandes et al., 2000; Sfetsos and Coonick, 2000; Kalogirou et al., 2002; Mellit et al., 2004; 2005a)

In addition, a suitable model for forecasting the future solar radiation data based on preceded data, using the wavelet-network model we had developed (Mellit et al., 2006). However, this model cannot be used for estimating the total solar radiation data in remote area, but it gives a good accuracy results for prediction when we had some preceded data. The purpose of this work was to develop a new approach for predicting of daily solar radiation from satellite image using image processing technique and it was transformed for predicting temperature by using mathematical model. The application of solar radiation and temperature were determined from experimental work, field observations and knowledge of satellite data (Yaiprasert et al., 2007)

In order to improve the current measures of severe heat controls in the environment, it was necessary to accurately predict and/or gather the amount of solar

radiation in order to be able to determine the possibility of excess amount of solar radiation causing increase SST. However, it was not practical to install a vast number of automatic solar radiation sensors throughout the remote area that could transmit this solar radiation information to achieve the measures. It was then desirable to look for a continuous source of weather information and the meteorological satellites could provide such information. Therefore, it would be of urgent task to determine the amount of solar radiation and correlate these quantities to water vapour satellite data by using image processing technique over Thailand region (Strong, 1991; Bonazountasa et al., 2007; Feidasa et al., 2007; Marconi, 2007; Pardé et al., 2007).

DATA SOURCES

Satellite images had been used extensively to study temporal changes. Information and knowledge of water vapour dynamic systems were crucial to heavy rainfall forecast the collection of large amounts of satellite data with high spatial and temporal resolutions was indispensable (Dalu, 1986; Kleespies and McMillin, 1990; Wong et al., 2007). For this purpose, satellite remote sensing images of the water vapour data, taken by the GMS-6 satellite (Figure 17). The meteorological data used in this work were the mean daily temperature and the solar radiation. These data had been recorded by a weather station network located in Walailak University, Nakhon Si Thammarat, Thailand. Through this weather station network data, as an example, Figure 18 and Figure 19 shown a daily mean temperature and mean solar radiation data, respectively.

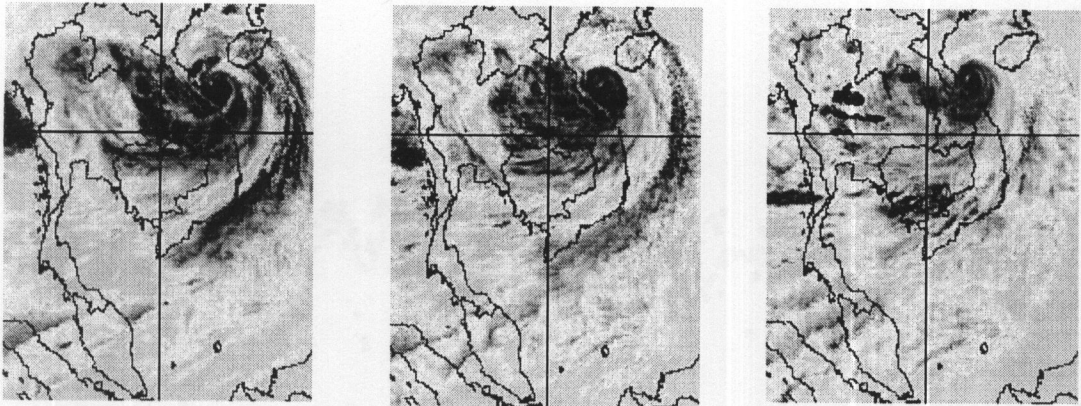


Figure 17 Snapshots of water vapour image from the GMS-6 satellite on Thailand (October 2007).

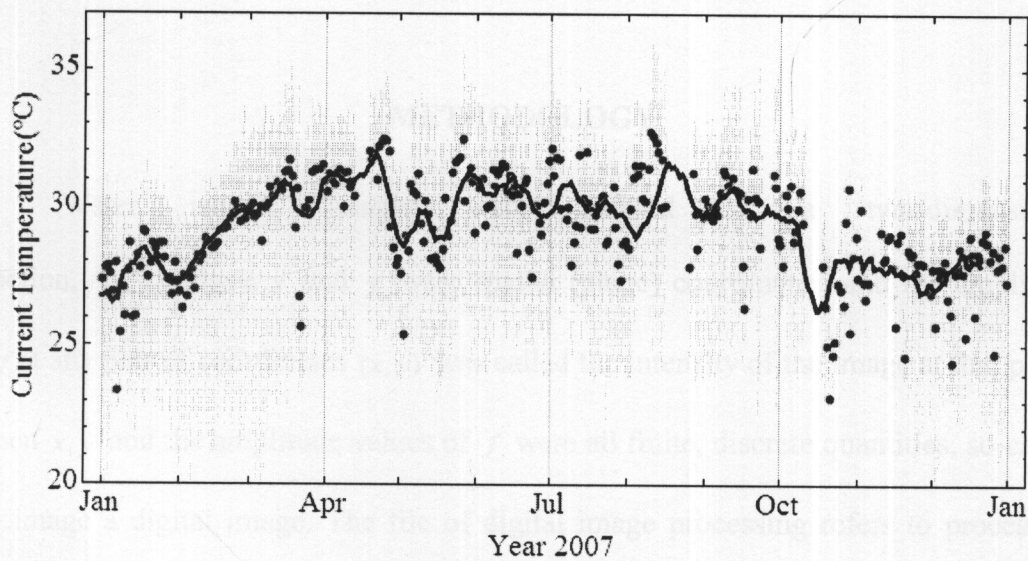


Figure 18 Daily mean temperature data (red points) and moving average temperature (blue solid line) during January-December 2007.

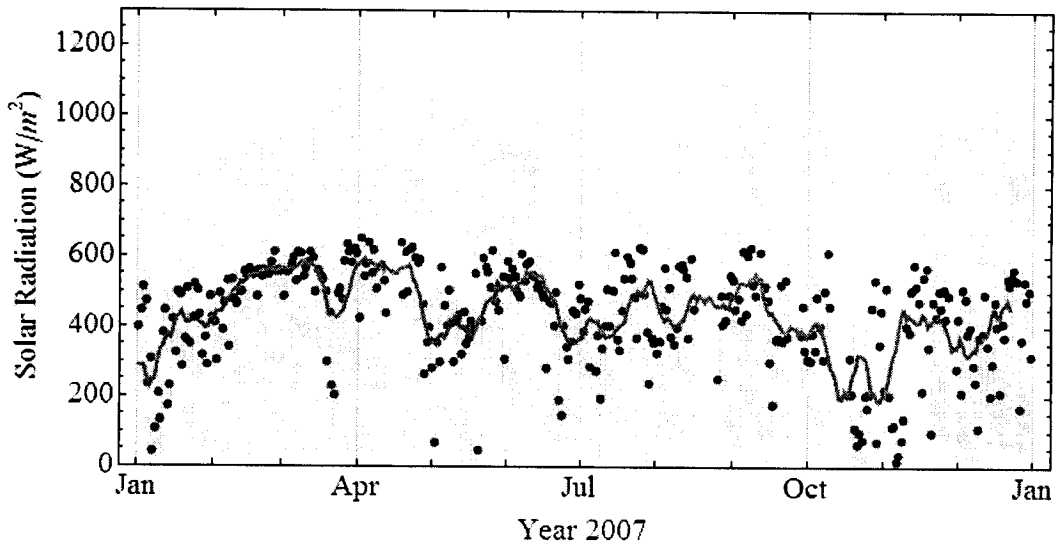


Figure 19 Daily mean solar radiation data (red points) and moving average solar radiation (green solid line) during January-December 2007.

METHODOLOGY

Water vapour images were defined as a two-dimensional function, $f(x, y)$, where x and y were spatial (plane) coordinates, and the amplitude of f at any pair of coordinates (x, y) was called the intensity of the image at that point. When x, y and the amplitude values of f were all finite, discrete quantities, so-called the image a digital image. The field of digital image processing refers to processing digital images by mean of a digital computer (Gonzalez and Woods, 2002). A digital image results from a sampling of water vapour was produces a finite 2D array of values uniformly distributed over the field of view, while the brightness was restricts the sample values to a finite integer range. These necessary operations converted real-world analogue sensory data to a form suitable for computer processing and storage.

Water vapour data from GMS-6 were obtained from IR sensors, which came in 0 to 255 values. Water vapour data were then transformed to RGB colours by Naval Department, USA, in JPEG format. We downloaded the vapour maps from the navy website to our local archive automatically at half an hour intervals. After that we were read and wrote of these common image formats of water vapour data from GMS-6 satellite and store in one of the computer supported image formats. The RGB colour scheme of water vapour was just one of many colour representation methods used in practice. The three so-called primary colours were combined (added) in various proportions to produce a composite, full-colour image (Wolfram, 2004).

For image processing applications, it was often useful to change the colour format of the image. Colour format conversions were implemented as point operations. The RGB colour was converted to returns a three-channel image given specifies real colours in terms of hue, saturation and brightness, each between 0 and 255. Then, point transformations image processing technique was used convert the image data to 0 to 255 values. Figure 20 was illustrated colour bar value and mathematical point transformations image processing technique.

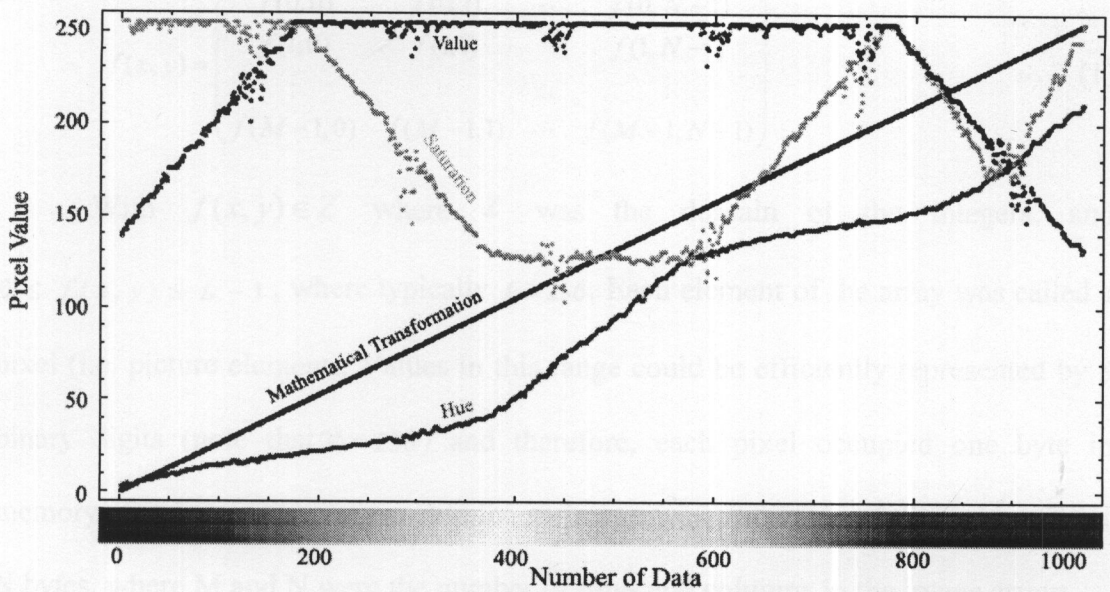


Figure 20 Colour bar diagram; hue value (red), saturation (green), value (blue), and mathematical transformation (black).

When processing colour images, it automatically adjusted the overall tonal range of an image, specified clipping percentages, and assigned colour values to shadows, midtones, and highlights

Besides, it desired to change the colour format of the image. Colour format conversions were implemented as point operations. The RGB colour was converted to returns a three-channel image given specifies real colours in terms of hue, saturation and brightness, each between 0 and 1. Then, we were used point transformations image processing technique convert the image data to 0 to 255 values.

Equation (1) was shown the digital image $f(x, y)$ in a 2D array of luminance (brightness) values.

$$f(x, y) = \begin{pmatrix} f(0,0) & f(0,1) & \cdots & f(0,N-1) \\ f(1,0) & f(1,1) & & f(1,N-1) \\ \vdots & & \ddots & \vdots \\ f(M-1,0) & f(M-1,1) & \cdots & f(M-1,N-1) \end{pmatrix} \quad (1)$$

With $f(x, y) \in Z$ where Z was the domain of the integers, and $0 \leq f(x, y) \leq L - 1$, where typically $L = 256$. Each element of the array was called a pixel (i.e. picture element). Values in this range could be efficiently represented by 8 binary digits (note that $2^8 = 256$) and therefore, each pixel occupied one byte in memory. Total storage requirements for an image were therefore of the order of $M \times N$ bytes, where M and N were the number of rows and columns in the image arrays.

The water vapour map was a two-dimensional geographic coordinate system. We transformed the plane coordinates (east and north or x, y) to geographic coordinates (longitude and latitude). Then it was deducted of the scale map, because the real earth's shape was irregular (Zhilin, 2007). Some information was lost in the first step of satellite products, in which an approximating, regular model was chosen. The scale was considered to be part of transforming plane coordinates to geographic coordinates. We used interpolating computational technique transform plan coordinates of water vapour image to geographic coordinates.

An equation of the geometry correction for an image had been expressed as follows:

$$G = a_0 + a_1 T + a_2 T^2 + \dots + a_n T^n \quad (2)$$

Where $T = t - t_0$, t_0 was constant, $a_i (i = 0, 1, 2, 3, \dots, n)$ were adjustable parameter. In general, a_0 was a position parameter, a_1 was a size parameter, a_2 was a Correction parameter (C) and a_3 was a Correction parameter (S). The definition of

the parameters were rather different according to demanded accuracy of the correction

An image sequence was various full-colour images and whose active ratios were not constant and widely range in value. Therefore, there needed to vary the size and the position parameters according to input and full-colour images. However, mismatches between the correction pixel value and the image occur because one correction parameter was independent of other correction parameters. For example, when the position was varied, one saw unbalance distortion in the image and one needed to vary the C correction parameter in connection with the position parameter.

Furthermore, the position parameter needed to correlate with the size parameter because the vertical size was affected by C correction parameter. This also held true with the S correction parameter. These were the reasons why there needed for correlative equations and interpolative calculations using pre-set data of these control parameters and tracking adjustment with the size, the position, C correction and S correction.

In order to eliminate correlative equations and interpolative mathematical calculations of control parameters and tracking adjustment, a concept of imaginary position coordinate for the satellite image was introduced into a geometric correction pixel value generator. This concept realised constant pixel value of correction for image through the following procedure.

Arbitrary reference points were select on the image and decide corresponding values of the correction pixel value generator's output. It seems to be convenient that one reference point was in the upper and lower side on the image.

An input parameter (x) was define to the correction pixel value generator including the colour value (V), number of full-colour image data (n) and parameters

as equation (3) .

$$x = \frac{n}{255} V_i; i = 0 - 255 \quad (3)$$

A function of the correction pixel value generator was selected and automatic calculated. The image distortion was corrected as this function:

$$y_{n+1} = y_n + h_n f(t_n, y_n) \quad (4)$$

$$y_{n+1/2} = y_n + \frac{h_n}{2} f(t_n, y_n) \quad (5)$$

$$y_{n+1} = y_n + h_n f(t_{n+1/2}, y_{n+1/2})$$

$$y_{n+1} = y_n + h_n f(t_{n+1}, y_{n+1}) \quad (6)$$

$$y_{n+1} = y_n + h_n f(t_{n+1/2}, \frac{1}{2}(y_{n+1} + y_n)) \quad (7)$$

$$y_{n+1} = y_n + \frac{h_n}{2} (f(t_n, y_n) + f(t_{n+1}, y_{n+1})) \quad (8)$$

$$(I - h_n J)(y_{n+1} - y_n) = h_n f(t_n, y_n) \quad (9)$$

$$\begin{aligned}
(I - \frac{h_n}{2} J)(y_{n+1/2} - y_n) &= \frac{h_n}{2} f(t_n, y_n) \\
(I - \frac{h_n}{2} J) \frac{(\Delta y_n - \Delta y_{n-1/2})}{2} &= \frac{h_n}{2} f(t_{n+1/2}, y_{n+1/2}) - \Delta y_{n-1/2}
\end{aligned} \tag{10}$$

Here $\Delta y_n = y_{n+1} - y_{n+1/2}$, I denoted the identity matrix and J denoted the Jacobian matrix $\frac{\partial f}{\partial y}(t_n, y_n)$. In a typical case, if it had differential equations with up to n^{th} derivatives, then it needed to either give initial conditions for up to $(n-1)^{th}$ derivatives, or give boundary conditions at n points.

The method was an automatic extracted pixel value data from the satellite image sequence. It was automatic contribution geographic coordinates of weather station network locations over water vapour images. Besides, the pixel values were got from the images, which were extracted date and time from file name of water vapour image. The spatial and temporal data of pixel value was integrated the intrinsic spatial correlations between the image information and the observed solar radiation data values.

GMS-6 satellite images were used for number solar radiation from weather station network. Solar radiation in the solar radiation was short time scales (generally 7.00-17.00) over small spatial scales. Therefore, 3 satellite images (1 hr) were used for number solar radiation from weather station network. An image was designed to search the qualified pixels in the satellite images, whose weather station network values satisfy. This was followed by a general data analysis process, which aimed to segment the remaining qualified pixels image into several different clusters.

The method was an automatic extracted pixel value data from the satellite

image sequence. It was automatic contribution geographic coordinates of weather station network locations over water vapour images. Besides we were get pixel value form the images. It was extracted date and time from file name of water vapour image. The spatial and temporal data of pixel value was integrated the intrinsic spatial correlations between the image information and the observed solar radiation data values.

Temperature and solar radiation data were imported data from a file, assuming that it was in the format indicated by the file extension, and converts it to a *Mathematica* expression. It could handle numerical and textual data and graphics. The weather station network data were operated in date and time. It could use *Mathematica* functional programming to convert a date string into a date list, as long as the date format was sufficiently unambiguous.

The *Mathematica* functional programming returns whatever weather data system gives as the current date and time. It assumed that any corrections for daylight saving time and so on had already been done by our computer system. In addition, it assumes that our computer system had been set for the appropriate time zone. The variable time zone returns the current time zone assumed by our computer system. The time zone was given as the number of hours which must be added to Greenwich Mean Time (GMT) to obtain the correct local time.

Pixel value and weather station network data were correlated by using date and time matrix operating system in *Mathematica* programming. The technique was founds a least-squares fit to a list of data as a linear/nonlinear combination of the functions of variable.

EXPERIMENTAL RESULTS

A computer program for modelling of daily solar radiation data based on the developed algorithm presented above image processing technique had been implemented using *Mathematica* functional programming. So the empirical function for this system as applied to solar radiation monitoring was following:

$$S_a = 261.623 + 3.277x \quad (11)$$

Where S_a was the calculated irradiance and x was the pixel value recorded by the acquisition image processing technique.

A typical correlation graph was shown in Figure 21. In order to examine the correctness of the linear combination of the functions, the data acquisition system readings were recorded against corresponding pixel value readings and equation (11) used to estimate the irradiance.

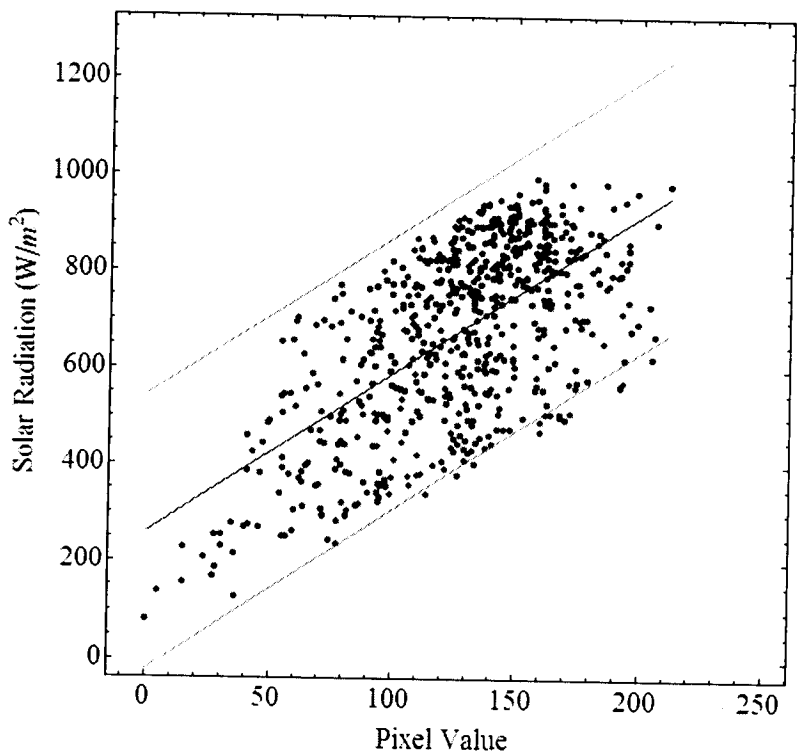


Figure 21 The 95% confidence interval predicted responses of solar radiation (W/m^2).

However, during partly cloudy days, relatively wide scatters were obtained. This was mainly due to the difference in response times of the GMS-6 satellite images, with the satellite images less able to respond quickly to rapid changes in irradiance levels. The data acquisition system takes about 30 minutes. So the wide scatters were primarily due to the satellite images being unable to follow rapid changes of radiation associated with clear-cloudy transitions during partly cloudy conditions. Consequently some significant calibration errors occurred during the transition period. This aspect was discussed by Suereke et al., 1990 and Michalsky et al., 1991.

The mathematical model was an abstract model that used mathematical language to describe the behaviour of a system. Mathematical model considers a solar radiation which describes a sea surface light intensity. It was modelled by a function:

$$L = -3.913 + 0.339S \quad (12)$$

Where L was the calculated sea surface light intensity and S was the digital irradiance data value recorded by the acquisition system.

Figure 22 shown the scattering diagram, which allow the comparison of predicted values of sea surface light intensity. The strong scattering of the points and good agreement was observed between the irradiance and sea surface light intensity. In other words, the irradiance was the more it tends to sea surface light intensity. Thus, the developed model seems to be adequate to fit daily sea surface light intensity data.

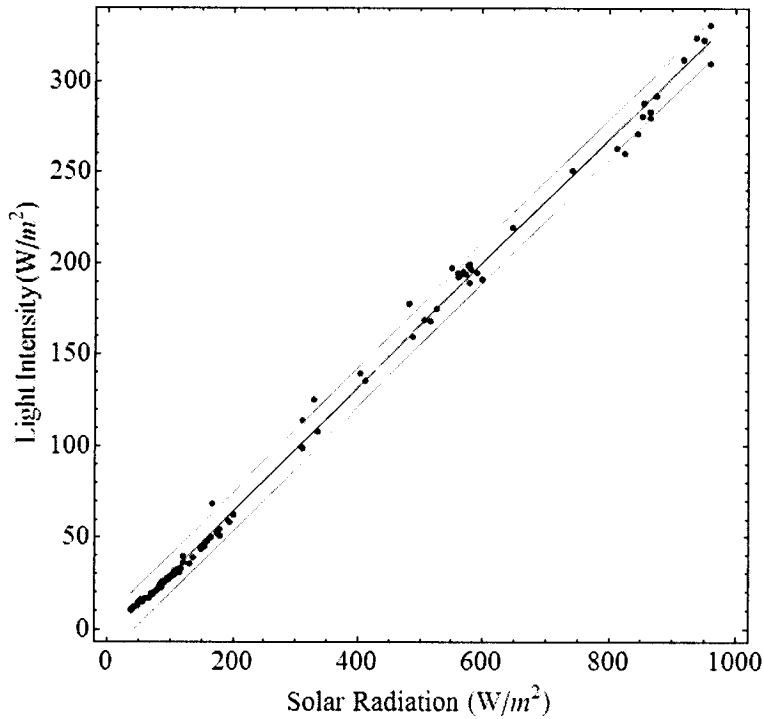


Figure 22 The 95% confidence interval predicted responses of sea surface light intensity (W/m^2).

The mathematical model considers a sea surface light intensity which describes a SST. So the empirical function for this system as applied to SST monitoring was following:

$$T_{sst} = 28.39 + 0.019 L \quad (13)$$

Where L was the calculated sea surface light intensity and T_{sst} was the measurement sea surface light intensity data value recorded by the acquisition system.

Figure 23 shown the scattering diagram, which allow the comparison of predicted values of SST. According to this scatter diagram, there seem to be a positive correlation between the sea surface light intensity and SST. A strong relationship

between the two variables was observed when most of the points fall along an imaginary straight line with a positive slope.

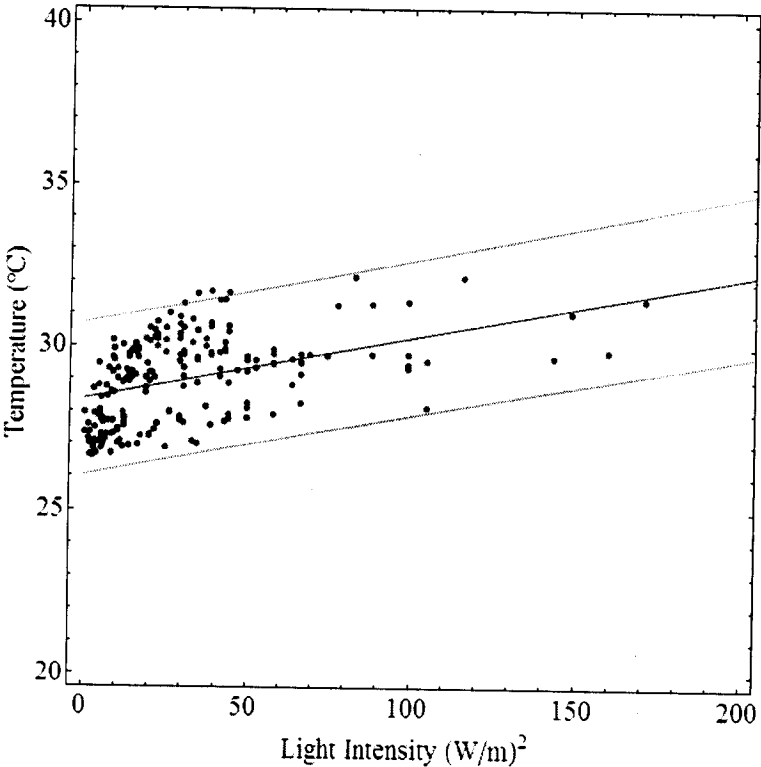


Figure 23 The 95% confidence interval predicted responses of SST (°C).

Figure 24 illustrates clearly the superposition of measured SST data and simulated SST output of the proposed pixel value mathematical model, corresponding to year 2007. The measured and simulated temperature data was plotted. This model was validated by comparison between the simulated temperature results, the actual temperature data and NOAA SST that were a good agreement between the three series.

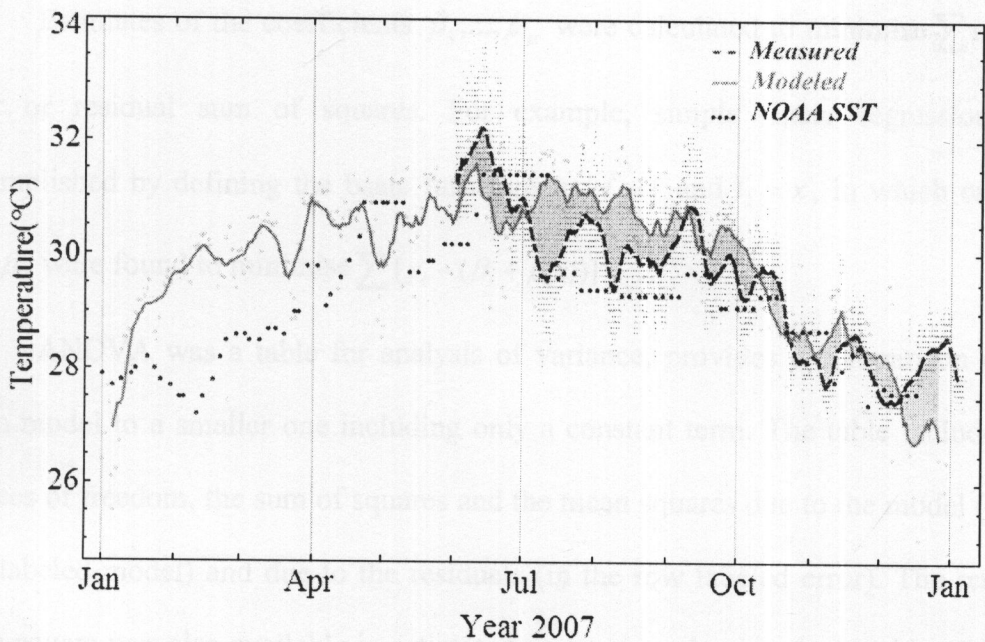


Figure 24 Comparison between measured SST data (red dash line), calculated SST data (green solid line) by the proposed mathematical model and NOAA SST data (blue points), corresponding to year 2007.

The mathematical model was obtained from a least-square fit to a list of data as a linear combination of the specified basis functions. The fit function was giving a list of commonly required diagnostics such as the coefficient of determination R^2 , the analysis of variance ANOVA table, and the mean squared error estimated variance. The output of regression functions could be controlled so that only needed information was produced. The basic functions f_i specify the predictors as functions of the independent variables.

The resulting model for the response variable was $y_i = \beta_1 f_{1i} + \beta_2 f_{2i} + \dots + \beta_p f_{pi} + e_i$, where y_i was the i^{th} response, f_{ij} was the j^{th} basis function evaluated at the i^{th} observation, and e_i was the i^{th} statistical error.

Estimates of the coefficients β_1, \dots, β_p were calculated to minimise $\sum e_i^2$, the error or residual sum of squares. For example, simple linear regression was accomplished by defining the basic functions as $f_1 = 1$ and $f_2 = x$, in which case β_1 and β_2 were found to minimise $\sum_i [y_i - (\beta_1 + \beta_2 x_i)]^2$.

ANOVA was a table for analysis of variance, provides a comparison of the given model to a smaller one including only a constant term. The table includes the degrees of freedom, the sum of squares and the mean squares due to the model (in the row labeled model) and due to the residuals (in the row labeled error). The residual mean square was also available in estimated variance, and was calculated by dividing the residual sum of squares by its degrees of freedom. The F -test compares the two models using the ratio of their mean squares. If the value of F was large, the null hypothesis supporting the smaller model was rejected.

To evaluate the importance of each basis function, we could get information about the parameter estimates from the parameter table. This table included the estimates, their standard errors, and t -statistics for testing whether each parameter was zero. *The p -values were calculated by comparing the obtained statistic to the t distribution with $n-p$ degrees of freedom, where n was the sample size and p was the number of predictors.* Confidence intervals for the parameter estimates, also based on the t distribution. We could be specified parameter confidence region the ellipsoidal joint confidence region of all fit parameters associated with basic functions $\{f_{i1}, f_{i2}, \dots\}$, a subset of the complete set of basic functions.

The square of the multiple correlation coefficients was called the coefficient of determination R^2 , and was given by the ratio of the model sum of squares to the total

sum of squares. It was a summary statistic that describes the relationship between the predictors and the response variable. Adjusted R squared was defined as $\bar{R}^2 = 1 - \left(\frac{n-1}{n-p}\right)(1 - R^2)$, and gives an adjusted value that we could use to compare subsequent subsets of models. The coefficient of variation was given by the ratio of the residual root mean square to the mean of the response variable. If the response was strictly positive, this was sometimes used to measure the relative magnitude of error variation.

The averaged pixel value of daily water vapour images was positively associated with the amount of solar radiation. The F -test using the ratio of their mean squares which the value of F was large and P lesser than 0.001 ($F_{1,416} = 337.809$, $P < 0.001$). The null hypothesis supporting the model was rejected (see Table 6). This means that when we had a high averaged pixel value of daily water vapour data, we could also had a high amount of irradiance.

The daily mean solar radiation was positively associated with the daily mean temperature. The F -test using the ratio of their mean squares which the value of F was large and P lesser than 0.001 ($F_{1,329} = 520.714$, $P < 0.001$). The null hypothesis supporting the model was rejected (see Table 7). This means that when we had a high amount solar radiation data, we would also have a high amount of temperature.

Table 6 The regression output of pixel value and solar radiation for fitting the

model $y_i = \beta_0 + \beta_1x_i + e_i, P < 0.001$.

ANOVA	df	SS	MS	F
Model	1	5.400 x 10 ⁶	5.400 x 10 ⁶	337.809*
Error	416	5.950 x 10 ⁶	14303.200	
Total	417	1.140 x 10 ⁷		
Parameter	Estimate	SE	t-Value	
Constant	86.339	20.335	4.246	
x	3.163	0.163	19.437	
R ²	Adjust R ²	Estimated Variance		
0.475	0.476	14303.200		

Table 7 The regression output of solar radiation and temperature for fitting the model $y_i = \beta_0 + \beta_1 x_i + e_i$, $P < 0.001$.

ANOVA	df	SS	MS	F
Model	1	796.550	796.550	520.714*
Error	329	503.280	1.529	
Total	330	1299.830		
Parameter	Estimate	SE	t-Value	
Constant	25.038	0.235	106.890	
x	0.009	0.396×10^{-3}	22.819	
R ²	Adjust R ²	Estimated Variance		
0.613	0.612	1.529		

CONCLUSION

The distribution of temperature over the world and its variations through the year depend primarily on the amount of radiant energy received from the sun in difference regions. This in turn depends mainly on latitude but was greatly modified by location of continents and ocean, prevailing wind, oceanic circulation, topography, and other factors.

Developed model offers the possibility to predict the daily temperature data from the values of solar radiation and correlation of pixel value and irradiance that was statistically indistinguishable from the real ones where the later exist to be compared. The prediction of data was done in a very simple manner using a simple mathematical model. This model was suitable to use it in the case where there were no

recorded daily temperature data (missing data) for locations where measurements were not available. Possible application of the proposed model could be found in meteorological for predicting SST in coral reef sites. A developed model was generated to predict a daily SST data in the future. The validation of the model was performed with field investigation data, which the model had not seen before. Therefore, the pixel value of water vapour was a new way to predict the solar radiation and temperature.

We showed that solar radiation cycles coincide with SST cycles for the study site, and should be considered as one of the primary variables driving coral bleaching. Similar solar radiation principles might drive bleaching in other geographic locations, and might lead to predictions of coral bleaching in localities for which no field investigation information was available (e.g., along the east and west coast of Thailand). These remote sensing mathematical modelling techniques would facilitate predictions of SST schedules and determine stress thresholds when coral bleaching.

The key difference between January-April 2007 SST events on the study site lays not in the intensity of the solar radiation anomaly that caused each event, but in the proximity of the anomaly to the study site. The fact that the low SST occurred during a tropical storm and Southern wind occurred outside and it might be an important factor in the position of this site. The correlation between SST variability on the Gulf of Thailand and climatic events such as tropical storm, El Niño and the Pacific Decadal Oscillation need further investigation. The relationship between SST in the Gulf of Thailand and other relevant environmental parameters also need to be investigated to better understand potential cause and effect relationships. For instance,

it was known that factors such as light, turbidity, salinity, pollution, etc. also cause stress and could lead to bleaching in certain circumstances (Reaser et al., 2000).

SST trends from satellite and in-situ techniques were providing scientists with the tools to help understand the role of climate change on coral bleaching frequency and intensity over the Gulf of Thailand. However, to more accurately monitor and predict coral bleaching, satellite observations of additional environmental parameters such as wind, currents, cloud cover, and solar radiation were necessary to better relate environmental measurements and predictions to the biological response that causes coral bleaching. In addition to these, the spatial resolution and accuracy of the current data sets need to be improved. The high spatial resolution of other SST products currently in development as a joint NOAA project (Skirving et al., 2002) would help improve our capacity to understand spatial variability in this important and increasing environmental stress.

Then in the future, we could use these data to predict coral bleaching areas from SST. Moreover, this technique could be used to study climate change in terms of anomalies in the amount of water vapour data because our results could provide a more accurate estimation of climate change and more data points because we could estimate the water vapour data every half an hour. The methodology could be applied to any geographical area in the world.

ACKNOWLEDGEMENTS

This work was supported in part by PTT Public Company Limited, TOTAL Foundation and TOTAL E&P Thailand, TRF/Biotec special program for Biodiversity Research Training grant BRT T_550001, Commission on Higher Education, and

CXKURUE, the Institute of Research and Development, Walailak University. The authors thank Complex System Research Unit and Computational Science Graduate Program Walailak University for their supporting the amount of irradiance and temperature at weather station network in Thailand, The Naval Research Laboratory Marine Meteorology Division for their supporting the water vapour satellite images. The authors were also grateful to the editors and reviewers for their valuable comments and suggestions on this manuscript.

REFERENCES

- Aguiar R. and Collares-Pereira M. (1992). TAG: a time dependent autoregressive, Gaussian model for generating synthetic hourly radiation. *Solar Energy*, 49, 167-174.
- Bonazountasa M., Kallidromitoub D., Kassomenosc P. and Passasd N. (2007). A decision support system for managing forest fire casualties. *Journal of Environmental Management*, 84, 412-418.
- Dalu G. (1986). Satellite remote sensing of atmospheric water vapour. *International Journal of Remote Sensing*, 7, 1089-1097.
- Egido M. and Lorenzo E. (1992). The sizing of sand-alone PV systems: A Review and a proposed new method. *Solar Energy Materials and Solar Cells*, 26, 51-69.
- Feidasa H., Kontosa T., Soulakellisa N. and Lagouvardosb K. (2007). A GIS tool for the evaluation of the precipitation forecasts of a numerical weather prediction model using satellite data. *Computers and Geosciences*, 33, 989-1007.
- Gonzalez R. C. and Woods R. E. (2002). Image Segmentation. *Digital Image Processing (2nd edition)*, Euclid W. M., (Editor), Pearson Education (Singapore) Pte. Ltd., Indian Branch, 567-636.
- Guessoum A., Boubkeur S, and Maafi A. (1998). A total irradiation model using radial basis function neural network. *Proceeding of WREC VI*, UK, 332-336.
- Hokoi S., Matsumoto M. and Kagawa M. (1990). Stochastic models of solar radiation and outdoor temperature. *ASHRAE Transaction*, 2, 245-252.
- Kalogirou S. A., Michanelides S. and Tymoios F. (2002). Prediction of maximum solar radiation using artificial neural networks. *Proceeding of WREC VII*, Germany.

- Kleespies T. J. and McMillin L. M. (1990). Retrieval of precipitable water from observations in the split window over varying surface temperatures. *Journal of Applied Meteorology*, 29, 851-862.
- Marconi M. L. (2007). A kinetic model of Ganymede's atmosphere. *Icarus*, 190, 155-174.
- Mellit A., Benghane M. and Kalogirou S. A. (2006). An adaptive wavelet network model for forecasting daily total solar radiation. *Applied Energy*, 83, 705-722.
- Mellit A., Benghane M., Hadj A. A. and Guessoum A. (2003). Modelling of sizing the photovoltaic system parameters using artificial neural network. *Proceeding of IEEE Conference on Control Applications*, Istanbul, Turkey, 1, 353-357.
- Mellit A., Benghane M., Hadj A. A. and Guessoum A. (2004). Modelling of total solar radiation data from sunshine duration and temperature using the RBF networks. *The IASTED, MIC*, February 22-25, Grindelwald, Switzerland.
- Mellit A., Benghane M., Hadj A. A. and Guessoum A. (2005a). A simplified model for generating sequences of global radiation data for isolated sites: using artificial neural network and a library of Markov transition Matrices. *Solar Energy*, 79, 468-482.
- Mellit A., Benghane M., Hadj A., A. and Guessoum A. (2005b). An adaptive artificial neural network model for sizing of stand-alone photovoltaic system: Application for isolated sites in Algeria. *Renewable Energy*, 80(10), 1501-1524.
- Michalsky J. J., Perez R., Harrison L. and Lebaron B. A. (1991). Spectral and temperature correction of silicon photovoltaic solar radiation detectors. *Solar Energy*, 47, 299-305.

- Mohandes M., Balghonaim A., Kassas M., Rehman S. and Halawani T. O. (2000). Use of radial basis functions for estimating monthly mean daily solar radiation. *Solar Energy*, 68, 161-168.
- Mora Lopez L. L. and Sidrash-de-Cardona M. (1998). Multiplicative ARMA models to generate hourly series of total radiation. *Solar Energy*, 63, 283-291.
- Pardé M., Goïta K. and Royer A. (2007). Inversion of a passive microwave snow emission model for water equivalent estimation using airborne and satellite data, *Remote Sensing of Environment*, 111(2-3), 346-356.
- Reaser J. K., Pomerance R. and Thomas P. O. (2000). Coral bleaching and global climate change: Scientific findings and policy recommendations. *Conservation Biology*, 14, 1500–1511.
- Sfetsos A. and Coonick A. H. (2000). Univariate and multivariate forecasting of hourly solar radiation with artificial intelligence techniques. *Solar Energy*, 68, 169-178.
- Shrestha G. B. and Goel L. (1998). A study on optimal sizing of stand-alone photovoltaic stations. *IEEE Transactions on Energy Conversion*, 13, 373-378.
- Skirving W. J., Mahoney M. and Steinberg C. R. (2002). Sea surface temperature atlas of the Great Barrier Reef, 1990–2000, Version 1. *AIMS Data report*.
- Strong A. E. (1991). Sea surface temperature signals from space, *Encyclopedia of Earth System Science*, Nierenberg W.A. (Editor), Academic Press, San Diego, CA, 4, 69-80.
- Suereke H., Ling C. P. and McCormick P. G. (1990). The dynamic response of instruments measuring instantaneous solar radiation. *Solar Energy*, 44, 145–148.

Wolfram S. (2004). The Mathematica Book. *Book News (5th edition)*, Oregon.

Wong N. H., Jusuf S. K., Win A. A. L., Thu H. K., Negara T. S. and Xuchao W.

(2007). Environmental study of the impact of greenery in an institutional campus in the tropics. *Building and Environment*, 42, 2949-2970.

Yaiprasert C., Jaroensutasinee K. and Jaroensutasinee M. (2007). The Pixel Value

Data Approach for Rainfall Forecasting Based on GOES-9 Satellite Image Sequence Analysis. *International Journal of Mathematic and Engineering Science*, 1(4), 222-227.

Zhilin S. I. (2007). Simple method for outlier detection in fitting experimental data under interval error. *Chemometrics and Intelligent Laboratory Systems*, 88, 60-68.

CURRICULUM VITAE

Name: Mr. Chairote Yaiprasert.

Date of Birth: April 20, 1978.

Office: School of Science, Walailak University, 222 Thaiburi,
Thasala District, Nakhon Si Thammarat. 80161.
Tel: +66 75672050, +66 848460690.
Fax: +66 75672004.
E-mail: a.cirrus@gmail.com.

Education:

- Doctor of Philosophy Program in Computational Science, Walailak University, 2007.
- Master of Science Program in Computational Science, Walailak University, 2004.
- Bachelor of Science in Marine and Coastal Resources Management Technology (2nd Class Honors), Walailak University, 2002.

Awards and Honors:

- Her Majestic Queen scholarship in Bachelor of *Science*, Walailak University, 1998 - 2001.
- Commission on Higher Education scholarship in Master of Science (Computational Science), 2002 – 2003.
- Commission on Higher Education scholarship in Doctor of Philosophy (Computational Science), 2005 – 2007.

- PTT Public Company Limited, TOTAL Foundation and TOTAL E&P Thailand, TRF/Biotec special program for Biodiversity Research Training grant BRT T_550001, 2007-2008.

List of Publications:

- Jaroensutasinee, K. and Yaiprasert, C. (2003). Land cover analysis of Pakpanang watershed, Nakhon Si Thammarat using satellite image data. *29th Congress on Science and Technology of Thailand*, Khonkaen, Thailand. 20th-22nd October, SH290, 252.
- Jaroensutasinee, K., Yaiprasert, C., May, P. and Wirathtipong, T. (2003). Ocean circulation and sea elevation simulation system with POM. *29th Congress on Science and Technology of Thailand*, Khonkaen, Thailand. 20th-22nd October, SA36, 7.
- Jaroensutasinee, K., Yaiprasert, C., May, P. and Wirathtipong, T. (2003). Ocean circulation and sea elevation simulation system with POM. *DPST conference, Windsor Hotel, Bangkok*. 27th-28th September, 20.
- Jaroensutasinee, K., Jaroensutasinee, M., Yaiprasert, C., Ruairuen, W., Aungsakul, K., Uraichuen, Y. Kulsri, S. and Phetkeaw, W. (2004). Water quality and land use: an integrated study of the Lipanoi River system, Samui Island. *The 8th Annual GLOBE Conference*, Colourado, USA. 25th-30th July.
- Yaiprasert C. and Jaroensutasinee K. (2004). A computational technique for generating a digital elevation model (DEM). *30th Congress on Science and Technology of Thailand*, Bangkok, Thailand. 19th-21st October.

I0011, I210.

- Yaiprasert C. and Jaroensutasinee K. (2004). Floating Circle of Objects (FCO) Simulation with Hydrodynamic Model. *Proceedings of The 8th Annual National Symposium on Computational Science and Engineering*, Nakhonratchasima, Thailand. 21st-23rd July, HPCCM-O25.
- Yaiprasert C. and Jaroensutasinee K. (2005). Floating Circle of Objects (FCO) Simulation with Princeton Ocean Model for the Gulf of Thailand. *Walailak Journal of Science & Technology*, 2, 99-113.
- Yaiprasert C., Jaroensutasinee M. and Jaroensutasinee K. (2006). Pasak Jorasid Dam Affecting Soil and Hydrology measurements of Oxbow Lakes. *10th GLOBE Annual Conference*, Phuket, Thailand. 30th-4 August.
- Jitkue K., Srisang W., Yaiprasert C., Jaroensutasinee K. and Jaroensutasinee M. (2007). *Integration of Multi-Source Data to Monitor Coral Biodiversity. International Journal of Mathematical, Physical and Engineering Sciences*, 1(4), 238-242.
- Jitkue K., Yaiprasert C., Surabun S., Wongkoon S., Jaroensutasinee M. and Jaroensutasinee K. (2007). Coral growth forms, biodiversity index and physical factors at Racha Islands, Phuket. *The 33rd Congress on Science and Technology of Thailand*, Nakhon Si Thammarat, Thailand. 18-20th October, 127-128.
- Surabun S., Yaiprasert C., Wongkoon S., Jaroensutasinee M. and

Jaroensutasinee K. (2007). Coral growth forms and biodiversity indices at kha nom mu koh talae tai marine national park. *The 33rd Congress on Science and Technology of Thailand*, Nakhon Si Thammarat, Thailand. 18-20th October, 129.

Yaiprasert C., Jaroensutasinee K. and Jaroensutasinee M. (2007). The Pixel Value Data Approach for Rainfall Forecasting Based on GOES-9 Satellite Image Sequence Analysis. *International Journal of Mathematical, Physical and Engineering Sciences*, 1(4), 222-227.

Yaiprasert C., Surabun S., Wongkoon S., Jaroensutasinee M. and Jaroensutasinee K. (2007). Comparing two estimating techniques on coral growth forms using random and quadrat sampling techniques. *The 33rd Congress on Science and Technology of Thailand*, Nakhon Si Thammarat, Thailand. 18-20th October, 125-126.

Yaiprasert C., Jaroensutasinee K. and Jaroensutasinee M. (2007). Mathematical Model for Solar Radiation and Temperature Field Verification. (in preparation).